STRUCTURE BASED MECHANISTIC STUDIES ON 2-KETOPROPYL COENZYME M OXIDOREDUCTASE / CARBOXYLASE FROM *XANTHOBACTER AUTOTROPHICUS* AND [FEFE] HYDROGENASE FROM *CLOSTRIDIUM PASTEURIANUM*

by

Arti Sharma Pandey

A dissertation submitted in partial fulfillment
of the requirements of the degree

of

Doctor of Philosophy

in

Biochemistry

MONTANA STATE UNIVERSITY
Bozeman, Montana

July 2007

© COPYRIGHT

By

Arti Sharma Pandey

2007

All Rights Reserved

APPROVAL

of a dissertation submitted by

Arti Sharma Pandey

This dissertation has been read by each member of the dissertation committee and has been found to be satisfactory regarding content, English usage, format, citations, bibliographic style, and consistency, and is ready for submission to the Division of Graduate Education.

Prof. John W. Peters

Approved for Department of Chemistry and Biochemistry

Prof. David Singel

Approved for the Division of Graduate Education

Dr. Carl A. Fox

STATEMENT OF PERMISSION TO USE

In presenting this dissertation in partial fulfillment of the requirements for a doctoral degree at Montana State University, I agree that the Library shall make it available to borrowers under rules of the Library. I further agree that copying of this dissertation is allowable only for scholarly purposes, consistent with "fair use" as prescribed in the U.S. Copyright Law. Requests for extensive copying or reproduction of this dissertation should be referred to ProQuest Information and Learning, 300 North Zeeb Road, Ann Arbor, Michigan 48106, to whom I have granted "the exclusive right to reproduce and distribute my dissertation in and from microform along with the non-exclusive right to reproduce and distribute my abstract in any format in whole or in part."

Arti S. Pandey

July 2007

ACKNOWLEDGEMENTS

I express my thanks to the Principal Investigator on my projects, Prof. John Peters, for providing me the opportunity to learn and apply X-ray crystallography to meet larger scientific ends. His enthusiasm and passion for his projects were always inspiring.

I would also like to thank my graduate committee member, Prof. Martin Lawrence, for patiently explaining any questions I had about crystallography. I consider myself fortunate to have been his student. I thank Prof. Valerie Copié for her constant encouragement and support. I would like to thank Prof. Trevor Douglas, Prof. Brenda Spangler and Prof. Brian Bothner for their insights into these projects.

I would like to thank my fellow lab members who made this a fun experience.

I would like to thank my family for their staunch support throughout. I dedicate my thesis to my two boys, who were 3 and 5 yrs old when I started, and were my companions throughout this journey.

TABLE OF CONTENTS

TABLE OF CONTENTS-CONTINUED

TABLE OF CONTENTS - CONTINUED

LIST OF FIGURES

LIST OF FIGURES - CONTINUED

LIST OF FIGURES-CONTINUED

LIST OF TABLES

Table Page

ABSTRACT

X-ray crystallography was employed to probe the mechanism of the enzyme 2-ketopropyl coenzymeM oxidoreductase / carboxylase (2-KPCC). We were able to determine the enzyme structure in various catalytically relevant states, providing insights into substrate binding, intermediate stabilization, product formation and release. Structures of 2-KPCC were obtained with the substrate 2-ketopropyl coenzyme M (KCoM), product acetoacetate, 6-oxoheptanoic acid (OHA), 2-oxopropyl phosphonate (OPP), $NADP^+$ and coenzymeM (CoM), the oxidized and reduced states. The binding sites for these ligands in relation to one another have led to important sights into the mechanism. CO_2 binds at the base of a hydrophobic channel at the interface of a hydrophobic pocket and the substrate binding site. Acetoacetate binds at an alternate anion binding site, as revealed in the bicarbonate and CoM disulfide bound structures. The enolate intermediate can be stabilized by an Ala430 carbonyl stabilized water molecule as revealed in the OHA bound structure, at a site different from that in KCoM bound structure. Together, the structures reveal a mechanism of concerted attack of a CO_2 molecule on the enolate intermediate formed by the nucleophilic attack of Cys82 on the C-S bond of KCoM. Acetoacetate is stabilized at the alternate anion binding site, with the concomitant formation of a mixed disulfide. A nucleophilic attack by a water molecule on the mixed disulfide, accompanied by a weakening of interactions between CoM and Arg residues due to charge sharing with the acetoacetate carboxyl group, aids the release of CoM acetoacetate. Decarboxylation of acetoacetate occurs at the alternate anion binding site with the release of carboxyl group perhaps as bicarbonate.

Structural refinement at 1.39Å in conjunction with density functional theory (DFT) optimization has been applied to address undefined aspects of the active site H-cluster that could impact the mechanism of reversible H_2 oxidation by [FeFe] hydrogenase from *Clostridium pasterianum*. The model with highly accurate positioning of the H-cluster atoms was used for sequential structural optimization. The results of this optimization challenge the established paradigm that the dithiolate ligand bridging the Fe atoms of the 2Fe H-subcluster is a dithiomethylammonium and supports the assignment of a dimethyl ether.

INTRODUCTION

X-ray crystallography is a widely used method of obtaining a detailed picture of a molecule through interpretation of diffraction of x-rays from an ordered array of molecules as in a crystal. The structures of macromolecules (proteins/DNA) obtained by this method provide a graphical view of its secondary structure and the domains that it folds into. In addition, it reveals the various interactions that hold the protein together, or that bind cofactors/ligands to their respective binding sites. A study of these interactions provides a basis for designing drugs that might bind in an analogous manner to the substrate for a protein and inactivate it. This approach has successfully been used to design drugs for malfunctioning proteins. For example, 25% of the currently marketed drugs are small molecule drugs against G protein coupled receptors[1]. Small molecules that modulate the function of ion channels, proteases, kinases and nuclear hormone receptors make up another 22% of the market [2]. Co-crystallization studies in which the target molecule is crystallized with a small molecule inhibitor is invaluable for the determination of a good target site. The detailed interactions of the ligand to the residues that constitute its binding site are utilized to design inhibitors that are structural analogs of the substrates, but lack a feature that causes them to resist getting turned over by the enzyme. The same method is also used to elucidate details of mechanism of an enzyme with the target of capturing the enzyme bound to its substrate, products or any intermediates. This is achieved by using substrates/products or their non-hydrolyzable structural analogs for cocrystallization. The accuracy of interactions seen in the resulting x-ray structures depends on the resolution to which the structure has been determined.

Together, such analog bound structures at high resolutions can provide important information in elucidation of mechanisms of enzymes. In this work, this technique has been applied to two enzymes for providing insights into their mechanisms:

1. 2-ketopropyl coenzyme M oxidoreductase/carboxylase (2-KPCC) from *Xanthobacter autotrophicus*: A novel disulfide oxidoreductase that performs the additional role of carboxylation without using any of the conventional cofactors used by other carboxylases. This enzyme is the terminal enzyme in the epoxide carboxylation pathway of short chain alkenes in the organism *X. autotrophicus* strain Py2.

2. The Fe-only hydrogenase from *Clostridium pasteurianum*: Catalyzes the production of hydrogen gas from protons and electrons. A higher resolution structure combined with application of the Density Functional Theory and provides a better basis for correlation of geometry of its [Fe-S] and its mechanism of H_2 production with that of its synthetic mimics.

2-Ketopropyl Coenzyme M Oxidoreductase / Carboxylase

Over 200 million tons of gaseous alkenes are produced annually from biogenic and anthropogenic processes [3]. Bacteria that are able to grow by using short-chain alkenes as sources of carbon and energy are believed to play an important role in remineralization of this carbon in the global carbon cycle [4].

Diverse bacteria, including various strains of *Rhodococcus*, *Mycobacterium*, *Nocardia*, *Xanthobacter*, *Alcaligenes*, *Pseudomonas* and *Corynebacterium*, are capable of aerobic growth with short-chain aliphatic alkenes (C2 to C6) as the sole added carbon source [4]. While some alkene oxidizing bacteria are restricted to growth on a single

alkene, e.g., ehtylene or isoprene (2-methylbutadiene), others exhibit less selectivity for the growth substrate. For example, *Xanthobacter* strain Py2, a bacterium isolated with propylene, can also grow using ethylene, 1-butylene, 2-butylene, 1-pentene and 1-hexene as carbon sources [5, 6]. An interesting feature of alkene-oxidizing bacteria is the diversity of additional growth substrates that the bacteria are capable of using. For example, some of the alternative growth substrates for *Xanthobacter* strain Py2 include glucose, fructose, organic acids, C-1 to C-4 alcohols, acetone, 1,2-propanediol and H_2 plus CO_2.

All of the alkene oxidizing bacteria isolated to date are aerobic bacteria that initiate alkene oxidation by O_2- and reductant dependent monoxygenase reactions. Alkene monooxygenases (AMOs) have been purified and characterized from two propylene -oxidizing bacteria: *Rhodobacter rhodochrous* strain B276 [7] and *X. autotrophicus* strain Py2 [8]. Both enzymes are NADH-dependent, multicomponent enzymes that catalyze alkene epoxidation according to the reaction:

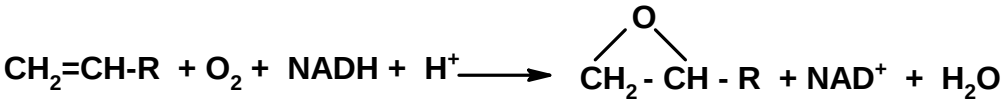

Aliphatic epoxides are highly reactive molecules with mutagenic and in some cases carcinogenic properties [9]. The toxicity of aliphatic alkenes arises from their ability to serve as substrates for broad-substrate specificity oxygenases resulting in the formation of highly reactive electrophilic epoxides [10, 11]. Depending upon the organism, epoxides formed in this way can undergo one of several fates. Epoxides may react abiotically with cellular nucleophiles e.g. proteins and DNA, to form covalent

adducts, a process that accounts for the toxic properties of these compounds [12]. To counteract this, some organisms contain detoxification enzymes, specifically glutathione-S-transferases (GSTs) and epoxide hydrolases that use glutathione or water, respectively, as nucleophiles to attack and open the oxirane ring (Figure 2.1). These adducts may then be excreted or further metabolized. Alkene-oxidizing bacteria are unique in being able to carry out the productive catabolism of aliphatic epoxides by their conversion to central metabolites that meet the carbon and energy needs of the bacteria. The reactivity of these compounds derives from their electrophilicity and the resultant reaction with cellular nucleophiles (e.g. proteins and DNA). These epoxidation reactions may be catalyzed fortuitously, i.e. in place of the natural oxygenase substrate as the first step in the detoxification of alkenes or as the first step in the utilization of alkenes as primary carbon and energy sources of growth (Figure 1.2).

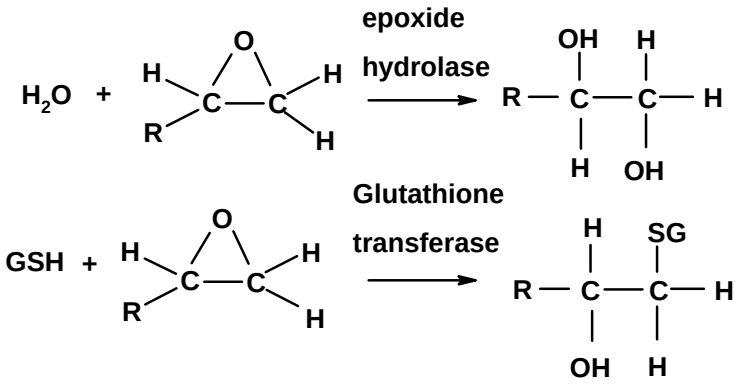

Figure 1.1: Detoxification of epoxides by epoxide hydrolase and glutathione transferase

or *Nocardia* strain A60, the metabolism of propylene oxide occurs via hydration to 1, 2 propanediol [13]. The metabolism of styrene oxide (phenylepoxyethane) by styrene

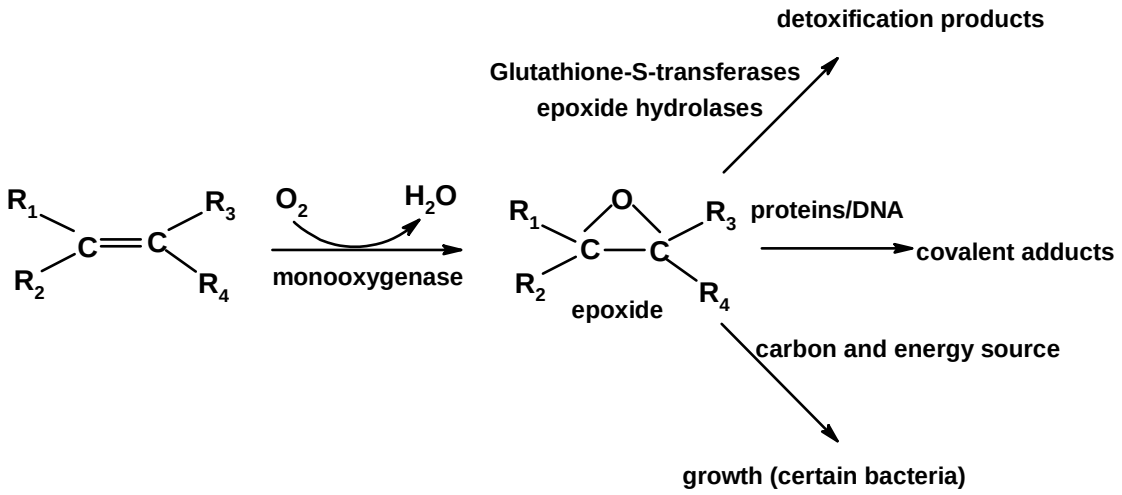

Figure 1.2: Fates of epoxides formed from short chain alkenes.

utilizing bacteria proceeds by isomerization to the corresponding aldehyde [14]. A fundamentally distinct strategy for aliphatic epoxide utilization occurs in some other bacteria that carboxylate the epoxides to β - keto acids as for example *X. autotrophicus* strain Py2.

X. autotrophicus strain Py2 is a gram-negative, nutritionally versatile, bacterium isolated with propylene as the source of carbon and energy [6]. In addition to linear, short-chain (C-2 to C-7) aliphatic alkenes and epoxides, *X. autotrophicus*, strain Py2 can grow using ketones (acetone and 2-butanone), aldehydes, diols, sugars, organic acids and H_2 / CO_2 as carbon and energy sources [6]. *X. autotrophicus* grows rapidly with aliphatic alkenes, typical doubling times with propylene as the carbon source are 4-8 h [15]. The alkene and epoxide degrading enzymes of this bacterium are repressed during growth on other carbon sources and are induced by the presence of a range of aliphatic and

chlorinated alkenes and epoxides [16]. The alkene monooxygenase of *X. autotrophicus* Py2 is also capable of oxidizing chlorinated alkenes of environmental concern, e.g. trichloroethylene and vinyl chloride [17] and the epoxide converting enzyme has a similar ability to degrade halogenated epoxides [18]. These various features make the alkene/epoxide metabolizing system of *X. autotrophicus* strain Py2 an attractive one for studying the pathway of aliphatic alkene and epoxide metabolism. The pathway for alkene metabolism in *X. autotrophicus* strain Py2 and *Rhodococcus rhodochrous* strain B276 have been extensively studied with regard to propylene metabolism [15, 19, 20]. In both of these organisms, propylene metabolism is initiated by highly stereoselective NADH-dependent monooxygenases producing an enantiomeric excess of (*R*)-epoxypropane [7, 8, 21]. In the presence of CO_2, the enantiomers of epoxypropane are further metabolized to acetoacetate by four enzymes constituting the "epoxide carboxylase system" [22, 23]. Coenzyme M (CoM), a cofactor once thought to be restricted to methanogenic Archae, was discovered as the central C3 carrier in the *Xanthobacter* Py2 epoxide carboxylase system [24]. This discovery revealed the epoxide carboxylase system as not a true multiprotein complex but actually a three step metabolic pathway with distinct intermediates (Figure 1.3) [20].

The Epoxide Carboxylation Pathway

The first enzyme of the epoxide carboxylase pathway is an epoxyalkane:CoM transferase [24](Figure 1.3). This enzyme is a homohexameric zinc metalloenzyme (42 KDa subunits) that catalyzes the conjugation of CoM an *(R)*- or *(S)*- enantiomer of 2-hydroxypropyl-CoM. In the second step, these enantiomers are oxidized by stereospecific

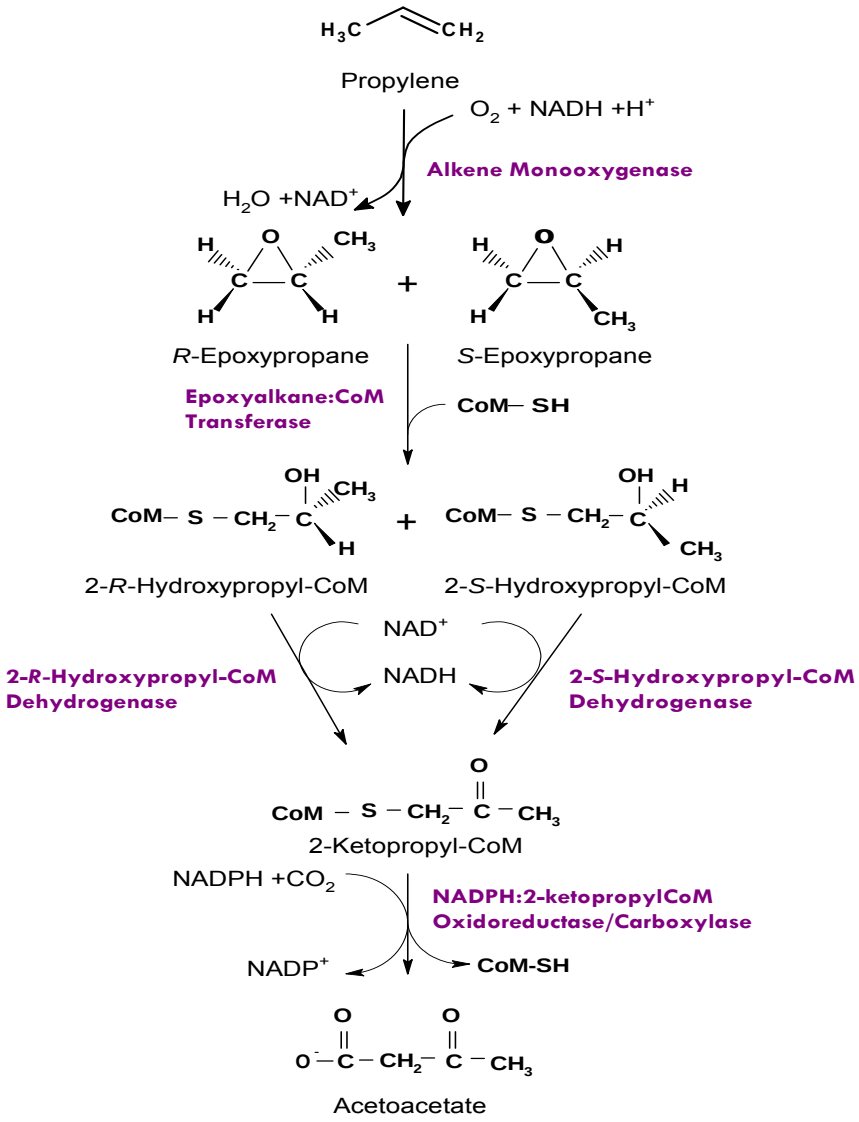

Figure 1.3: The epoxide carboxylation pathway in *X. autotrophicus* [20] CoM-SH, Mercaptoethanesulfonate (SO_3^{2-}-CH_2-CH_2-SH)

R- or (*S*)-2-hydroxypropyl-CoM dehydrogenases to the common intermediate 2-ketopropyl-CoM [24]. The terminal enzyme of the *Xanthobacter* Py2 epoxide carboxylase pathway is the NADPH:2-ketopropylCoM oxidoreductase/carboxylase (2-

KPCC). This enzyme catalyzes the reductive cleavage and carboxylation of 2-ketopropyl CoM to acetoacetate, with the concomitant regeneration of CoM for use by the epoxyalkane:CoM transferase.

The primary sequence and biochemical properties of 2-KPCC place it in the family of NADPH:disulfide oxidoreductases (DSORs) [25-27]. The chemistry of the reaction catalyzed by 2-KPCC is unprecedented for a DSOR enzyme. In all but one case, members of this family catalyze the reduction of a disulfide bond in an organic substrate, as, for example, in the case of glutathione reductase and dihydrolipoamide dehydrogenase [28]. Mercuric reductase is an atypical member of this family, which catalyzes the reduction of mercuric ion to elemental mercury [29]. However, mercuric reductase shares the common feature of catalyzing a two-electron reduction of substrate.

The DSOR Family

All members of the DSOR family contain a highly conserved redox active cysteine pair, separated by four intervening residues, that participate in substrate reduction [28]. The well characterized members of this group are lipoamide dehydrogenase, glutathione reductase, thioredoxin reductase NADH peroxidase and mercuric ion reductase [30]. Other members of this family include trypanothione reductase, CoA-disulfide reductase, cystine reductase, asparagusate reductase, bis-γ -glutamylcystine reductase and sulfhydryl reductase. With the exceptions of mercuric ion reductase and sufhydryl oxidase, all enzymes in this family catalyze electron transfer between NAD(P)H and a disulfide/dithiol. A general mechanism for the inital reactions of the DSOR enzymes, which diverge into the specialized reactions of those enzymes that

reduce organic substrates is shown in the figure 1.4. The first step in the catalytic cycle is the binding of NADPH to the fully oxidized enzyme. NADPH reduces FAD to $FADH_2$ and is followed by the nucleophilic attack of the C4a carbon of $FADH_2$ on the proximal cysteine thiol of the disulfide. Heterolytic cleavage of the C4a-thiol bond leaves FAD oxidized and the redox active disulfide in its two-electron reduced form. In the case of the disulfide reducing DSOR enzymes, the distal cysteine thiol then attacks one of the S atoms of the disulfide substrate. This releases one organic thiol in its reduced form and forms a mixed disulfide with the other thiol. Attack of the proximal cysteine thiol on the distal thiol promotes heterolytic cleavage of the mixed disulfide, which releases the second substrate to complete the catalytic cycle.

Glutathione Reductase : Glutathione reductase from *E.coli* and mammalian cells has been very well characterized both structurally and functionally, and serves as a model for comparison to other DSORs. Cells maintain high levels of GSH relative to glutathione disulfide, GSSG by the action of glutathione reductase (GR), which catalyzes the NADPH-dependent reduction of GSSG to GSH.

$$GSSG + NADPH + H^+ \rightleftharpoons 2GSH + NADP^+$$

Human GR has been thoroughly studied by X-ray crystallography. Structures of the native enzyme [31] at high resolution (1.54 Å) [31, 32] as well as complexes of the oxidized and reduced enzymes with pyridine nucleotides, GSSG, and of a mixed disulfide

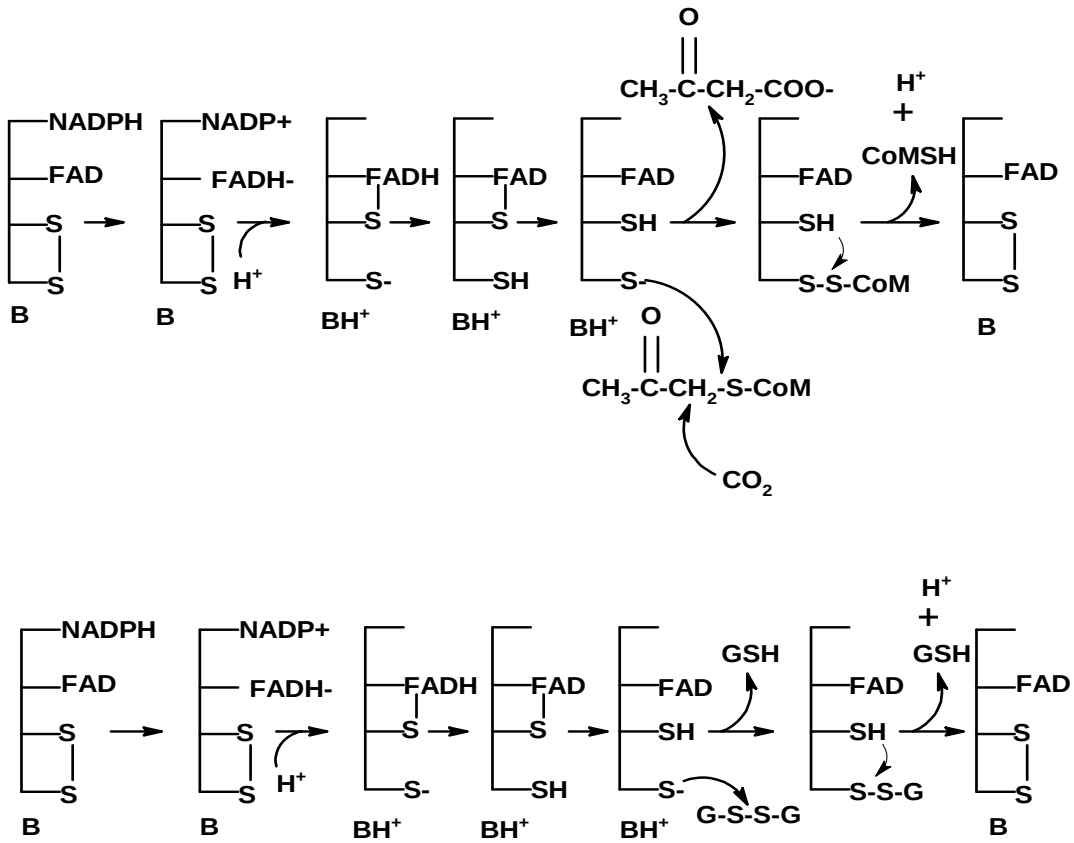

Figure 1.4: Top-The general reaction catalyzed by 2-KPCC, reductive cleavage of a C-S bond of the substrate 2-ketopropyl coenzyme M and subsequent addition of CO_2 to form acetoacetate and free coenzyme M. Bottom: General reaction catalyzed by members of the DSOR family. Reduction of FAD by NADPH to form $FADH^-$, nucleophilic attack of C4a of $FADH^-$ on the proximal cysteine sulfur to form a covalent adduct that collapses into a charge transfer complex, nucleophilic attack of the distal cysteine sulfur on the disulfide substrate (eg G-S-S-G) to form a mixed disulfide, nucleophilic attack of the proximal cysteine sulfur on the mixed disulfide. Both leaving groups (GSH in the example shown above) are protonated by histidine of the catalytic dyad and leave as thiols

intermediate [33-35] have been determined (Figure 1.4). In *E. coli* GR, a mutation of the histidine residue of the His-Glu catalytic dyad resulted in the dramatic accumulation of FADH2.$NADP^+$ intermediate [36] due to interruption of intramolecular electron transfer to the disulfide facilitated by the dyad. GR from human erythrocytes [37], yeast, [38, 39] and mouse liver [40] has been shown to be inactivated by preincubation with NADPH.

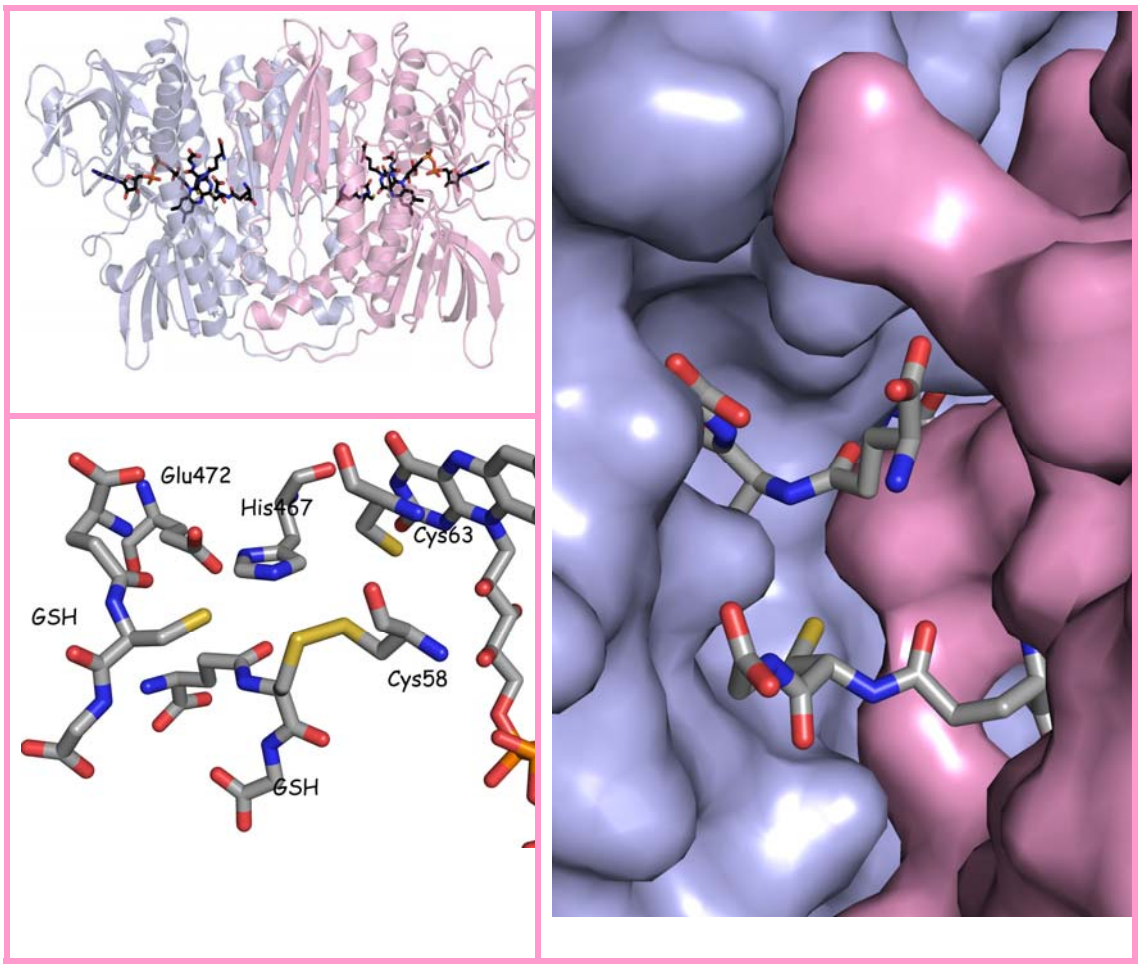

Figure 1.5: Top left: Glutathione reductase dimer with FAD and glutathione bound**.** Right.Substrate binding pocket at the dimer interface with two glutathiols bound. Bottom left: Substrate binding site in GR, showing a mixed disulfide between one of the glutathiols and the distal cysteine while the other glutathiol is positioned in proximity to the catalytic His-Glu dyad

In human erythrocytes, this inactivation was accompanied by aggregation nd was completely reversed by GSH suggesting that inactivation is due to intermolecular thiol oxidation [37].

Lipoamide Dehydrogenase: Lipoamide dehydrogenase is the E3 component of the pyruvate dehydrogenase, alpha ketoglutarate dehydrogenase, branched chain 2-oxoacid

dehydrogenase and glycine reductase multienzyme complexes [41]. It functions in reoxidation of the dihydrolipoyl cofactors that are colvalently linked to the lipoylacyltransferase subunits of these complexes.

$$Lip(SH)_2 + NAD^+ \overset{LDH}{\rightleftharpoons} Lip(S)_2 + NADH + H^+$$

Formation of the reduced flavin intermediate, $FADH_2.NAD^+$ charge transfer complex was observed for the first time in LDH from *Mycobacterium tuberculosis*. This was due to slower internal electron transfer to the the redox active disulfide to generate EH_2. The $FADH_2.NAD^+$ complex is stabilized a 1000-fold relative to the wild type LDH from *Azotobacter vinelandii* when the His of the catalytic dyad is replaced by serine, showing impaired transfer of electrons from FAD to the redox disulfide [42].

Trypanothione Reductase: Trypanothione [T(S)2; N1,N8 –bis (glutathionyl) spermidine], is used as a protective thiol in trypanosomatids [43]. Trypanothione is maintained in its reduced form by trypanothione reductase (TR), which catalyzes the NADPH-dependent reduction of $T(S)_2$ to $T(SH)_2$.

$$T(S)_2 + NADPH + H^+ \overset{TR}{\rightleftharpoons} T(SH)_2 + NADP^+$$

The substrate binding site in TR is wider than that of human GR. [44] to accommodate the bulkier $T(S)_2$ and TR also provides a hydrophobic patch to interact with the hydrophobic spermidine moiety of $T(S)_2$. In human GR, the hydrophobic patch is replaced by cationic residues which interact with the negatively charged carboxylate of

GSSG. This causes the substrates for TR and GR to be mutually exclusive even though they have a common glutathione core [45].

Thioredoxin reductase (TrxR): TrxR catalyzes the NADPH-dependent reduction of a disulfide bond in thioredoxin [$TR(S)_2$], a 12-kDa protein.

$$TR(S)_2 + NADPH + H^+ \overset{TrxR}{\rightleftharpoons} TR(SH)_2 + NADP^+$$

High molecular weight TrxRs (~55kDa) are termed high to distinguish them from low molecular weight TrxRs (~35 kDa), which lack an interface domain [46]. High molecular weight TrxRs have been found in *P.falciparum*, mammals and *Drosophila melanogaster* whereas low molecular weight TrxRs are found in bacteria, yeast, fungi and plants.. In high molecular weight TrxRs, a 15-20 residue extended C-terminus harbors an essential second non-flavin redox center [47-49]. This auxiliary redox center is either a second enzymic disulfide (*D.melanogaster* and *P. falciparum*) or a selenenylsulfide (mammals).

Low molecular weight TrxRs contain an essential redox active sulfide [50, 51], but its cysteines are separated by two amino acids rather than four, and are located in the pyridine-nucleotide-binding domain rather than in the FAD-binding domain. TrxR in *E. coli* lacks an interface domain where the His-Glu catalytic dyad is normally located, they use an Asp as the general acid catalyst [52]. The redox active disulfide is located on the *re* face of FAD as opposed to the *si* face as in other DSORs and positioned favourably for electron transfer from FAD to the disulfide (Figure 1.6 Left). However, the subsequent

reduction of $Trx(S)_2$ by dithiol-disulfide interchange is sterically restricted, the NADPH binding site is too far from FAD and access of NADP to the *re* face of FAD is blocked by the redox disulfide. [53] (PDB 1TDF). A structure of TrxR-Trx complex (PDB 1F6M) [54] cocrystallized with 3-aminopyridine adenine dinucleotide phosphate ($AADP^+$) provided structural evidence for an earlier proposal [53] that a conformational change involving a relatively unrestricted 66 ° rotation of the pyridine nucleotide binding domain relative to the FAD binding domain occurs juxtapositioning NADP and FAD for electron transfer (Figure 1.6, Right).

Mercuric Ion Reductase: Organomercurials and mercuric ion are highly toxic to living organisms because of the high affinity of Hg(II) for thiolates [55]. Detoxification by bacteria involves uptake of these compounds and separation of the organic moiety by organomercuric lyase and reduction of Hg (II) to the less toxic and volatile elemental mercury (Hg0) by mercuric ion reductase (MR).

$$\text{R-S-Hg(II)-S-R} + \text{NADPH} + \text{H}^+ \overset{\text{MR}}{\rightleftharpoons} \text{Hg(0)} + 2\text{RSH} + \text{NADP}^+$$

MR, like mammalian TrxR also uses an additional cysteine disulfide at its C-terminus [56], which are essential for in vitro activity with some [57, 58] but not all [59, 60] Hg (II) substrates. The presence of auxiliary cysteines has been found to be essential for organomercurial substrates with bulkier organic groups, [61] suggesting the presence of two different channels for small and large substrates, which deliver smaller substrates bypassing the auxiliary cysteines [62]. In order to sequester Hg (II) followed by its

thermodynamically unfavourable reduction, the two active sites in homdimeric MR communicate such that while one binds Hg(II) tightly, the other reduces it, and this timing of events is regulated by pyridine nucleotide [63].

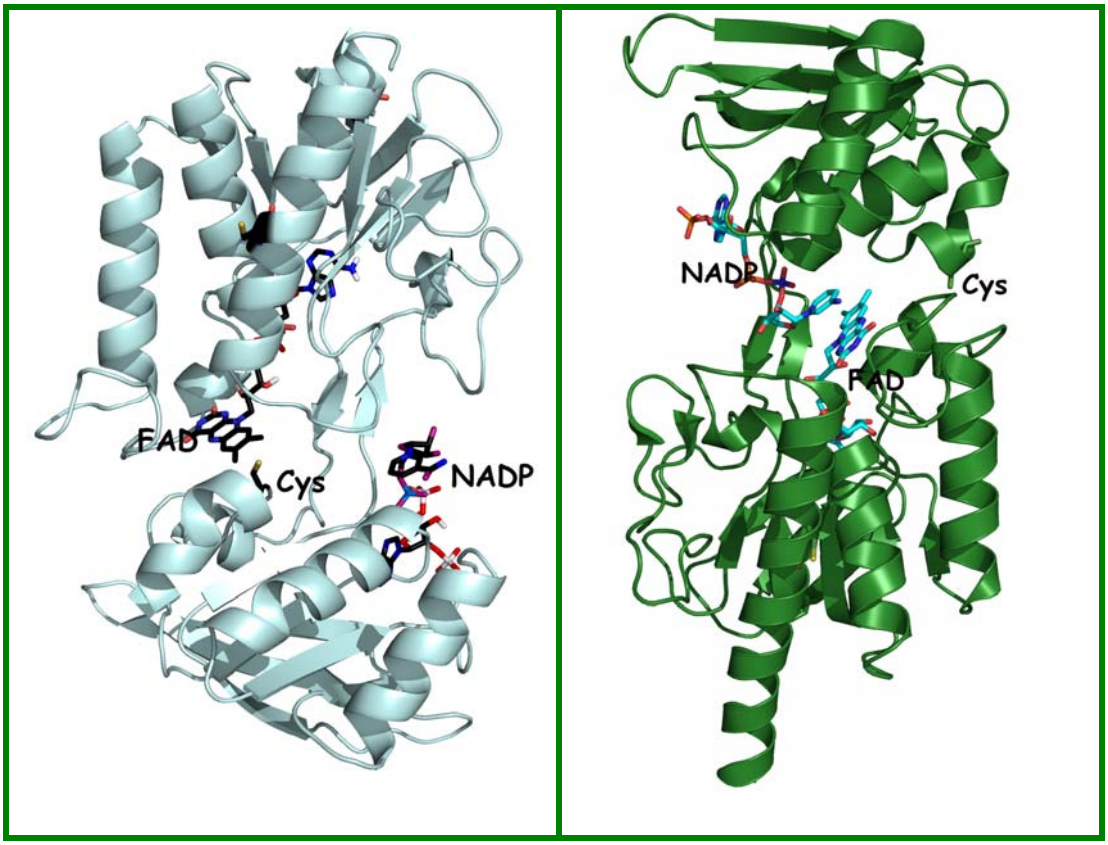

Figure 1.6: Thioredoxin reductase from *E. coli* Left: The flavin oxidized conformation with the redox active cysteine positioned close to FAD while the NADP nicotinamide positioned away from both. Right: A rotation of the NADP domain with respect to the FAD domain causes the correct positioning of NADP, FAD and redox active cysteine for electron transfer

Coenzyme A Disulfide Reductase, NADH oxidase and NADH peroxidase: These enzymes do not contain a redox active disulfide, but instead use a single redox-active cysteine sulfenic acid residue, (NADH oxidase and peroxidase) and Cys-S-S-CoA mixed disulfide (CoA disulfide reductase) [64]. Gram positive bacteria, eg. *Bacillus subtilis* and

Staphylococcus aureus, produce and maintain high levels of reduced coenzyme A (CoASH) as the predominant low-molecular-weight thiol [65]. A homodimeric flavoprotein reductase from *S. aureus* has been identified and characterized [66]. Coenzyme A disulfide reductase (CoADR) catalyzes the NADPH-dependent reduction of coenzyme A disulfide (CoASSCoA). NADH- oxidase and NADH peroxidase enzymes from *Enterococcus faecalis* do not catalyze the reduction of disulfide bonded substrates, but rather catalyze the four-electron reduction of molecular oxygen to water or two electron reduction of hydrogen peroxide to water, respectively [67].

Reaction Catalyzed by 2-KPCC

Based on the kinetic and mechanistic studies of the 2-KPCC catalyzed reaction [68], together with the information from kinetic and spectroscopic studies performed by Westphal and coworkers using 1,3- propanedithiol before the physiological substrate for 2-KPCC was identified [27], a catalytic mechanism was proposed according to which the distal thiol attacks the thioether linkage of 2-ketopropyl CoM, which forms a mixed disulfide of Cys and CoM with formation of the enolate (or enol) of acetone (Figure 1.7). An early piece of evidence supporting the formation of enolacetone as a reaction intermediate was the observation that acetone was formed as the product of epoxide degradation when CO_2 was excluded from assays [18, 69]. After the identification of CoM, it was verified by Ensign and coworkers that acetone is indeed formed as the product of the 2-KPCC catalyzed reaction in the absence of CO_2, 2-KPCC catalyzed acetone formation occurs at about 40% of the maximal rate of acetoacetate formation [68]. Enolacetone is a strong nucleophile, and if formed in the absence of CO_2, it would

be expected to abstract a proton from the bulk solvent to form acetone. This step would be essentially irreversible due to the high pKa of the methyl group proton of acetone. As expected, 2-KPCC was unable to catalyze the reverse reaction with acetone, CO_2, NADP and CoM as substrates. However, 2-KPCC did catalyze the reverse reaction when acetoacetate was used as the substrate, as well as the decarboxylation of acetoacetate and exchange of CO_2 into acetoacetate in the absence of other substrates.

Carboxylation by 2-KPCC

Aliphatic epoxide carboxylation appears to be a general strategy for epoxide metabolism in bacteria that grow using aliphatic alkenes as carbon sources [70]. In the epoxide carboxylation pathway in *X. autotrophicus*, it was discovered that the actual CO_2-fixing step is catalyzed by 2-KPCC. Although diverse in terms of structure, substrate specificity and cofactor usage, all carboxylases share an important common feature: the ability to generate a stabilized carbanion for attack on electrophilic CO_2 or an activated CO_2 species (eg carboxyphosphate). The reductive carboxylation of 2-ketopropyl coenzyme M by 2-KPCC occurs through the formation of a carbanion that is proposed to get stabilized as an enolate intermediate by a histidine coordinated water molecule in the active site [68, 71]. The enolate intermediate being a strong nucleophile adds to a CO_2 molecule to form acetoacetate. In the absence of CO_2, the nucleophilic enolate extracts a proton from bulk solvent to form acetone.

2-KPCC also catalyzes the decarboxylation of acetoacetate, which in the presence of coenzyme M and $NADP^+$ results in the formation of 2-ketopropyl coenzyme M. Enzymatic decarboxylation of common types of organic acids (β- keto acids, β- hydorxy

acids, α- keto acids and α- amino acids) occurs through the formation and stabilization of a carbanion / enolate [68]. 2-KPCC has been shown to neither utilize a metal ion or a Schiff's base for stabilization of enolate intermediate. Also, neither thiamin pyrophosphate (TPP) nor pyridoxal phosphate, cofactors used by enzymes that catalyze α – amino acid decarboxylations, are associated with 2-KPCC. This implicates the role of a catalytic acid mediated proton donation to the carbonyl oxygen or electrostatic stabilization using a positively charged amino acid side chain. It was also shown [68] that decarboxylation of acetoacetate by 2-KPCC is ~77 fold slower in the absence of coenzyme M.

Structure of 2-KPCC

The three dimensional structure of substrate bound 2-KPCC was determined by the multiple isomorphous replacement and anomalous scattering (MIRAS) method and refined to 1.65 Å [71] (Figure 1.8). The structure of the native enzyme was also solved using the substrate bound structure as a model for molecular replacement. The overall structure of KPCC was found to be very similar to the dimeric structure observed for the classic members of the DSOR family [28] [72].

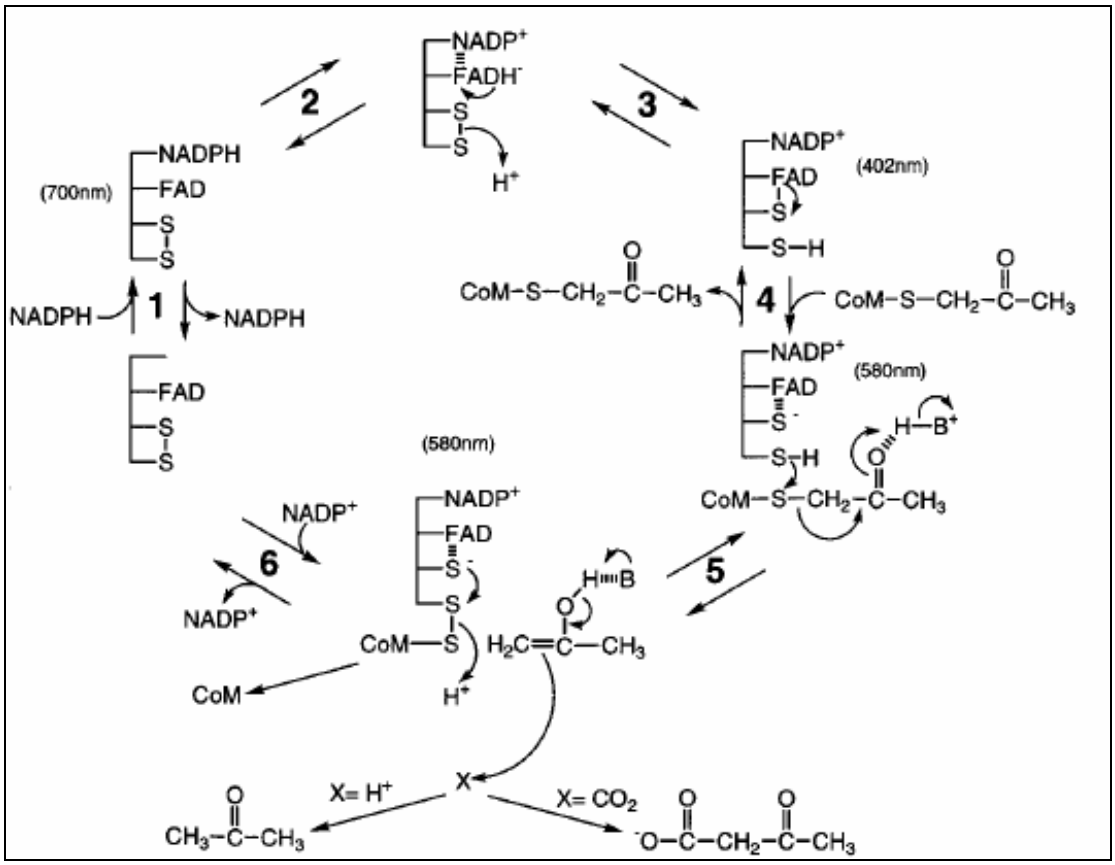

Figure 1.7: The proposed mechanism of 2-KPCC [27]

Each monomer can be divided into three domains, including the FAD binding domain, the NADPH binding domain and the dimerization or interface domain (Figure 1.8) [28]. The three domains make up two interlocked L-shaped monomers having the interface domain of one subunit interacting with both the interface domain and the FAD domain of the opposing subunit. The NADPH and FAD binding domains are oriented such that both nucleotide binding sites are located at the interface of these two nucleotide binding domains.

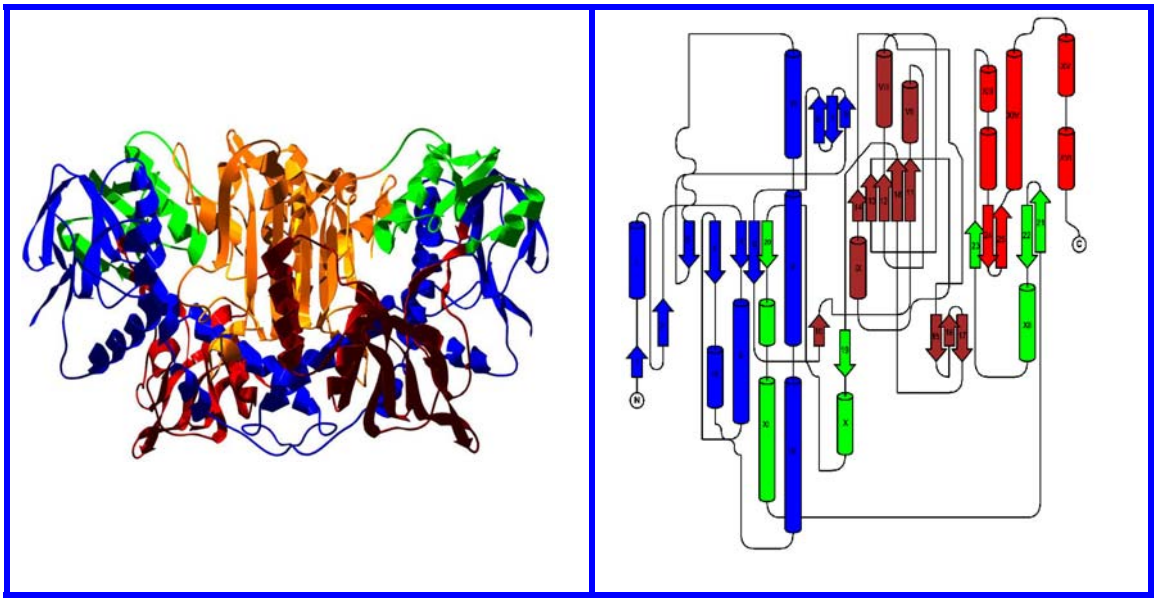

Figure1.8: The crystal structure and topology diagram of 2-KPCC color coded by domain. FAD domain in blue, NADP domain in brown, central domain in green and dimerization domain in orange

Substrate Binding Cleft: Substrate access in the other dimeric members of the DSOR family is defined by a large open cleft that separates the FAD domain of one monomer of the dimer and the interface domain of the other monomer of the dimer. The redox active disulfide is located at the base of the cleft . For a majority of the enzymes of the DSOR family, the reaction path involves reductive cleavage and protonation of the substrate with protons presumably supplied from the bulk solvent. An open cleft allows easy access for substrate binding and release, providing a continuous source of protons from the bulk solvent. Access to the substrate binding site of 2-KPCC is distinct from all other members of the family. In comparison to other members of the family, 2-KPCC has notable differences at the N – terminus and a 13-amino acid long stretch of residues within the interface domain. These regions occur as parts of the walls of the substrate binding cleft of 2-KPCC and move considerably on substrate binding (Figure 1.9). The

N-terminal region which forms one of the peripheral β -strands of the central β- sheet of the FAD domain and an α helix contacts the insertion within the interface domain, effectively blocking the large cleft observed in the other dimeric members of the family.

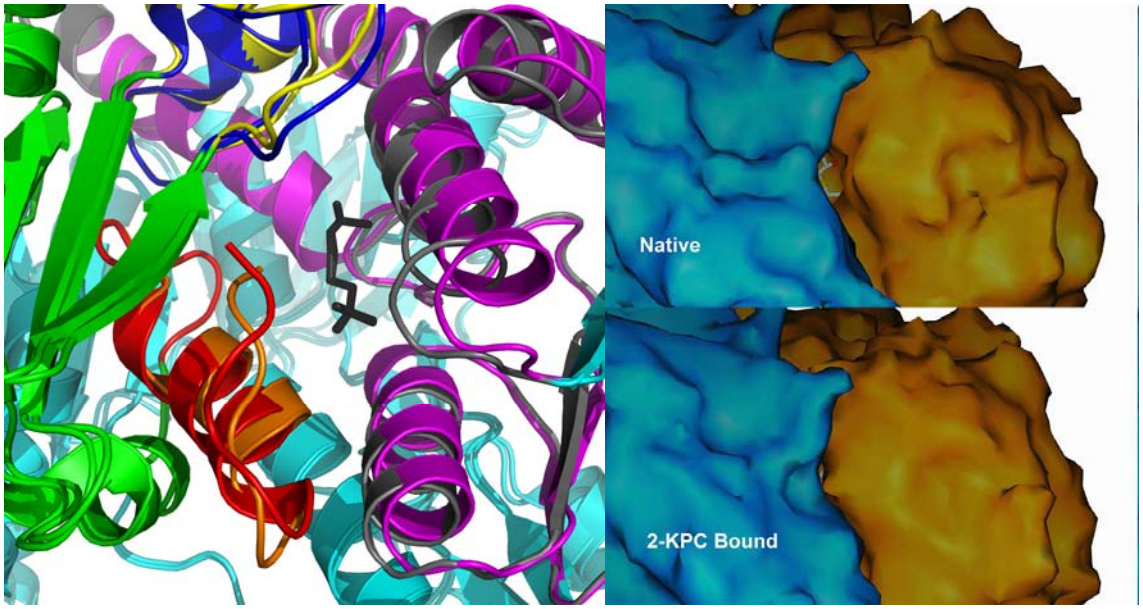

Figure1.9: Movement of the N- and C-terminii and the proline flanked insertion loop on substrate binding Left: Superposition of the C α atoms of the substrate bound 2-KPCC on native 2-KPCC.. N- and C-terminii and loop in the ligand free enzyme are shown in magenta, red and blue respectively. The same are shown in gray, orange and yellow in the substrate bound enzyme. Right: Surface rendering of 2-KPCC showing the view from the exterior of the molecule. The substrate binding cleft between the two monomers closes on substrate binding

Interestingly, the inserted region is flanked by two *cis*-proline residues (Pro420 and Pro432) which approach each other very closely. In the substrate bound form, 2-ketopropyl CoM is virtually buried within the protein such that a substrate accesss channnel is not discernible. Access to the substrate binding site is limited to a narrow hydrophobic channel.

Substrate Binding Site: The substrate is bound by specific interactions with CoM. The sulfonate moiety of CoM is bound by two Arg side chains (Arg 56 and Arg365) which approach from the sides and interact directly with additional side chain and main chain atoms through hydrogen bonding (Figure 1.10). The Arg side chains approach from the sides and an adjacent phenyalanine side chain (Phe 57) acts as a "backstop" preventing further translation of the substrate and thus allowing proper alignment of the thioether linkage with respect to the enzyme disulfide for reductive cleavage. Reductive cleavage occurs when NADPH initiates the reduction pathway through direct hydride transfer to the isoalloxazine ring of FAD. The binding site for NADPH is a large cleft at the interface between the nucleotide binding domains. Although NADPH was not present in this structure, the docking of NADPH into its binding site requires very little repositioning of amino acid side chains. The nicotinamide must be in close contact with the isoalloxazine moiety of FAD for direct hydride transfer from the C4 position of the nicotinamide ring to the N5 position of the isoalloxazine. The active site Cys82 and Cys87 residues form a disulfide bond.

Hydride transfer to FAD results in reduction of the enzyme disulfide via the presumed formation of a covalent adduct between the isoalloxazine ring at the C4A positon and the proximal thiol of the reduced disulfide, by analogy to other members of the DSOR family [29]. The resulting free thiol is then available for substrate thioether cleavage. The structure reveals a linear reduction pathway, and the modulation between oxidation and reduction of the redox active disulfide only requires changes in the conformation of the side chains of the active site Cys residues. In this regard, the interchange thiol can be placed within binding distance of the S of the substrate.

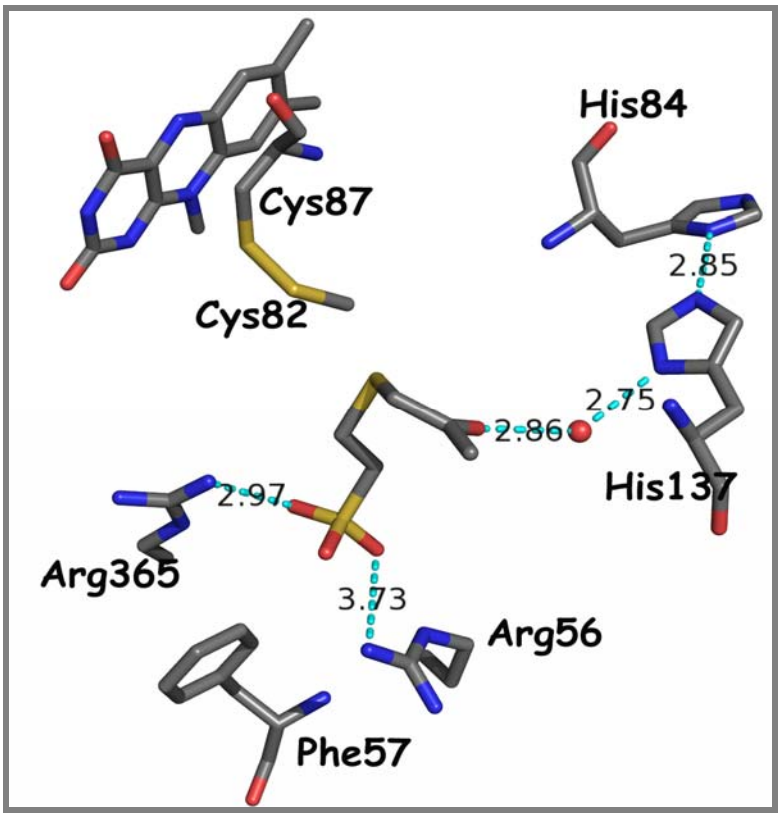

Figure 1.10: Substrate binding and stabilization, 2-ketopropyl CoM showing the interactions of sulfonate moiety of 2-ketopropyl coenzyme M with Arg365 and Arg56. A lone water molecule stabilized by His137 and His84 hydrogen bonds to the carbonyl group of 2-ketopropyl coenzyme M and has been proposed to stabilize the enolate intermediate during catalysis.

Stabilization of an Enolate Intermediate : In contrast to the specific side chain interactions observed for the substrate CoM moiety, the ketopropyl moiety is observed to have limited interactions with the protein (Figure 1.11). It was hypothesized that the presence of a hydrogen bond donor near the keto group of the substrate could serve to stabilize an enolate intermediate, facilitating the reductive cleavage of the thioether linkage analogous to bound Mg^{2+} observed in Rubisco [73]. Although the electron density is not unambiguous with respect to the positioning of the ketopropyl moiety of the

substrate, the best fit places the keto group of the substrate within hydrogen bonding distance of an ordered water molecule that is oriented by hydrogen bonding interactions with the peptide bond carbonyl of Leu78 and a side chain imidazole nitrogen of His137. The side chain of His137 is in turn oriented in its proper position by a specific interaction with the adjacent His84 (Figure 1.10). The His-oriented water molecule could conceivably act as a proton donor for reaction with an enolacetone intermediate analogous to the enediol intermediate of ribulose 1,5-bisphosphate in Rubisco [73]. The enolacetone intermediate provides an appropriate nucleophile for attack on the electrophilic carbon dioxide. The water molecule could also act in the stabilization of the intermediate as a hydrogen bond acceptor, serving a role analogous to that of Mg^{2+} in Rubisco. Since Mg^{2+} ion is isoelectronic with water, the assignment of water at this position is based on the coordination environment of this atom since the interaction of a His side chain nitrogen and a single peptide bond carbonyl would be an atypical coordination environment for Mg^{2+} ion. In addition, the results of previous biochemical studies indicate that Mg^{2+} is not required for 2-KPCC-catalyzed carboxylation, and its addition in enzyme assays does not stimulate activity (J. R. Allen and S. A.Ensign, unpublished results). With the exception of the bound water molecule possibly involved in enolacetone formation and stabilization, the remaining environment of the ketopropyl moiety of the substrate is distinctly hydrophobic (Figure 1.11). The interactions of the keto group with the His-bound water molecule serve to orient the methylene group which undergoes carboxylation toward the hydrophobic cavity.

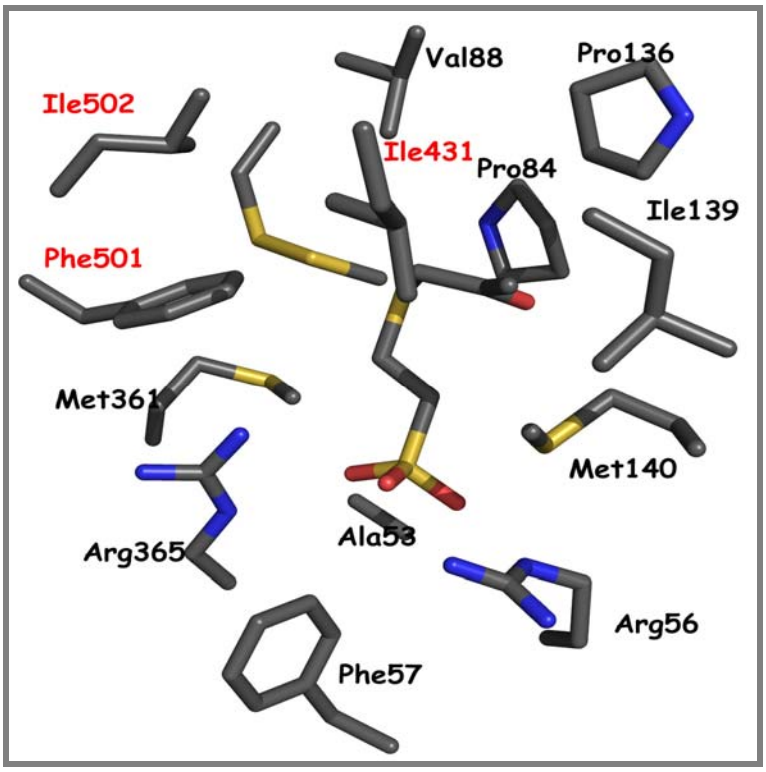

Figure 1.11: Protein environment of 2-ketopropylCoM. Residues contributed by the other subunit are labeled in red

This water molecule is more than 5 Å from the methylene group of the ketopropyl moiety of the substrate and fixed in position by a hydrogen bonding interaction with both the His side chain, a peptide carbonyl, and the substrate keto group, perhaps making it an unlikely candidate as a proton donor for the reaction that would lead to acetone formation. Among these hydrophobic residues are two methionine residues which flank the CoM moiety of the substrate and act to shield the carboxylation site from the sulfonate moiety. An additional *cis*-amino acid conformation (Leu502) is observed in the substrate binding region, which allows the side chains of two hydrophobic residues, Phe501 and Leu502, to be oriented toward the substrate. Along these lines, a hallmark of

other members of the DSOR family is the presence of a His side chain in the proximity of the interchange thiol to stabilize the thiol in the reduced state. The His at this position in 2-KPCC has been replaced with the side chain of Phe501, perhaps as an adaptation to eliminate the availability of protons to the reactive methylene group formed upon reductive cleavage.

Substrate-Induced Conformational Change: The distinctly hydrophobic nature of the active site could serve to exclude solvent interactions and thereby limit protonation of the enolate intermediate and formation of the undesired product acetone. The structure of the native enzyme indicates that substrate access in 2-KPCC occurs through a well-defined channel directly opposite the NADPH binding cleft through a channel that is 8 Å long and 5 Å wide leading directly to the active site disulfide. Comparison of the native and substrate-bound forms of the enzyme indicates that substrate binding brings about a conformational change as a likely result of the specific interactions of the CoM moiety of the substrate with the N-terminal region of the protein. The main chain of the helical N-terminal region is displaced 3.0 Å and results in additional conformational changes in the adjacent secondary structure elements within the FAD binding domain. The conformational change results in a collapse of the substrate binding channel, limiting access to the substrate binding site to only a narrow hydrophobic channel (Figure 1.9).

Unanswered Questions

Stabilization of Enolate Intermediate: The kinetic and structural analysis provides a solid foundation for the proposed mechanism of reductive cleavage and subsequent carboxylation of 2-ketopropyl coenzyme M by 2-KPCC. The ambiguity in assigning the carbonyl oxygen atom in the substrate bound structure cannot be overlooked. The ketopropyl group was modeled into the density based on the nature of the surrounding residues and whether the assignment was chemically reasonable. To resolve this, either a higher resolution structure of the KCoM bound form or a structure with a non-hydrolysable substrate analog is required. Since 2-ketopropyl CoM is bound at the active site primarily through interactions of the sulfonate group with Arginine residues, it is conceivable that a non hydrolysable ketopropyl CoM analog with similar binding properties would bind at the active site and because of the enzymes inability to turn it over, would show better occupancy than the substrate itself. This would in turn be expected to provide a clearer picture of the positioning of atoms of the carbonyl group and corroborate / refute the role of the His137 bound water molecule in the stabilization of the enolate intermediate.

Carboxylation: Enzymatic carboxylations often involve a reaction of CO_2 or an enzyme-bound form of CO_2 with a carbanion. Inherently unstable, a carbanion can be stabilized by electron delocalization with an adjacent electron-deficient atom such as a carbonyl or imine carbon [68] . The imine carbon/nitrogen double bond is readily reduced to a secondary amine by agents such as sodium borohydride ($NaBH_4$) and $NaBH_4$ inhibition of an enzyme in the presence of its substrate has been a classical way to detect

Schiff's base formation [74]. Using this technique it has been detemined that 2-KPCC does not employ the formation of a Schiff's base during its carboxylation activity [68]. Also, some acetoacetate decarboxylases are known to utilize a metal ion to stabilize enolate formation by way of accelerating the mechanism [74]. 2-KPCC has been shown to be devoid of metals. Common α-keto acid decarboxylating enzymes accomplish decarboxylation by participation of the cofactor thiamin pyrophosphate (TPP). Neither TPP nor pyridoxal phosphate, cofactors utilized in alpha amino acid decarboxylation reactions, are associated with 2-KPCC [20].

Addition of CoM to the enzyme increases decarboxylation and CO_2 exchange activities of 2-KPCC 77-fold. CoM is postulated to form a mixed disulfide with the proximal redox active cysteine thiol and cause an enhancement in the formation of the carbanion intermediate to which CO_2 can add to form the product acetoacetate. Since it is hard to capture CO_2 alone at the active site, a prudent approach would be to try to get a crystal structure of 2-KPCC with the product acetoacetate bound in the presence as well as absence of CoM. An alternative approach would be to get co-crystals of 2-KPCC with a non hydrolysable analog of acetoacetate in the presence and absence of CoM. It has been shown [68] that modifying the redox active cysteines of 2-KPCC with N-ethylmaleimide (NEM) does not affect the acetoacetate low decarboxylation or CO_2 exchange activity of NADPH reduced 2-KPCC in the absence of CoM. However the acetoacetate decarboxylation rates in the presence of CoM are reduced to <10% when NADPH reduced 2-KPCC has been treated with NEM, showing that the decarboxylation of acetoacetate by 2-KPCC in the presence of CoM is dependent on redox active disulfide. Co-crystal structures of non hydrolysable analogs of acetoacetate in the

oxidized and reduced forms might be expected to shed light on binding modes of acetoacetate and coenzyme M for decarboxylation of the former and formation of 2-ketopropyl CoM as one of the products.

Protonation and Product Release: DSOR members like glutathione reductase, thioredoxin reductase, dihydrolipoyl lipoamide dehydrogenase, all possess a catalytic dyad comprised of a conserved histidine and glutamate residues. The former has been proposed to act as a proton aceeptor from the redox active cysteine residue distal to the substrate binding site and a donor to the S atom of the leaving group. The Glu residue hydrogen bonds to Nε of this His so that it is not allowed to move during the catalytic cycle. In the sequence alignment of 2-KPCC with some well characterized DSORs, a Phe (501) and a His (506) align with the His and Glu residues of the dyad. 2-KPCC differs from the members of the DSOR family in cleaving a C-S bond instead of an S-S linkage, and subsequently carboxylating one of the resulting moieties (ketopropyl) and protonating the other (coenzyme M). However, protonation of both moieties resulting after the C-S bond cleavage does occur in the absence of carbonate species, gaseous CO_2 or HCO_3^-, resulting in the formation of acetone and free coenzyme M [68]. His506 in the substrate bound structure of 2-KPCC is not close enough to the thioether sulfur to be able to protonate it. The Phe residue aligning with the His of the catalytic dyad, on the other hand, has been implicated in providing an environment conducive to preferential carboxylation of the enolacetone intermediate over protonation.

Role of *cis*-proline Flanked Loop: The sequence alignment of 2-KPCC to members of DSOR shows the presence of an insertion region (residues 420-432) in 2-

KPCC, that is flanked by two Cis proline residues. This insertion sticks out as a loop in the substrate bound structure with *cis*-Pro420 and *cis*-Pro432 in close proximity to each other. A structural alignment of 2-KPCC with structurally characterized DSORs shows this region to be a very short linker or a 3_{10} alpha helix in the latter. The role of this loop so far is not clear. The loop lines the subunit interface and is observed to move towards the interface on substrate binding.

Fe-only Hydrogenase from *Clostridium pasteurianum* (*Cp*I)

Background

Hydrogenases, first discovered in 1931 by Stephenson and Stickland in colon bacteria [75] are found in diverse organisms. These include methanogenic, acetogenic, nitrate and sulfate reducing bacteria; anaerobic archaea, rhizobia, protozoa, fungi; and anaerobically adapted algae. These enzymes catalyze the reversible conversion of protons to H_2 gas. They are classified according to their metal content as [NiFe] hydrogenases, [FeFe] hydrogenases [76] and Fe-S-cluster-free hydrogenases [77]. The latter seem to be restricted to methanogenic archaebacteria, whereas the other two types occur in many bacteria. Some bacteria possess [NiFe] enzymes only eg. *E. coli*, *A. aeolicus*, others only Fe enzymes (*T. maritime*). In others yet, both types of hydrogenases coexist within the same cell (genus *Desulfovibrio*). No [FeFe] hydrogenase genes have yet been found in Archaea [76]. Likewise, [NiFe] hydrogenase encoding genes have so far remained undetected in Eukarya. Evidence for the existence of [NiFe] hydrogenases in Eukarya is restricted to biochemical and immunological data on the green alga *S. obliquus* [78-80] unsupported by gene cloning and sequencing. In contrast,

four different [FeFe] hydrogenase sequences from the green algae *S. obliquus* [81]. *C. reinhardtii* and *C. fusca* have been determined. It may therefore be inferred that for the time being, [FeFe] hydrogenases are restricted to bacteria and Eucarya while [NiFe] hydrogenases occur only in Bacteria and Archaea [76]. Both types need accessory proteins for posttranslational processing to yield an active enzyme. [NiFe] hydrogenases depend on the action of six proteins encoded by the *hyp* genes (hydrogeases-pleiotropic genes) and a protease [82]. [FeFe] hydrogenases seem to need only two or three additional proteins encoded by hydE, hydF and hyd G to get active [83]. Sequence comparisons show that hydrogenases are related to other redox proteins and enzymes. Fe-S containing subunits and modules of [FeFe]- and [NiFe] hydrogenases are homologous to soluble ferredoxins and parts of respiratory chain complexes, in particular NADH-ubiquinone oxidoreductases (Complex I) [84-90].

Hydrogenases catalyze the simple reaction:

$$2H^+ + 2e^- \xrightleftharpoons{\text{hydrogenase}} H_2$$

In fermentative bacteria of the clostridial type, the reduction of protons into dihydrogen by hydrogenases is a means of disposing of excess reducing equivalents [91]. Various microorganisms can use H_2 as an electron source either aerobically [92], or anaerobically eg. methanogens [93] [94, 95], the sulfate reducers [96] and the photosynthetic bacteria [97, 98]. These various functions are associated with different cellular localizations eg. hydrogen evolution is most often cytosolic, whereas hydrogen uptake is usually periplasmic or membrane localized [76]. However, cytoplasmic

bidirectional hydrogenases also mediate hydrogen uptake. Some bacteria contain two or more different hydrogenases, localized in different cell compartments. The multiplicity of hydrogenases in such organisms reflects the importance of H_2 in their metabolism and also ensures a rapid and efficient response to variations in energetic needs under changing growth conditions. The distinction between soluble intra- cytoplasmic hydrogenases and membrane-bound hydrogenases is made at the genetic level. The protein to be exported to the periplasm or imported into an organelle is tagged by a signal peptide at the N-terminus.

The [NiFe] hydrogenases are minimally heterodimers composed of a small and a large subunit. The membrane targeted hydrogenases are characterized by the presence of a large signal peptide (30-70 amino acid residues) at the N-terminus of the small subunit [99]. It is inferred that [NiFe] hydrogenases missing this signal peptide remain in the soluble cytoplasmic compartment. [99,100]. A number of [FeFe] hydrogenases are cytosolic and therefore devoid of signal sequences. These include enzymes from C.*pasteurianum*, [101], *Megasphaera elsdenii* [102] as well as the tetrameric NADP-reducing hydrogenase from *Desulfovibrio fructosovorans* [103]. Hydrogenases from anaerobic eukaryotes not containing hydrogenosomes eg. *Entamoeba histolytica* are also cytosolic [104] while the ones containing hydrogenosomes eg. *Trichomonas vaginalis* appear to be located in these organelles. [105] [106]. In the case of dimeric periplasmic [FeFe]-hydrogenases of *Desulfovibrio vulgaris*, the small subunit possesses a tat (twin arginine translocation)-type signal sequence ([107, 108] which is homologous to the C-terminal region of monomeric cytoplasmic hydrogenases . In these enzymes, the large subunit includes a C-terminal extension that is cleaved off post translationally [109, 110].

[NiFe] Hydrogenases

The first Ni-containing hydrogenases were isolated as αβ-heterodimers with large and α and small β subunits having average masses of 60 and 30 kDa respectively [96, 111-113] [86]. The X-ray structure of the [NiFe] hydrogenases from *Desulfovibrio gigas* [114] and *D. vulgaris* [115] showed that the two hydrogenase subunits interact very extensively through a large contact surface and form a globular heterodimer. (Figure 1.2.1). The bimetallic [NiFe] center of the active site is located in the large subunit and is deeply buried inside the protein (figure 1.2.1 C and D). The small subunit contains up to three Fe-S clusters which conduct electrons between the hydrogen activating center and the physiological electron acceptor or donor of hydrogenase. The [4Fe-4S] cluster that is proximal to the active site is 'essential' to H_2 activation in [NiFe] hydrogenases [87, 114, 116]. Hydrophobic channels expanding through both subunits have been identified by crystallographic analysis of xenon binding and molecular dynamics simulations of xenon and H_2 diffusion within the interior of the enzyme [117]. Those channels linking the active site to the surface of the molecule were suggested to facilitate gas access to the active site. Sequence alignments of large subunits of [NiFe] hydrogenases reveal two very conserved regions surrounding the two pairs of cysteine ligands of the [NiFe] site, near the N- and C-terminus of the sequence [111, 112, 118]. All large subunits sequenced have the sequence R-X-C-X-X-C fully conserved in the amino terminal region and the sequence D-P-C-X-X-C fully conserved in the carboxy terminal region. These conserved sequences ligand the Ni atom in the large subunit and form the so called L1 and L2 patterns respectively [119]. These patterns define groups of [NiFe] hydrogenases

which are in good agreement with the groups derived from cellular functions and full sequence alignments. [76].

Group 1: Membrane associated respiratory uptake [NiFe] hydrogenases: This group of [NiFe] hydrogenases transfer electrons from H_2 to a cytochrome that is bound to a membrane located complex coupling electron transfer to transmembrane proton translocation. H_2 oxidation is linked to reduction of various electron acceptors such as O_2, NO_3^-, SO_4^{2-}, fumarate or CO_2. eg. Nitrogen fixing bacteria like *A. vinelandii* [120], *A. chroococcum* [121], *R. capsulatus* [97] and in cyanobacteria [122, 123]. Bacteria of the genus *Desulfovibrio* contain peroplasmic hydrogenases that transfer electrons from H_2 to low potential c-type cytochromes [124-126].

Group2: Cytoplasmic heterodimeric [Ni- Fe] hydrogenases. These include the cyanobacterial uptake hydrogenases [127-129] and the cytoplasmic soluble hydrogenases involving hydrogen sensing [130-132]. They all lack the membrane targeting signal peptide at the N-terminus of the small subunit.

Group3: Cytoplasmic heteromultimeric reversible [NiFe] hydrogenases. These include subunits able to bind a soluble cofactor eg. F420 (methanogenic archaea), NAD or NADP and function reversibly [133, 134].

Group 4: Membrane associated H_2 evolving respiratory hydrogenases. These membrane bound hydrogenases appear to be able to couple the oxidation of a carbonyl group (originating from formate, acetate or carbon monoxide) with the reduction of protons to H_2 [89, 94, 95, 135-139].

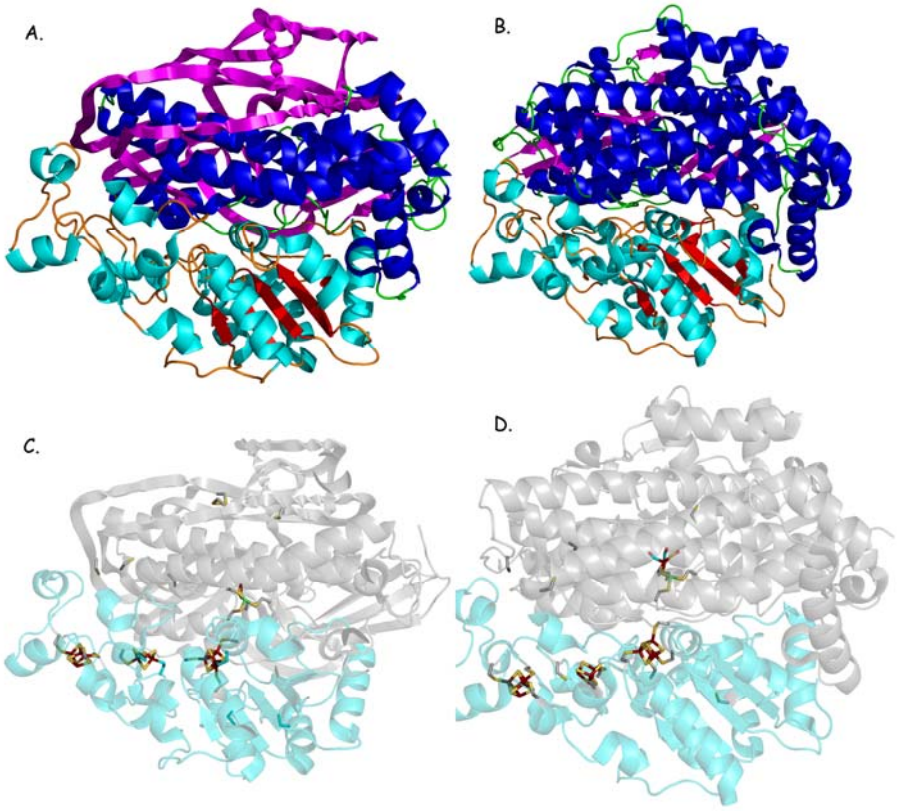

Figure 1.2.1**:** [NiFe] hydrogenases from A: *D. gigas* and B: *D. vulgaris* strain Miyazaki F, showing the dimer with color coded secondary structure (blue helices, magenta sheets and green loops) for large subunit and (cyan helices, red sheets and orange loops) for small subunit. C and D: Localization of the [NiFe] cluster in the large subunit (gray) and [4Fe-4S] clusters in the small subunit (cyan) in *D. gigas* and *D. vulgaris* respectively.

[FeFe]- Hydrogenases

Unlike [NiFe] hydrogenases which are composed of at least two subunits, many Fe-hydrogenases are monomeric and consist of the catalytic subunit only. However, dimeric, trimeric (HydABC hydrogenase from *T. maritima* [140] and tetrameric enzymes (HndABCD from *D. fructosovorans* [103] are also known. A number of Fe hydrogenases are cytosolic and are therefore devoid of signal sequences. These include enzymes from clostridia eg. *C. pasteurianum* (Figure1.2.2) [101] and *M. elsdenii* [102] as well as the tetrameric NADP-reducing hydrogenase from *D. fructosovorans* [103]. Dimeric

periplasmic [FeFe] hydrogenases eg *D. desulfuricans* (Figure 1.2.2), contain a large and small subunit [141].

Sequence and structure comparison have shown that the small subunit of periplasmic [FeFe] hydrogenases is homologous to the C-terminal region of monomeric cytoplasmic hydrogenases. [141]. In these enzymes, the large subunit includes a C-terminus extension that is cleaved off post translationally [109, 110]. The small subunit is a counterpart of the C-terminus of the monomeric enzymes, with regard to sequence as

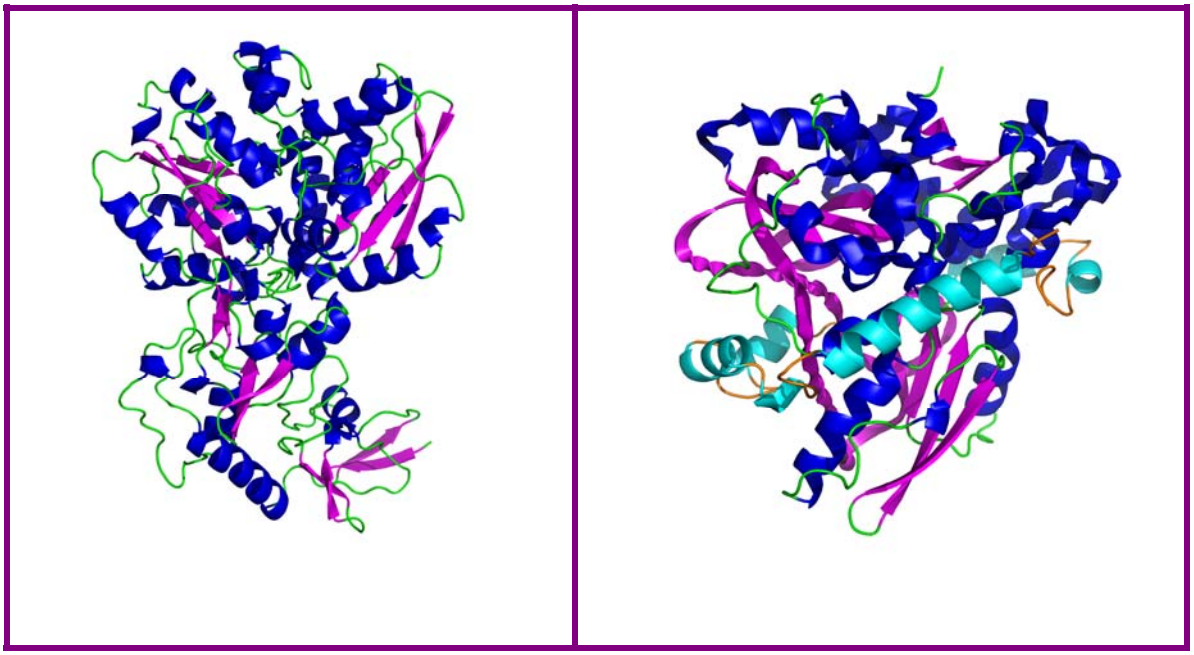

Figure1.2.2: Left: Crystal structure of the Fe-only hydrogenase monomer from *C. pasteurianum*. Right: Fe-only dimer from *D. desulfuricans* . The small subunit is shown in cyan

well as structure; it contains no prosthetic group and wraps around the large subunit [141]. The small subunit also carries the signal sequence allowing export of the whole enzyme to the bacterial periplasm in members of the genus desulfovibrio [107, 108].

Unlike [NiFe] hydrogenases, many [FeFe] hydrogenases are monomeric and consist of the catalytic subunit only. The catalytic subunits of [FeFe] hydrogenases show

considerable variations in size. In addition to a conserved domain of ca. 350 residues containing the active site H-cluster [141-143], they most often comprise additional domains which accommodate Fe-S clusters and which may altogether consist of more than 800 residues.

The conserved domain housing the H-cluster is formed by the C-terminus and is present in all [FeFe] hydrogenases [81], [102]. Many [FeFe] hydrogenases possess an N-terminal domain similar to the 2[4Fe-4S] bacterial ferredoxins eg. two short monomeric *T. vaginalis* hydrogenases [105] and the *M. elsdenii* hydrogenase [102]. The clostridial type [FeFe] hydrogenases are significantly larger [101, 142] and contain three domains in addition to the H-domain: starting from the N-terminus, a [2Fe-2S] plant ferredoxin like domain [143-145], a unique [4Fe-4S] containing fold and a 2[4Fe-4S] domain [143] The catalytic subunit of the tetrameric NADP-reducing hydrogenase from *D. fructosovorans* also has the same size and domain composition as clostridial hydrogenases [103]. The trimeric *T. maritime* hydrogenase is clostridial like but has a C-terminus extension homologous to the NuoE subunit of NADH-ubiquinone oxidoreductases (Complex I) and bacterial thioredoxin-like [2Fe-2S] ferredoxins [146, 147]. The largest catalytic subunit known so far (ca. 130 kDa) is the putative monomeric hydrogenase from the anaerobic eukaryote *Nyctotherus ovalis* [148] which possesses an additional C-terminal domain homologous to the NuoF subunit of Complex I besides all the other domains of *T. maritima* hydrogenase.

The Active Site

The active sites of [FeFe] and [NiFe] hydrogenases share a dimetallic framework and the unique presence of CO and CN as iron ligands [109, 149-151] (Figure 1.2.3). These similarities appear to be requirements of their common catalytic activity [151, 152]. Otherwise, the hydrogenase active sites differ not only in their metal composition but also in their attachment to the protein moiety: the [NiFe] site is bound to the polypeptide chain through the thiolate functions of four cysteine residues [149, 151, 153] while the 2Fe site has only one protein ligand, a cysteine which bridges it to a [4Fe-4S] cluster (Figure 1.2.3). The main characteristics and sequence signatures are highlighted by crystal structures [141, 143] and multiple sequence alignments [76]. The most conserved sequence patterns encompass the cysteine ligands of the H-cluster.

The [NiFe] hydrogenase from *D. gigas*, as aerobically isolated in the inactive form, has been characterized by X-ray crystallography [114, 154]. This shows the active site, where the dihydrogen is converted to protons and electrons, is a dinuclear thiolate-bridged nickel-iron complex. The nickel atom is coordinated by four cysteinate-sulfur atoms, two of which bridge to the iron atom. In the aerobically isolated crystals there is an additional bridging feature, probably oxo- or hydroxo, which is not present in the active form of the enzyme. The other ligands to iron, as shown by crystallography and spectroscopy [114, 154] are diatomic cyanide and carbon monoxide. Several other, similar structures of [NiFe] hydrogenase have been reported [155].

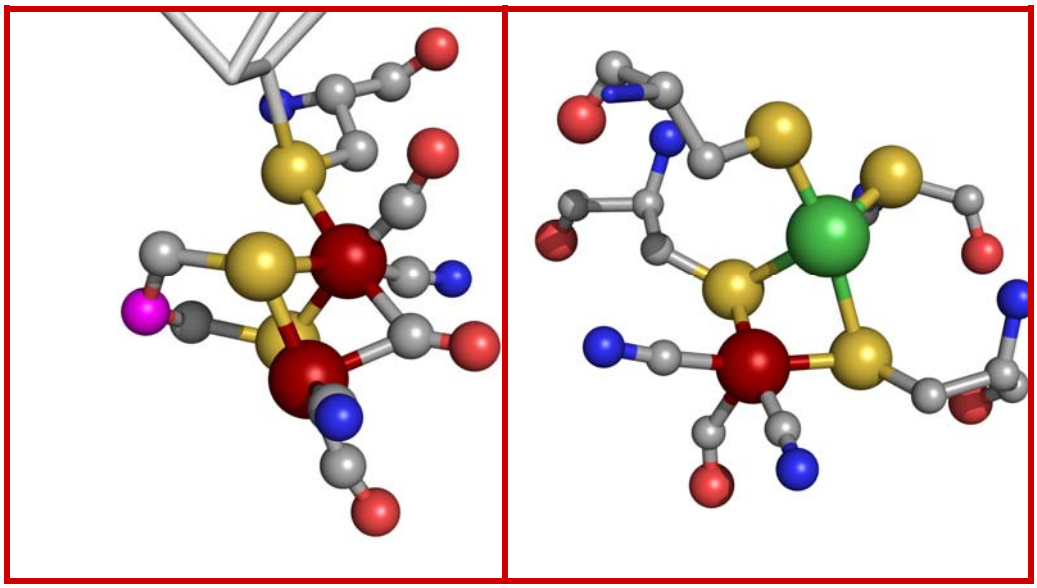

Figure 1.2.3: Left: [2Fe-2S] H-subcluster of Fe-only hydrogenase from *C. pasterianum* . The dithiolate ligand bridging the two Fe atoms is either a propandedithiolate of dithiopropylamine. The unresolved central atom is shown in magenta. Part of the [4Fe-4S] cluster attached to the [2Fe-2S] cluster through a cysteine sulfur is shown in gray sticks. Right: [NiFe] cluster from *D. degigas*, Ni atom is shown in green

X-ray crystallographic structures of the Fe-only hydrogenases from *D.desulfuricans* and *C. pasteurianum* [141, 143] together with spectroscopic data on Fe-only hydrogenase from *D. vulgaris* [156] [157, 158] show that the H-cluster, the active site at which protons are reduced to dihydrogen, is a conventional [4Fe-4S] cluster linked by a bridging cysteinyl sulfur to an organometallic 2Fe subsite.

At the subsite a terminal carbon monoxide, a bridging carbon monoxide and a cyanide ligand are bound at each iron atom which also share two bridging sulfur ligands of a 1,3 propanedithiolate or possibly the related di(thiomethy)amine unit. The Fe atom distal to the [4Fe-4S] cluster has a coordinated water molecule in the resting paramagnetic oxidized state of the enzyme, [Hox]. This site is occupied by carbon monoxide in the CO inhibited form of the enzyme [Hox(CO)] and is therefore thought to be where hydride / dihydrogen is bound during turnover.

Crystal Structure of Fe-only Hydrogenase
from *Clostridium pasteurianum* (*Cp*I)

The crystal structure of the Fe-only hydrogenase from *C. pasteurianum* was determined by MAD phasing in 1998. [143]. The overall structure of *Cp*I was found to resemble a mushroom with a large cap connected to a stem (Figure 1.2.4). The H-cluster and four accessory clusters are housed within four domains, the largest of which (res. 210-574) forms the mushroom cap and houses the H-cluster. The domain directly interacting with the active site domain contains two clusters of the [4Fe-4S] type, designated FS4A and FS4B. FS4A is ~9Å from the active site H-cluster while FS4B is ~10 Å away from FS4A, suggesting an in-line electron pathway from FS4B to FS4A to H-cluster. A histidine coordinated [4Fe-4S] cluster (FS4C) and a [2Fe-2S] cluster (FS2) are present ~8 Å and 11 Å away from FS4B respectively in the remaining two domains. The domains housing FS4 (A, B &C) and FS2 clusters together form the stem of the overall mushroom like structure of *Cp*I.

The presence of the [2Fe-2S] cluster (FS2) in *Cp*I independent of the active-site cluster was indicated from the results of resonance Raman studies [159, 160]. A sequence comparison of this domain reveals considerable sequence similarity to a number of [2Fe-2S] ferredoxins, including arrangement of cysteine residues involved in the coordination of the [2Fe-2S] cluster [143]. The conservation in sequence translates into conservation of overall fold of this domain which is very similar to the [2Fe-2S] domain from eg. *Chlorella fusca* (PDB code 1AWD) (Figure 1.2.5, Top). The FS4A-FS4B domain contains two [4Fe-4S] clusters, each coordinated by four cysteines.

The sequence and hence secondary structure for this domain shows similarities to a number of ferredoxins containing two [4Fe-4S] clusters eg. ferredoxin from *C. vinosum* (PDB code 1BLU) [161] (Figure 1.2.5, Bottom), including a distinctive arrangement of cysteine residues with two sets of Cys-X-X-Cys-X-X-Cys-X-X-X-Cys sequences.

The FS4C domain binds a single [4Fe-4S] cluster coordinated through three cysteines and a histidine (Figure 1.2.6). Histidine ligation of a [4Fe-4S] cluster has been observed in the structure of [NiFe] hydrogenase from *D. gigas* [111]. The site of binding to Fe on this His is Nε, which is in contrast to known examples of His ligands to an [Fe-S] cluster where the Nδ is the coordinating atom. Histidine ligation has been observed in [2Fe-2S] containing Rieske proteins, which have higher midpoint potentials that that of the similar [2Fe-2S] clusters that are coordinated exclusively by cysteine ligands [162]. This suggests that a role of the single histidine ligand in the [4Fe-4S] cluster of the FS4C domain may be to tune the midpoint potential to accommodate an appropriate electron donor. However, experimental evidence suggests that the midpoint potentials of all accessory cluster of *Cp*I are equivalent at -420mV [163]. The effects of mutation of one of the cysteines ligating the [4Fe-4S] cluster of the DNA repair enzyme, MutY, have been studied. [164]. A C199H mutant form showed catalytic activity similar to that of the wild type and could be crystallized. It was noted that the occupancy of the His199 coordinated iron was reduced to 60% suggesting the presence of some [3Fe-4S] cluster which was also confirmed by EPR studies. It has also been shown for *C. pasteurianum* ferredoxin that while oxidation of the [4Fe-4S] cluster is relatively easy, the resulting 3Fe form was stable and resistant to further oxidation suggesting that this conversion might

help protect the enzyme activity in the presence of a highly oxidizing environment [165]. [3Fe-3S] clusters have also been found in variants of *Bacillus thermoproteolyticus* ferredoxin, with the x-ray structure showing that their 3Fe-3S cluster geometry is virtually indistinguishable from the [4Fe-4S] geometry [166]. Some Fe-S proteins are known to bind clusters of either the [3Fe-4S] or [4Fe-4S] type, and interconversion between these types of clusters has been extensively studied for several ferredoxins such as *Pyrococcus furiosus* Fd, Fd III from *Desufovibrio africanus* and DgFd [166] These ferredoxins, isolated in the [3Fe-4S] form, when subjected to reduction and addition of Fe^{2+} use an aspartate as a fourth ligand to form [4Fe-4S] clusters, which revert to 3Fe forms upon exposure to oxygen [167]. Replacement of this Asp with Cys by site directed mutagenesis results in a stable [4Fe-4S] cluster that can no longer be easily converted to [3Fe-4S]. This suggests that the His coordinated cluster in *Cp*I might be able to convert to 3Fe form. The domain binding this [4Fe-4S] cluster in *Cp*I, however, does not show structural similarity to the physiologically His-coordinated [4Fe-4S] domain of [NiFe] hydrogenase form *D. gigas*.

Both *Cp*I and *Dd*ase dislay extensive structural similarities at the H- and [4Fe-4S]- cluster domains [109, 141, 143] although their relative orientations are not the same in the two enzymes. The H-domain in *Cp*I is topologically equivalent to both the large and small subunit of DdH [109]. The fold of the active site domain consists of two four stranded twisted β-sheets, each flanked by a number of α-helices that appear to be two nearly equivalent lobes. The H-cluster provides a site of covalent attachment between the two lobes. The region of attachment exhibits a high degree of conservation in sequence

alignments of known Fe-only hydrogenases and putative Fe-only hydrogenases [168] [103, 108, 169-171].

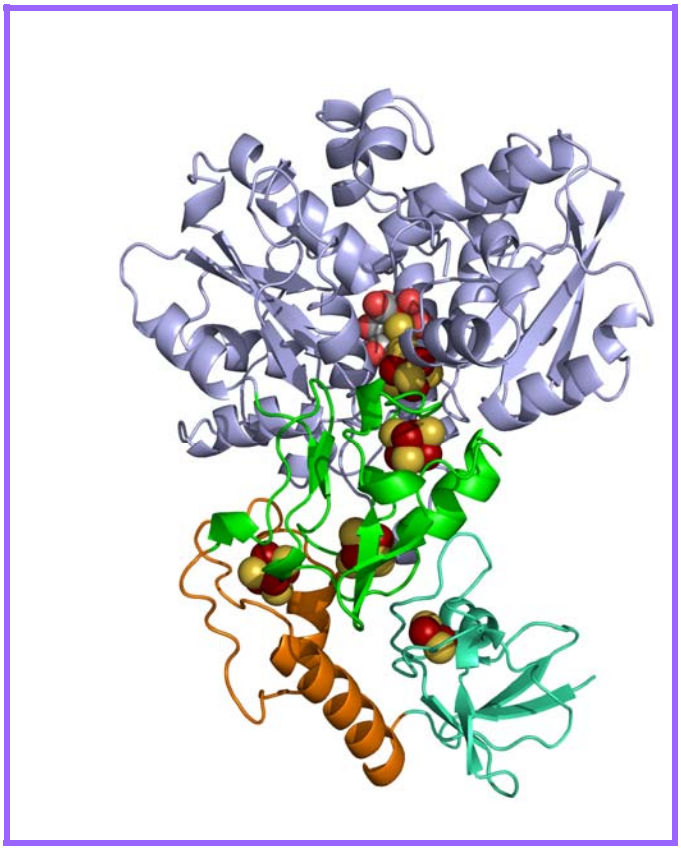

Figure1.2.4: Crystal structure of Fe-only hydrogenase from *C. pasteurianum* showing Fe-S clusters as spheres, the H-domain (mauve), FS4A-FS4B domain(green), FSH domain (orange) and FS2 domain (cyan).

The H-cluster: The H-cluster contains six Fe atoms arranged as a [4Fe-4S] subcluster bridged to a [2Fe] subcluster by a single cysteinyl S [143] (Figure 1.2.7). The [4Fe-4S] cluster is coordinated to the protein through four cysteines, one of which acts as the bridge to the other subcluster. The 2Fe cluster consists of two octahedrally liganded Fe atoms that together contain five CO/CN ligands, three S ligands, (one of which is

cysteine S), and one H_2O ligand. This water is not present in the Ddase H-cluster. Each of the irons of the 2Fe subcluster is bridged to the other by two S atoms and one CO/CN

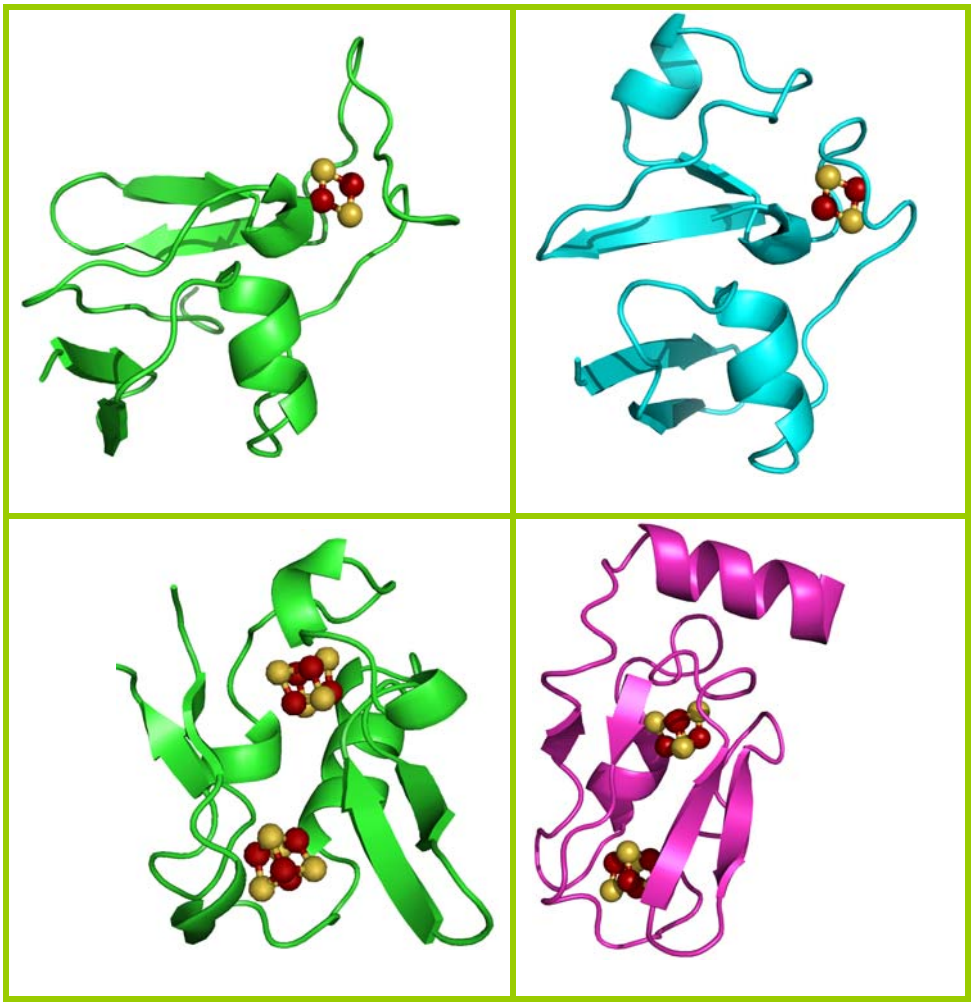

Figure 1.2.5**:** Top-The [2Fe-2S] domains of CpI (green) and ferredoxin from *C. fusca* (cyan). Bottom: The 2[4Fe-4S] domain of CpI (green) and *Chromatium vinosum* (magenta)

molecule. The sulfur atoms are bridged with each other through a dithiolate moiety thought to be either a propane dithiolate or dithiodimethylamine.

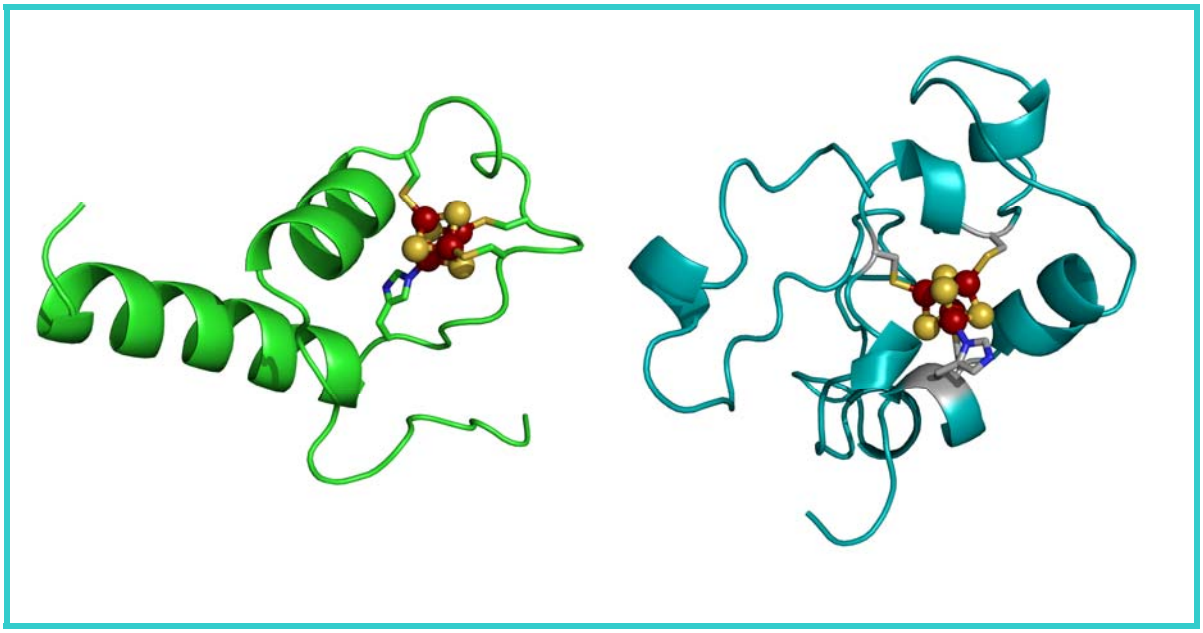

Figure1.2.6**:** The domain housing the His-coordinated [4Fe-4S] cluster in CpI (left) and [NiFe] hydrogenase from *D. gigas*

The [4Fe-4S] cluster of the active site is ligated to the protein through Cys300, Cys355, Cys499 and Cys503, which also bridges it to the [2Fe-2S] subcluster (Figure 1.2.7). The linkage of a [4Fe-4S] cluster to another metal containing prosthetic group is reminiscent of a sulfite reductase, where a [4Fe-4S] cluster is bridged to the Fe of a seroheme in a similar manner [172]. In addition to the four covalent cysteinyl ligands, there are a number of additional residues that define the active-site environment (Figure 1.2.8). Two Met residues, Met353 and Met497 are located near the H-cluster. Both of these Met residues are conserved within the sequence when compared to the other known Fe-only hydrogenases [103, 168-171]. The sulfur atom of Met497 is ~3.4 Å away from the atoms connecting the two bridging sulfur atoms of the 2Fe subcluster. The Met353 sulfur atom is ~3.2 Å from the CO/CN that bridges Fe1 and Fe2. Other amino acid side

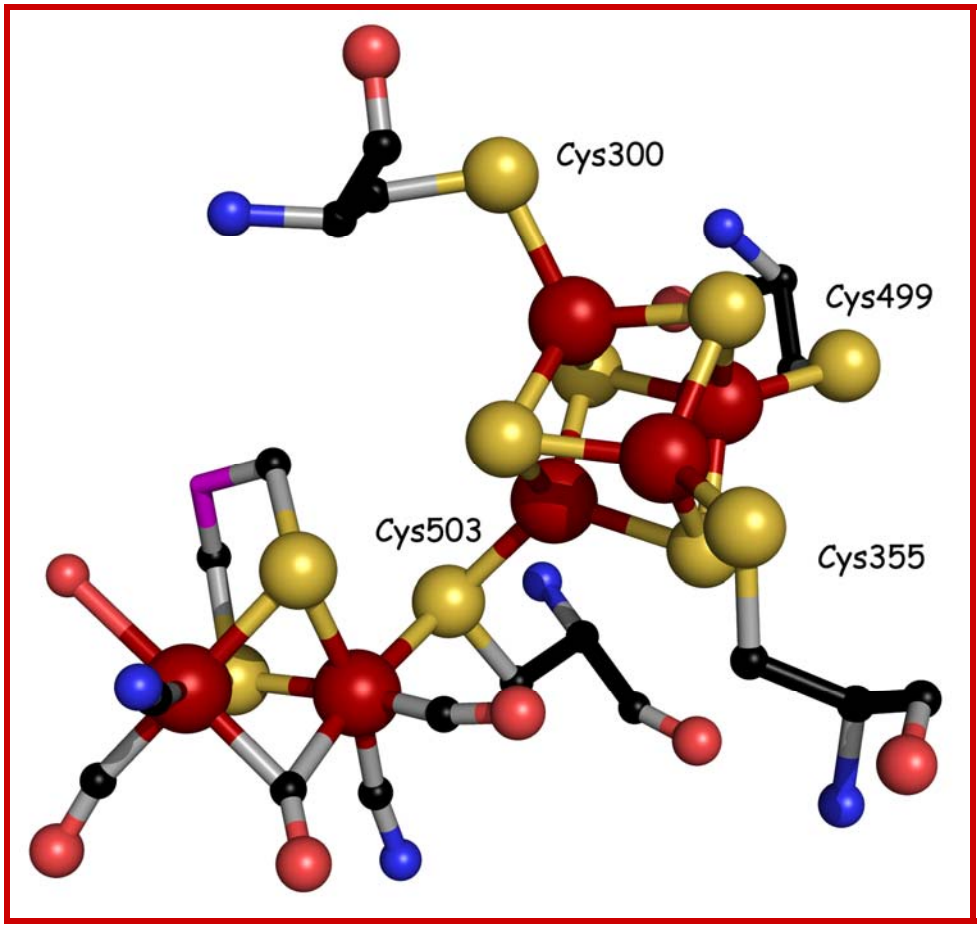

Figure1.2.7: The H-cluster of *Cp*I. The [4Fe-4S] cluster is coordinated to four cysteines from the protein, one of which serves to attach it to the [2Fe-2S] subcluster. The unknown atom of the bridging ligand is shown in magenta.

chains in close proximity to the terminal CO/CN ligands include Nε of Lys358 and Oγ of Ser232, both ~2.9 Å away from these ligands. The adjacent Pro231 is one of a number of hydrophobic residues that surround Fe2, potentially protecting the cluster from solvent access and regulating the availability of substrates such as protons. Additional hydrophobic residues in the polypeptide environment of Fe2 include Ile268, Ala272,

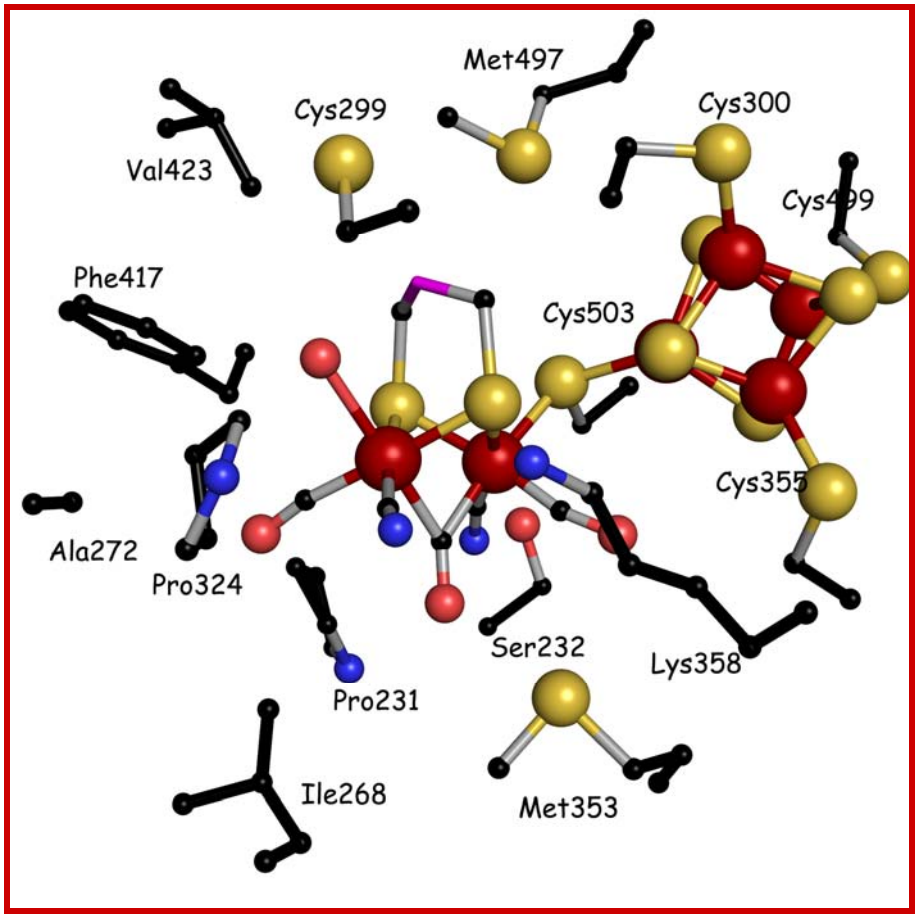

Figure 1.2.8: The protein environment around H-cluster of *Cp*I

Pro324, Phe417 and Val423. The peptide bond carbonyl of Phe417 is ~3.4 Å from one of the bridging sulfurs of the [FeFe] subcluster. The other bridging sulfur atom in the subcluster is in close proximity to the peptide bind carbonyl of Cys299. A free cysteinyl residue (Cys299) is ~ 5Å from Fe2 of the 2Fe subcluster and ~3 Å from the terminally bound water molecule.

Proton Reduction by *Cp*I: The location of the free cysteine residue, Cys299, with respect to the cluster bound water is suggestive of a potential mechanism of proton reduction catalyzed by *Cp*I [143]. An important function of this amino acid is supported

by the strict conservation of a comparable Cys in the sequences of all known Fe-only hydrogenases [103, 168-171].

Although the purification and crystallization of *Cp*I was accomplished in the presence of reductant, it was likely to be consumed over the course of the period of crystal growth. If this were indeed the case, the enzyme could be in an oxidized state. With the exception of the terminally bound water molecule, the remaining CO/CN and S ligands should be very strong ligands. If we are indeed examining the oxidized state of *Cp*I, a reasonable mechanism for proton reduction at this active site might be the displacement of the terminal water ligand bound to Fe2 upon reduction, with the subsequent generation of an Fe-hydride intermediate. Cys299 could act as a proton donor for the formation of dihydrogen. The pKa of free Cys (~8.0) would allow this residue to act as a general acid/base near physiological pH values. Such a mechanism would be consistent with the heterolytic cleavage of hydrogen inferred from isotopic studies [91]. CpI has been shown to undergo irreversible inactivation in the presence of CO [142, 163, 173, 174]. It is easy to envision that the binding of CO displaces the terminally bound water molecule of Fe2, and this would result in the inhibition of proton reduction by the mechanism proposed above.

A potential pathway for proton transfer exists from Cys299 12 Å to the protein surface, involving two Glu residues, a serine and a water molecule [143]. There are no free cysteines in close proximity to the active site of the *D. gigas* [NiFe] hydrogenase; in contrast there are number of His residues in the active-site environment, presumably acting as proton acceptors [114]. This difference in the two active-site environments may support the preference in the direction in which they catalyze reversible hydrogen

oxidation physiologically. Additionally, Ni at the active site may also contribute to the preference for hydrogen activation over hydrogen evolution in Ni-containing hydrogenases [111].

Carbon Monoxide Inhibition of *Cp*I: Although multiple carbon monoxide molecules serve as ligands to the 2Fe cluster, additional carbon monoxide has been shown to bind to *Cp*I both in a manner that results in the inhibition of reversible hydrogen oxidation and in a manner that does not [91, 142, 163, 174-176]. When carbon monoxide is added to the enzyme at high concentrations under turnover conditions, it results in complete and irreversible inhibition in a state of the enzyme that has not been characterized by spectroscopic methods. A site for the binding of exogenously added carbon monoxide was identified at the active site of *Cp*I crystallographically [176]. Carbon monoxide was shown to bind at the site of the terminally bound water molecule in the as crystallized native state of the *Cp*I that had been suggested to be the potential site of reversible hydrogen oxidation. Carbon monoxide binding and inhibition were also investigated by EPR in solution and crystal forms of *Cp*I [177]. The EPR spectrum of *Cp*I solution on addition of carbon monoxide in the presence of dithionite resulted in the inhibition of hydrogen evolution activity and a characteristic axial EPR signal (geff (1), geff (2) and geff (3)= 2.0725, 2.0061 and 2.0061 respectively). Hydrogen evolution activity was restored by successive sparging with hydrogen and argon and resulted in samples that exhibited the native oxidized EPR signature that could be converted to the reduced form upon addtion of sodium dithionite and hydrogen. EPR spectra of *Cp*I crystals in CO-bound state exhibit the same axial signal associated with CO binding that

was indistinguishable from that observed in frozen solution showing that the crystallographically characterized species corresponded to an inhibited species of *Cp*I containing a single molecule of reversibly bound to the H-cluster.

Oxidation states of the 2Fe H-subcluster are believed to be FeII-FeII (oxidized, active, EPR silent), FeII-FeI (oxidized, active, EPR active) and FeI-FeI (reduced, active and EPR silent) [64]. In the EPR active state [Hox], the proximal iron atom is almost certainly diamagnetic FeII because only weak magnetic coupling of the paramagnetic [4Fe4S] cluster is observed [178]. Thus the spin density in the sub-site resides on the distal Fe atom. The question is whether this metal atom has a formal oxidation state of FeIII or is in a biologically unprecedented FeI state [151]. It has been argued on the basis of Mossbauer data that the distal iron is in a conventional FeIII state, however FeI could not be excluded. On the other hand, FTIR ^{13}CO labeling studies of the enzyme by De Lacey and co workers strongly supports an FeI oxidation state for the distal iron center in [Hox(CO)] because the uncoupled v(CO) stretch at this center is lower in energy that that for the CO bound at the proximal FeII site [157]. Clear support for an [FeI distal-FeII] arrangement comes from studies of synthetic [2Fe-3S] systems [179] and from DFT calculations [180]. Whether the bridging dithiolate at the sub-site is 1,3 propanedithiolate or a di(thiomethyl)amine unit is still an open question. Re-anlaysis of the first structures of the Fe-only hydrogenases marginally favoured the latter ligand and led to the speculation that the amine group could function in proton delivery to the active site [109].

FTIR studies of *Cp*I have indicated that the bridging CO of [Hox] becomes terminally bound on reduction [157]. The mechanistic implications of this may be related to the exposure of a proton binding site at the distal iron when CO adopts the bridging

mode, with subsequent elimination of dihydrogen driven by rearrangement to a terminal CO bonding mode with concomitant metal-metal bond formatioin [151]. This mechanism invokes formation of terminal hydride/dihydrogen intermediates. Such intermediates remain spectroscopically undetected in the enzymic system although indirect evidence for the development of hydrides in biological system come from studies of H^+/D_2 exchange reactions [181].

Bridging or Terminal Hydride?: Synthetic tertiary phosphine di-iron dithiolate assemblies possessing a bridging hydride have been characterized crystallographically and are shown to be capable of catalyzing the H^+/D_2 exchange process [181]. Infrared studies have demonstrated that the irradiation of the CO-inhibited form results in two products, depending on temperature [182]. At temperatures above 150K, the exogenous CO dissociates and the structure otherwise remains intact, whereas below 80K, it is bridging CO that dissociates, either completely, or remaining bound only to the distal Fe. This implies that H_2 may bind to the proximal Fe, at a site that is made available by the bridge cleavage [64]. Although synthetic models of the type $[Fe_2(SR)_2(\mu\text{-}H)L_2(CO)_4]^z$ produce H_2 by electrocatalytic reduction of protons (L=CN-, PMe_3) [183-185] , Fe2(μ-H)

species [186] exhibit no inherent reactivity toward protons. Biophysical studies strongly implicate the role for a hydride at the axial site on distal Fe, such terminal hydrides are expected to be more hydridic than the isomeric bridging hydrides [187]. Diferrous species bearing a terminal hydride ligand was first reported by Vlugt and coworkers in 2005 [188]. Spectroscopic and crystallographic analyses of the complex [Fe2(edt)(μ-CO)(H)(CO)-(PMe_3)4]PF_6([α1HPF_6]) support the assignment of a terminal hydride trans

to the Fe-Fe vector . This along with the presence of the semibridging CO ligand matches with the crystallographic data from the Hred form of the Fe-only hydrogenase from *D. desulfuricans*. Characterization of the simplest known functional model of the [FeFe] subcluster, $Fe_2(S_2C_3H_6)(CO)_6$ capable of catalyzing proton reduction [185, 189] also supports the formation of a terminal hydride.

MECHANISTIC IMPLICATIONS OF THE STRUCTURES OF THE MIXED DISULFIDE INTERMEDIATE AND COENZYME M DISULFIDE BOUND 2-KPCC

Introduction

The NADPH:2-Ketopropyl-CoM carboxylase/oxidoreductase (2-KPCC) catalyzes the reductive cleavage and carboxylation of 2-ketopropyl-CoM (KCoM) to produce acetoacetate and free CoM [27, 68] as shown in Equation 1:

2-ketopropyl-CoM + NADPH + CO_2 → acetoacetate + $NADP^+$ + CoM ..... Eq. 1

This reaction is the final step in a bacterial pathway by which aliphatic epoxides such as epoxypropane are converted to beta-ketoacids for entry into central metabolic pathways [20, 22, 70, 190].

The stoichiometry of this reaction, and the molecular properties of KCoM, reveal a fundamentally new type of chemistry and associated mechanism for the carboxylation of an organic substrate, without precedent for all other known carboxylases [3, 191-193]. The biochemical [20, 22, 26, 68] and structural [71] features of 2-KPCC have shown that the enzyme is a member of the DSOR family of enzymes (Fig 2.1 A) [41] , which includes such well-characterized enzymes as glutathione reductase [33] [31, 35]and dihydrolipoamide dehydrogenase [194]. Mechanistic studies of 2-KPCC have provided evidence that the cleavage of 2-ketopropyl-CoM is facilitated by attack of the distal (interchange) thiol (Cys82) on the thioether bond of KCoM, forming a mixed disulfide of CoM and Cys82 as shown in Figure 2.1 B [68] . The other product of thioether bond cleavage, enolacetone, is subsequently carboxylated to form the product acetoacetate.

The mixed disulfide of CoM and Cys82 is then reduced by formation of a disulfide between Cys82 and the flavin thiol Cys87. NADPH then reduces the disulfide bond between Cys82 and Cys87 via flavin mediation as observed for other DSOR enzymes [195]. At present, 2-KPCC is the only known member of the DSOR family to catalyze thioether bond cleavage and organic substrate carboxylation.

A. B.

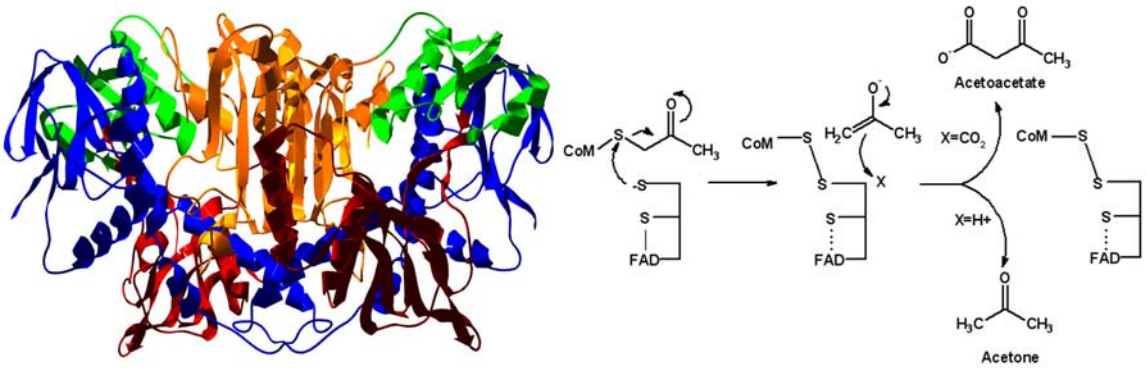

Figure 2.1. A. Ribbons representation of the homodimeric 2-KPCC (PDB code 1MO9) showing FAD-binding (brown), NADP binding (blue), central (green) and interface (orange) domains. B. Summary of 2-KPCC catalyzed acetoacetate and acetone formation both occurring via the formation of a mixed-disulfide and stable enolate intermediate

The three-dimensional structure of 2-KPCC has been solved by x-ray crystallography, both in the absence and presence of the substrate KCoM [71]. Relative to other DSOR enzymes, 2-KPCC has an extended N-terminus and a 13 amino acid insertion within the interface domain that effectively eliminates the larger cleft providing access to the active site for other members of this family. In the substrate-bound form, KCoM is oriented in the active site such that there is a linear pathway for electron pair

transfer between FAD, the redox active disulfide, and the thioether bond of the substrate. The sulfonate of 2-ketopropyl-CoM forms a salt bridge with two specific Arg residues. The carbonyl of the substrate is located within hydrogen bonding distance of an ordered water molecule that might donate a proton for stabilization of enolacetone. The remainder of the active site environment is largely hydrophobic. Together, these unique features of the 2-KPCC active site are believed to facilitate the sequestration of enolacetone to promote carboxylation rather than protonation, an undesirable side reaction producing acetone as a dead-end product.

In order to shed further light on the mechanism of 2-KPCC, we have, in the present work, established conditions for crystallizing the enzyme in a state where the mixed disulfide between CoM and Cys82 can be directly visualized, thereby providing direct evidence for the existence of this novel intermediate in the reaction pathway. Along with structural studies of a CoM-bound form of the enzyme, these studies provide new insights into the mechanism of thioether bond cleavage and substrate carboxylation catalyzed by this atypical member of the DSOR family.

Experimental Procedures

Xanthobacter autotrophicus (strain Py2) cells were grown as previously described [69] and 2-KPCC purified according to the method described previously [20]. Initial attempts at obtaining crystals of the mixed disulfide state of 2-KPCC using the previously characterized crystals used to determine the substrate bound state by the addition of reductant prior to data collection were unsuccessful. Subsequent attempts consisted of screening all available crystal forms by added exogenous reductant for defined time

periods prior to data collection. It was discovered that the mixed disulfide could be observed when reductant was added to crystals that were obtained when acetoacetate, CoM, and NADPH were added prior to crystallization. One possible explanation for this is that the mixed disulfide can only be obtained in the presence of NADP(H) as an electron transfer conduit for the reduction of the redox active disulfide. The crystals for this study were obtained by incubating purified 2-KPCC (~30 mg/ml) with acetoacetate, coenzyme M and NADPH for 10 minutes prior to the addition of an equal amount of precipitating solution of 0.1M ammonium acetate, 0.085M sodium citrate pH 5.6, 25% PEG 4000 and 30% glycerol. Drops of this mixture were allowed to incubate as hanging drops on siliconized slides with a reservoir of 0.8ml of the above precipitating solution. As observed previously for crystals grown in the presence of the substrate 2-ketopropyl-CoM, flat rectangular crystals appeared in three days and continued to grow to a maximum length of 0.5mm. The crystals obtained belong to monoclinic space group $P2_1$ with one dimer per asymmetric unit with the following unit cell dimensions: a=88.1 Å, b=60.0 Å, c= 105.9 Å and $\beta = 102.4^{\circ}$. Capturing the mixed-disulfide NADP(H) bound state of 2-KPCC required the incubation of these crystals with 10mM dithiothreitol dissolved in the crystallization mother liquor for 10 minutes prior to cryo-preserving the crystals by plunging in liquid nitrogen. Data were collected at SSRL beamline 9-1 equipped with a mar345 imaging plate detector (marUSA Inc.) with 1º oscillations.

Crystals of CoM disulfide bound 2-KPCC were obtained by incubating purified protein samples (~30mg/ml) with 20mM CoM prior to crystallization. Crystals were obtained by vapor diffusion using a precipitating solution consisting of 0.17M sodium acetate, 0.085 M Tris HCl pH 8.5, 25.5% (w/v) polyethylene glycol 4000 and 15% (v/v)

glycerol and cryo-cooled in liquid nitrogen before data collection as described previously [196]. These crystals also belonged to the monoclinic space group $P2_1$ with one dimer per unit cell of dimensions a=87.8 Å, b=60.1 Å, c=105.6 Å, and β=99.9º.

The data was processed with MOSFLM [64] and scaled with SCALA of the CCP4 program suite [197]. Since crystals of 2-KPCC grown in the presence of CoM or CoM + acetoacetate belonged to the same space group with unit cell dimensions similar to those of the substrate bound enzyme (a= 88.0 Å, b = 60.1 Å, c = 105.6Å, β =102.5˚) with one dimer per asymmetric unit, the substrate bound structure (1MO9) required limited repositioning for initial refinement of these structures using CNS [198]. Improvement of the structures was accomplished by iterative model building in O [199] using sigma A weighted 2*F*o-*F*c maps calculated with CNS. The structures were refined to the full resolution of usable data for the two data sets from 50 Å to 2.05 Å and 50 Å to 2.15 Å resolutions for the mixed-disulfide and CoM-disulfide bound 2-KPCC models respectively. A 1σ cutoff was applied to the data in the latter stages of the refinement.

The results of the refinement for all structures are given in Table 1. The final structural models obey reasonable stereochemistry with 100% of the residues occupying allowed regions of the Ramachandran plot calculated using PROCHECK [200]. Electron density and superimposition figures were generated using SWISSPDB VIEWER [201]. Surface rendering figures were generated with SPOCK [202]. Chemical pathway figures were created with the software ACD/CHEMSKETCH [203].

Results and Discussion

The Mixed-Disulfide State

The proposed mechanism of 2-ketopropyl CoM (KCoM) reduction and carboxylation assumes the formation of a mixed disulfide between the interchange thiol (Cys82) and coenzyme M (Figure 2.1 B). The mixed-disulfide state of glutathione reductase has been successfully captured and a 2.0 Å structure of this state has been determined providing insights into the thiol catalyzed reductive cleavage of the disulfide of the substrate.

We have been able to capture the mixed disulfide state in protein crystals of 2-KPCC and the structure of this state of the enzyme has been determined and refined to near 2.0 Å resolution. A number of unsuccessful attempts were made at stably capturing this intermediate state by the reduction of crystals grown in the presence of CoM prior to data collection. The mixed disulfide state was obtained by growing crystals in the presence of physiological products of the reaction acetoacetate, CoM, and $NADP^+$. Incubation of the crystals grown under these conditions with dithiothreitol (DTT) for ten minutes prior to data collection resulted in the stabilization of a high population of the mixed disulfide state. This mixed disulfide is well-defined in the electron density maps (Figure 2.2). Although NADP(H) is clearly visible in the electron density maps, density consistent with the presence of intact acetoacetate is not observed. In lieu of acetoacetate, density consistent with acetone, the product of acetoacetate decarboxylation, is observed at a site approximately 4.5 Å from the sulfur atoms of the disulfide. This electron density

Table 1. Data and refinement statistics of the mixed disulfide and coenzyme M disulfide bound structures of 2-KPCC

Data Collection Statistics		
	Mixed Disulfide	CoM Disulfide
resolution (Å)	2.15	2.15
no. of observed reflections	218816	226112
no. of unique reflections	62300	65514
R_{merge} (%)	9.3 (23.8)	8.3 (36.8)
completeness (%)	95.1 (82.8)	97.8 (76.4)
I/σ	5.5 (2.5)	7.6 (1.9)
Data Statistics for the highest resolution shell indicated in parentheses		
Refinement Statistics		
resolution range (Å)	20.0-2.15	20.0 -2.15
R_{cryst} (%)	17.7	19.2
R_{free} (%)	22.6	23.6
no. non-hydrogen atoms		
protein	8046	8046
cofactor/substrate	224	127
solvent	710	698
r.m.s.d. from target values		
bond lengths (Å)	0.008	0.006
bond Angles (deg)	1.440	1.290
average B factors (Å^2)		
protein main chain	21.7	21.3
protein side chain	23.7	22.3
FAD	19.2	21.4
NADP	35.5	-
Acetone	29.9	-
CoM	20.6	-
HOH	31.6	39.9
CoM-CoM	-	34.4

feature would also be consistent with acetate which is a component of the crystallization solution, However, density is not observed at this position in the native 2-KPCC (without substrates or products bound) and the structure of native 2-KPCC was determined from crystals that were also grown in the presence of acetate. It is reasonable that during the

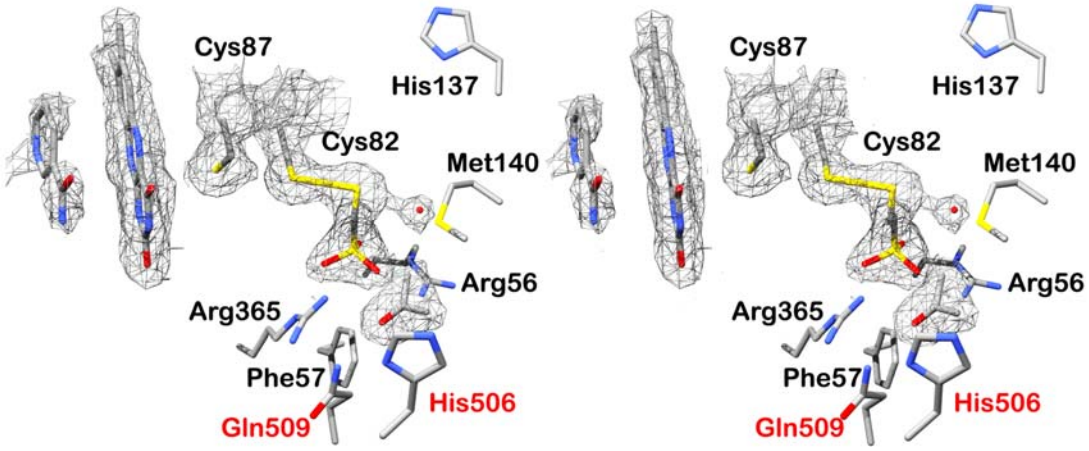

Figure 2.2. Stereo view of the active site of the mixed-disulfide bound state of 2-KPCC with electron density maps (2*F*o-*F*c) of the 2-KPCC mixed-disulfide state contoured (1σ) around NADP, FAD, Cys87,Cys82-CoM and acetone

course of crystallization or during the incubation with DTT, acetoacetate was reductively decarboxylated to form acetone and carbon dioxide, a previously reported 2-KPCC catalyzed reaction [68]. Unambiguous density consistent with CO_2 as a product of this reaction is, however, not observed. The binding mode of the acetone or acetate ion at the enzyme active site has some interesting implications on potential mechanisms for product formation and release that will be discussed in detail below.

The binding of the sulfonate moiety of CoM is analogous to the substrate bound state (Figure 2.3 A), primarily due to interactions with Arg56 and Arg365 at the active site. In our previous work [71], we have extensively characterized the substrate bound state of 2-KPCC and suggested a well-defined enclosed substrate binding pocket composed of largely hydrophobic amino acid residues was a critical factor in

A.

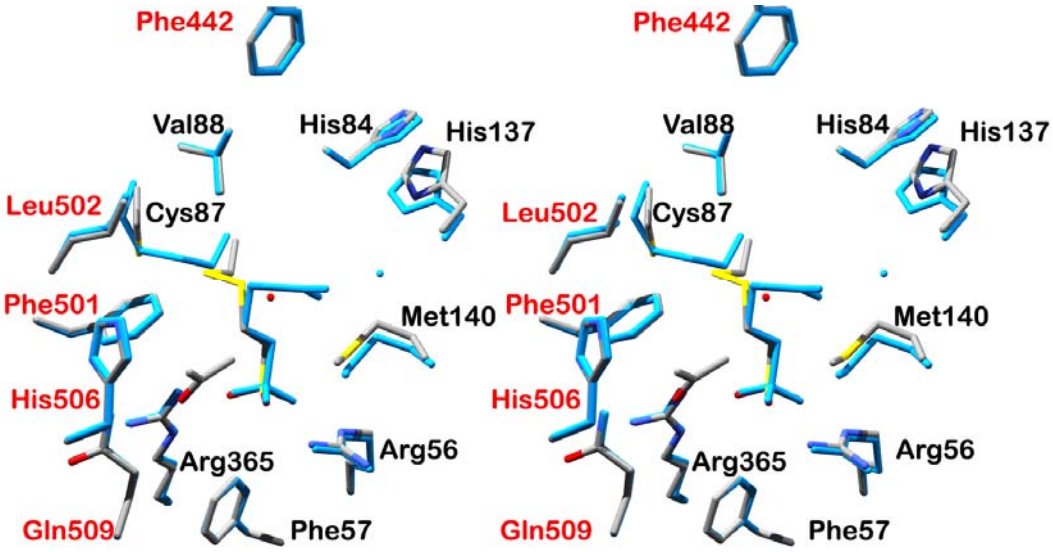

B. C.

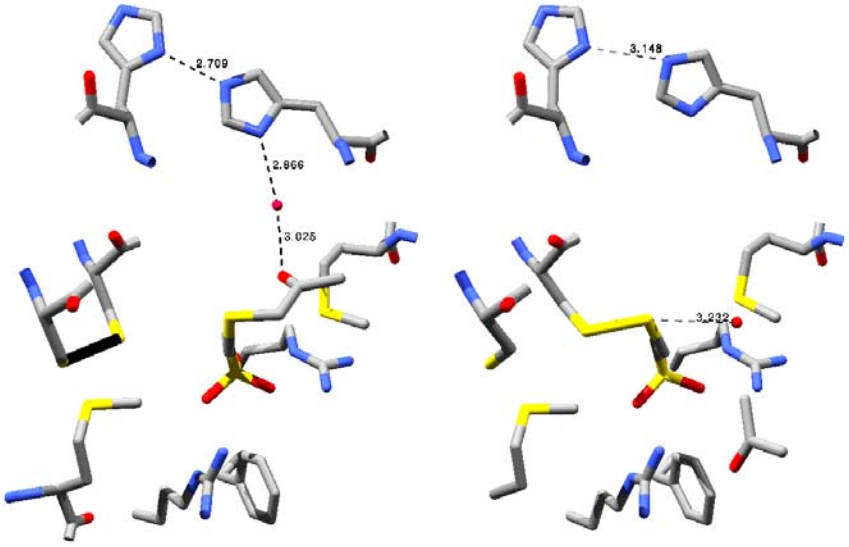

Figure 2.3. A. Stereo view of superimposition of the substrate binding site residues of Cys82-CoM mixed disulfide and acetone bound structure (CPK) on KCoM bound 2-KPCC (cyan). Residues from different subunits of the dimer are indicated in black and red labels. B. Structural representations of substrate binding in the previously characterized 2-KPCC substrate bound state (PDB code 1MO9) showing the redox active disulfide, bound substrate, and His oriented water molecule previously suggested to be involved in enolate formation /stabilization and (C) the same region in the mixed disulfide between 2-KPCC Cys82 and coenzyme M

discriminating between protons and CO_2 and favoring physiologically relevant carboxylation and acetoaectate formation.

In figure 2.3 B, substrate is bound at the active site in a manner such that a His oriented water molecule is interacting directly with the carbonyl group of the ketopropyl moiety of KCoM. We have suggested that this water molecule could be involved in the formation and stabilization of enolacetone generating a suitable nucleophile for the reaction with an electrophilic substrate such as a proton or carbon dioxide. These interactions poise the keto-propyl moiety of KCoM almost directly opposite of the sulfur of the attacking Cys residue in an appropriate orientation for a leaving group. In this mode of substrate binding, the site of the proposed formation of the enolacetone intermediate (Figure 2.1B) is largely hydrophobic and we have suggested that the exclusion of solvent at this site is a key factor in promoting carboxylation over protonation. In the structure of the mixed disulfide state, the pocket which bound the keto-propyl moiety is no longer occupied and it appears that the water molecule which was previously bound at His137 has migrated to within hydrogen bonding distance of the thiol sulfur of CoM (Figure 2.3C). This water molecule is now poised to protonate the free CoM product upon reoxidation of the enzyme disulfide.

Structural Changes in the Substrate Binding Site

As previously mentioned, the binding of substrate to 2-KPCC induces a conformational change that results in the sequestration of substrate at the dimer interface in an environment that favors carboxylation and the formation of acetoacetate [71]. The residues that are involved in this conformation change are predominantly in the region of

the N-terminus and the region of the His residue previously implicated in having a role in enolacetone formation/stabilization. These observations support the idea that substrate binding induces a structural change in N-terminus of 2-KPCC that leads to modulation of the substrate access channel, restricting the accessibility of bulk solvent to the channel. Interestingly, when the substrate bound state is superimposed onto the mixed disulfide state, very few differences are observed in the active site region (Figure 2.3 A). Only a slight movement of the Cys 82 side chain is required for formation of the mixed disulfide. The one significant difference that is clear in the active site in comparing these states is the position of the side chain of His137. In the substrate bound state this His is hydrogen bonded to a water molecule that is in turn hydrogen bonded to the substrate carbonyl group. In the mixed disulfide this water molecule is absent and the side chain of His137 rotates away from the active site cavity.

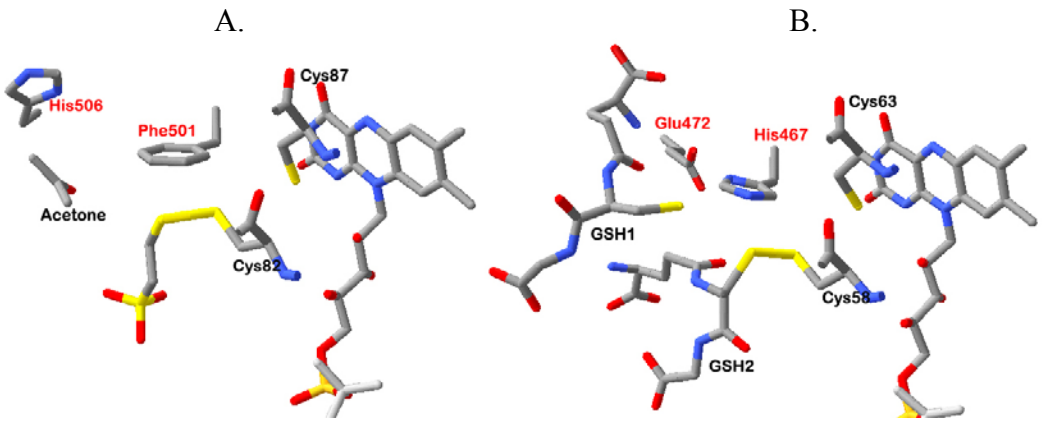

Figure 2.4. Comparison of the mixed disulfide states of 2-KPCC (A) and glutationine reductase (GR) (B) highlighting the position of the initial leaving groups, acetone and glutathione, for 2-KPCC and GR respectively

Electron density consistent with acetone/acetate was clear in the substrate binding pocket approximately 4.5 Å away from the sulfur of CoM. Binding of acetone/acetate is stabilized by a specific hydrogen bonding interaction (~3 Å) between the carbonyl group oxygen and the amide nitrogen of the side chain of Gln509 of the opposing subunit. In addition to being the product of reductive decarboxylation of acetoacetate, acetone is the product of the 2-KPCC reductive cleavage of KCoM in the absence of CO_2. Acetone as a leaving group during reductive cleavage of KCoM (Figure 2.4A) is in a similar relative position to the position of the reduced glutathione leaving group in the reductive cleavage of glutathione disulfide (Figure 2.4 B) in glutathione reductase (GR) [33]. Figure 2.4 also shows the positions of the catalytic dyad of GR which consists of His467 and Glu472 in a conserved motif (HXXXXE) among the many DSOR enzymes. These residues are contributed by the subunit opposite the subunit contributing the redox active disulfide. It has been proposed that this catalytic dyad in these enzymes facilitates catalysis by specific protonation of the initial leaving group by His, [41], His467 in the case of *E. coli* GR [33]. In 2-KPCC, this DSOR motif is not conserved and is replaced by (FLNPTH) and thus a Phe replaces the His observed in many DSOR enzymes. This difference is a likely reflection of the different chemical reactions catalyzed by the DSOR enzyme like GR and 2-KPCC. In GR, protonation of the leaving group is important for enzyme turnover to the productive product reduced glutathione. In 2-KPCC, protonation of the leaving group of reductive carbon sulfur bond cleavage is not desirable and instead carboxylation leads to the productive product acetoacetate. Thus the absence of this protonatable group in the active site may be very important for promoting carboxylation

of enolacetone intermediate and acetoacetate formation over protonation and acetone formation. There are no charged residues around the charge transfer thiol Cys87 that can be assigned a role in facilitating an attack on the enzyme-CoM mixed disulfide in 2-KPCC and we have suggested above that perhaps a water molecule that can only come into proximity of the active site Cys thiol after dissociation of the leaving group might be serving this role.

Potential CO_2 Channel

2-KPCC catalyzes the reductive cleavage and carboxylation of a β-ketothioether to form a β keto acid. It also catalyzes the reverse reaction which is the decarboxylation of the product acetoacetate to form 2-ketopropyl CoM and CO_2 in the presence of NADP and CoM (*16*). In the absence of CO_2, protonation of the proposed enolate intermediate occurs, resulting in the formation of acetone which is not a substrate for 2-KPCC. The characteristically hydrophobic region in the active site could be a possible binding site for CO_2. A CO_2 docking into this active site shows the molecule to be bound at the subunit interface just like the substrate and the other product acetone. A surface rendering of the region shows that CO_2 bound at this site is visible from the surface and is possibly the way in / out for CO_2 (Figure 2.5A). This potential channel for the CO_2 access is composed of hydrophobic residues from both subunits (Figure2.5B). Genetic-structural studies in the case of human carbonic anhydrase have indicated that a hydrophobic pocket is required for substrate (CO_2) association [204].

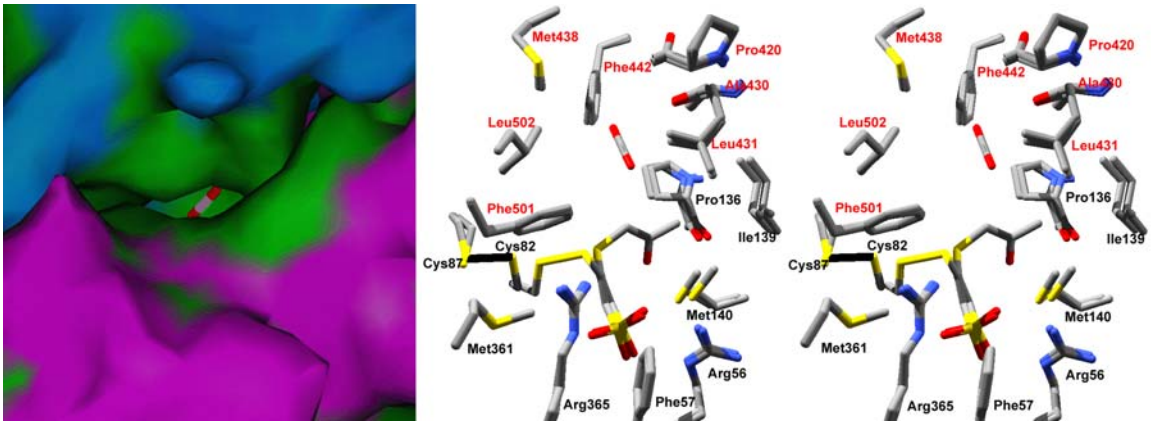

Figure 2.5. A. Surface rendering of potential CO_2 access channel generated using SPOCK showing CO_2 molecule docked into the hydrophobic pocket of the substrate binding site. The two subunits are shown in blue and pink respectively, with the surface due to hydrophobic residues are shown in green. B. Stereo view of the superimposition of the substrate and mixed disulfide bound states of 2-KPCC showing selected amino acid residues of the hydrophobic portion of the substrate binding pocket

With regard to the active species used by 2-KPCC, CO_2 rather than bicarbonate is believed to be the substrate for the enzyme, as assumed in the discussion above. Initial rate studies using CO_2 versus bicarbonate as substrate suggest this as well as ^{14}C fixation studies using $^{14}CO_2$ and $NaH^{14}CO_3$ as substrate (J.M.Boyd, J.W. Peters and S.A. Ensign , unpublished results). 2-KPCC does not require biotin or ATP, which are required for enzymatic activation of bicarbonate as an electrophile in enzymes that use bicarbonate as the active species, providing further support for the idea that CO_2 is the active species for 2-KPCC.

Genetic-structural studies in the case of human carbonic anhydrase have indicated that a hydrophobic pocket is required for substrate (CO_2) association [204, 205]. Although the conservation of a well-defined pocket in human carbonic anyhydrase is critical for proper substrate association, a deeper pocket does not severely hinder efficient catalysis, but a shallower pocket results in 3×10^5 – fold loss of CO_2

hydrase activity [205]. As stated for carbonic anhydrase, the hydrophobic pocket is probably involved in desolvation of the substrate as well as funneling the substrate toward the active site, and a variety of surface contours will satisfy this role as long as minimal requirements of pocket width and depth are met [206]. The potential CO_2 binding pocket of 2-KPCC possesses the aforementioned features in terms of the nature of the constituent amino acids as well as the location of the pocket. The CO_2 binding hydrophobic pocket is adjacent to the acetone/acetate binding site and is formed primarily from side chains of hydrophobic residues (Fig 2.5B). These include Ala17, Pro136, Ile139, Val88, Pro89 and Phe93 from one subunit. The residues from the other subunit are contributed by the residues of a proline flanked loop region unique amongst the DSOR enzyme to 2-KPCC and include Ala430, Leu431, Ala433, and Ser434 with the Cα of this Ser facing the CO_2 binding cavity. Phe501 and a *cis* Leu502 of the FLNPTH sequence and Phe442 from the interface domain of the other subunit are the residues forming the rest of the CO_2 binding pocket (Figure 2.5B).

Product Binding and Release

The structure of 2KPCC obtained from co-crystallization of the enzyme with coenzyme M reveals CoM disulfide at the active site (Figure2.6A). Although freshly prepared CoM thiol was added to the protein prior to crystallization, it appears that during the two-three week long period of incubation at room temperature in air required for crystallization, that the CoM has oxidized to form CoM disulfide. This CoM disulfide binds primarily through interactions between its sulfonate moiety with active site residues of both the subunits. In an earlier work [27], 1,3-propane dithiol (PDT) has been shown

A.

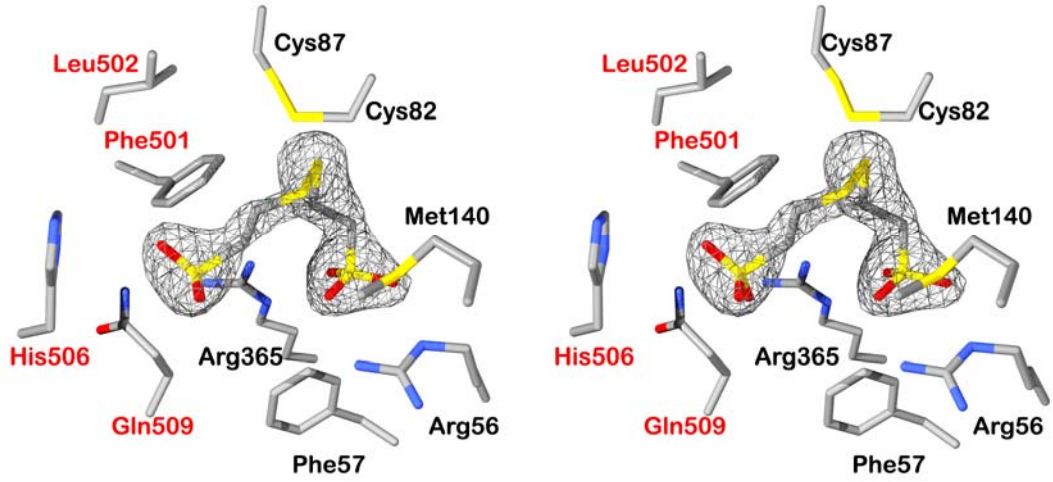

B.

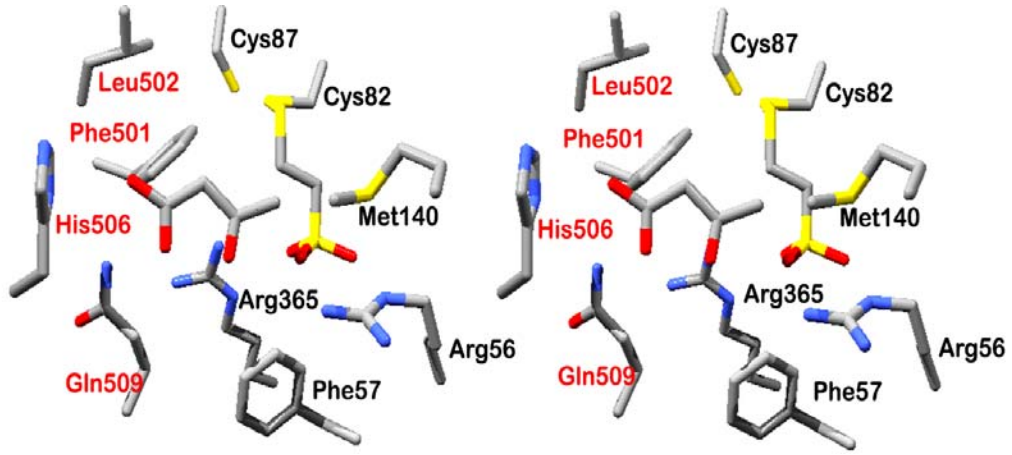

Figure 2.6. A. 2*Fo-Fc* electron density maps of the CoM 2-KPCC structure contoured (1σ) about the bound CoM disulfide. B. Acetoacetate modeled into the alternative anion binding site based on the position of the sulfonate oxygens (carboxylate of acetoacetate positioned at the site of sulfonate of CoM disulfide) in the CoM bound structure and the position of acetone in the mixed disulfide structure

to reduce 2-KPCC in the presence of $NADP^+$. The reduction of the enzyme by PDT is entirely dependent on the presence of $NADP^+$. According to the proposed mechanism, in the absence of $NADP^+$, a mixed disulfide between a PDT thiol and the redox active cysteine is formed along with the formation of an FAD C4a-thiol charge-transfer interaction. Such a mechanism is also observed in Glutathione reductase in the absence

of NADP with GSH as the reductant [207]. In 2-KPCC, the CoM disulfide assumes a bench-like conformation with the disulfide bridge forming the seat while the sulfonates form the legs. One half of this disulfide binds the same as the CoM part of 2-ketopropyl CoM , with ionic interactions between Arg365 and Arg56 of one subunit.

The sulfonate from the other CoM extends a little away from these Args to form interactions with the side chain carbonyl of Gln509 of the other subunit and water molecules but maintains proximity to Arg365, one of the oxygen atoms being 3.7 Å from NH_2 of the latter. One of the oxygens of this sulfonate is 3.3 Å from Nε of His506 of the other subunit, which has Pro432 and Pro420 of the insertion loop on top and towards its front respectively. During the course of the reaction leading to the formation of acetoacetate, the carboxylate moiety could be stabilized by the His and Gln of one of the subunits (Figures 2.6B, Figure 2.7), the interaction of the carboxylate with Arg365 concomitantly causing a weakening of the interaction between the CoM sulfonate and Arg365 and aiding the release of CoM. The binding interactions of acetoacetate as compared to a coenzyme M moiety can be speculated to be quite similar except in the vicinity of the carbonyl group, which could result in changes in the binding conformation conceivably favoring better stabilization of acetoacetate and destabilization of the CoM sulfonate – Arg binding interactions. The disulfide bond (S-S bond distance 2.4 Å) of the CoM disulfide faces a hydrophobic pocket formed by Val77, Pro83, Val88, Pro136 and Met361 of one subunit and Met438, Phe442, Phe501 and Leu502 of the other subunit. One of the sulfurs of the disulfide bridge is 3.8 Å away from the sulfur of Cys82 which in turn is 2.2 Å from the Cys87 sulfur.

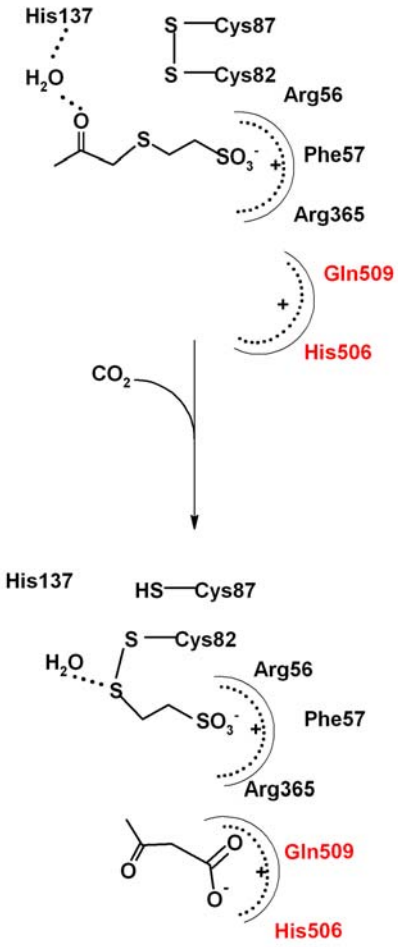

Figure 2.7: Schematic representation of the hypothetical mechanism of product formation/stabilization in 2-KPCC

Conclusion

In our previous work we have suggested that substrate binding induces conformational changes that result in the sequestration of substrate to favor carboxylation over protonation. This was based primarily on the observation that the substrate access channel becomes much more restricted in the substrate bound state in comparison to the

native state. For the mixed disulfide state in the current work, the substrate access channel is similar to that observed in the substrate bound state, however in the CoM disulfide state the channel widens slightly. This suggests an overall mechanism of the concerted stabilization of the developing charge of acetoacetate and the destabilization of the binding of substrates at the active site such that the electrostatic interactions at the active site that are generated during product formation are coupled to changes in the conformation of the N-terminal region of 2-KPCC that result in opening of the active site access facilitating product release and enzyme turnover.

SUBSTRATE AND NUCLEOTIDE BINDING INTERACTIONS IN 2-KPCC IN COMPARISON WITH DSORS

Introduction

The Flavin Disulfide Reductase Family

Flavoprotein disulfide reductases (FDRs) form a family of homodimeric enzymes catalyzing the pyridine nucleotide dependent reduction of a variety of substrates. The enzymes comprising this family show high sequence and structural homology, even though considerable variation in the mechanism of reduction occurs amongst the members. In each case, however, a tightly but noncovalently bound Flavin Adenine Dinucleotide (FAD) serves to transfer electrons from a reduced pyridine dinucleotide to a redox center on the protein, which is the final donor of reducing equivalents to the substrate. A majority of members have a protein disulfide as the single non-flavin redox center and are being referred to as the NADP(H)-dependent disulfide oxidoreductases (DSORs) in this work. An enzymic cysteine sulfinic acid and a mixed Cys-S-S-CoA disulfide constitute the non flavin redox center in other FDR members.

Disulfide oxidoreductases constitute group 1 of the FDR family [61] which consists of well characterized reductases namely glutathione reductase (GR), trypanothione reductase (TR), lipoamide dehydrogenase (LAD) [41] and the recently described mycothione reductase from *Mycobacterium tuberculosis* [208]. These DSORs are characterized by the presence of four domains per monomer: the FAD binding domain containing the redox active disulfide, the NADP(H) binding domain, the central

and the interface domains. In addition, there is a highly conserved HXXXXE sequence, where X denotes any amino acid, in the interface domain in all of group 1 FDRs with the conserved histidine and glutamate having been shown to be catalytically relevant [41].

2-KPCC bears ~30% sequence similarity with the group I FDRs / DSORs. The determination of its crystal structure [71] showed the presence of all four domains present in the DSORs, namely the FAD and $NADP^+$-binding domains, the central and the dimerization domains. A major difference in the sequence that is mechanistically relevant is the absence of the catalytic His-Glu dyad that has been shown to be involved in the protonation of the leaving groups [41, 61] in some DSORs and is highly conserved in all DSORs. A higher resolution (1.51 Å) substrate bound structure of 2-KPCC along with its previously determined NADP(H)/mixed disulfide bound structure [209] together provide structural and mechanistic aspects that can be compared to the same in DSORs. This sheds light on features that might be relevant to C-S bond cleavage and subsequent carboxylation of the leaving group, as opposed to S-S bond cleavage and protonation of both leaving groups.

General Reaction Catalyzed by DSORs and 2-KPCC

All known DSORs catalyze the reduction of a disulfide bond in an organic substrate (Figure 3.1). The direction of flow of electrons is from pyridine nucleotide to FAD to the active center disulfide to the substrate disulfide. [210-214]. Electron transfer between the flavin and the active center disulfide probably involves a covalent thiolate adduct at the C(4)a position of FAD [215-219]. The catalytically active species of these enzymes is the two electron reduced state EH2 [211]. The two cysteines in these enzymes

have distinct functions in the EH2 forms [41]. The cysteine towards the C-terminus forms the charge transfer complex with FAD and is hence termed the charge transfer cysteine [220-222]. The disulfide cysteine distal to FAD forms a mixed disulfide with the disulfide substrate during catalysis and is thus termed as the interchange cysteine.

2-KPCC is a novel DSOR that carries out the thioether bond reduction of its substrate 2-ketopropyl Coenzyme M and subsequent carboxylation to form acetoacetate and coenzyme M [68] (Figure 3.1). The reaction catalyzed by 2-KPCC is the final reaction in the carboxylation pathway of epoxypropane metabolism in *Xanthobacter autotrophicus* Strain Py2 whereby the citric acid cycle intermediate acetoacetate is produced with the concomitant regeneration of coenzyme M [68]. This reaction is unique in two aspects: One that this is the only known example of a DSOR catalyzing the reductive cleavage of a thioether substrate followed by CO_2 –fixation into the acetone-enolate intermediate to generate a product that can be utilized further. Reductive carboxylation of the intermediate is far preferred over its reductive protonation, which is in contrast with other DSORs in which both products are reductively protonated. Second, it utilizes coenzyme M as a cofactor for the carboxylation of the substrate 2-ketopropyl CoM as well as for the reverse reaction, the decarboxylation of acetoacetate to form 2-ketopropylCoM. Extensive kinetic analysis of 2-KPCC activity has been carried out [68] and suggests the formation of an enolate intermediate and its stabilization by proton donation by a nearby catalytic acid. This role was shown to be performed by a His coordinated water molecule in the substrate bound crystal structure of 2-KPCC [71].

2-KPCC can catalyze the decarboxylation of acetoacetate in the presence of coenzyme M and $NADP^+$ to form 2-ketopropyl coenzyme M. This rate of

decarboxylation is ~77 fold slower in the absence of coenzyme M. The mechanism of acetoacetate decarboxylation by 2-KPCC also proceeds through the formation of a carbanion that gets stabilized as an enolate intermediate. It has been shown [24] that the carboxylation of the enolate intermediate does not involve the formation of a Schiff's base, or the requirement of a metal ion for the stabilization of the carbanion.

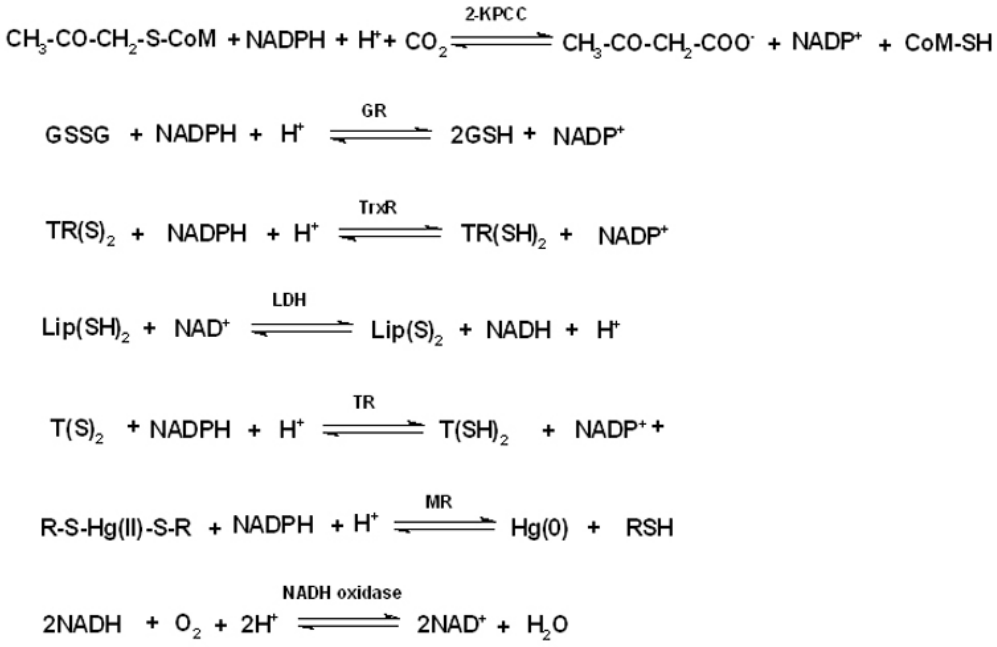

Figure 3.1. General reactions catalyzed by DSORs. GR-glutathione reductase, TrxR-Thioredoxing reductase, LDH-lipoamide dehydrogenase, TR-Trypanothione reductase, MR-Mercuric reductase.

Experimental Procedures

The ketopropyl CoM bound structure of 2-KPCC has been solved previously to a resolution of 1.65 Å [71]. The structure of the 2-ketopropyl CoM bound 2-KPCC has now been refined against higher resolution data good to 1.51 Å obtained at SSRL. This high resolution data was processed with programs of the CCP4 suite[197] and the

substrate bound structure (1MO9) was refined to 1.55 Å with REFMAC [224, 225] using all data. Co-ordinate and anisotropic TLS refinement [226] with each monomer designated a rigid group yielded an R_{free} of 0.19 and R_{work} of 0.15. SigmaA weighted 2*Fo-Fc* map was calculated within REFMAC [224,225] and viewed with the program O [199] at 1 σ contour levels. Alternate conformations of protein side chains were added where applicable. Data collection and refinement statistics are shown in Table 3.1.

Electron density and binding environment figures were generated using SWISSPDB VIEWER [201]. Surface rendering and superimposition figures were made with SPOCK [202], while the secondary structure alignment figure was generated with ESpript [227].

PDB files of the enzymes Glutathione reductase (3GRS), mammalian Thioredoxin reductase (1H6V), Trypanothione reductase (1FEC), lipoamide dehydrogenase (3LAD) and mercuric reductase (1ZK7) were obtained from the PDB Bank. Structure based alignment was done using the programs JOY [228] and COMPARER [229]. A molecular topology map for 2-KPCC protein structure was created with PROMOTIF of the CCP4 suite [197] and the topology diagram was created with TOPDRAW [230].

Results and Discussion

Structure

The crystal structure of 2-KPCC has been solved in the absence and presence of the substrate 2-ketopropyl CoM [71] (Figure 3.3) The overall structure of the dimer is very similar to those of the other DSORs as shown by the crystal structures of glutathione reductase [31], Lipoamide dehydrogenase [231], trypanothione reductase [232] etc.

Some examples of crystal structures of some of the DSORs are shown in figure 3.2. There is one active site per monomer that occurs at the subunit interface and is nestled amongst residues of the first three domains of one subunit and of the interface domain of the other subunit. Based on structural alignment with the well characterized human glutathione reductase [233], the overall secondary structure of 2-KPCC monomer shows distinct FAD-binding (41-181), NADP-binding (182-316), central (317-384) and interface (385-523) domains (Figure 3.4).

Table 3.1: Data and refinement statistics for 2-KCoM bound 2-KPCC

Data Collection Statistics	
	KCoM
resolution (Å)	1.51
no. of observed reflections	494604
no. of unique reflections	164833
R_{merge} [a] (%)	6.7(4.9)
completeness (%)	98.2(98.2)
I/σ	7.8(1.5)
Refinement Statistics	
resolution range (Å)	20.0-1.55
R_{cryst}	0.154
R_{free}	0.189
no. non-hydrogen atoms	9789
protein	8185
cofactor/substrate	215
solvent	1389
rmsd from target values	
bond lengths (Å)	0.009
bond Angles (deg)	1.233

As with the Group 1 FDR enzymes, the redox active disulfide is present within the FAD-binding domain as the CX_4C motif. A secondary structure alignment of 2-KPCC with the DSORs shows an 18-amino acid (420-437) loop insertion in the interface region that is either very short or absent in the DSORs. The loop curves inwards such that cis-Pro432 is brought in close proximity to cis-Pro420.

The substrate bound crystal structure (1.55 Å) shows a hexacoordinated metal bound at the center of the proline flanked loop and residues from the second 3_{10} helix of the peptide chain (Figure 3.5). To our knowledge, none of the group 1 FDRs has a metal

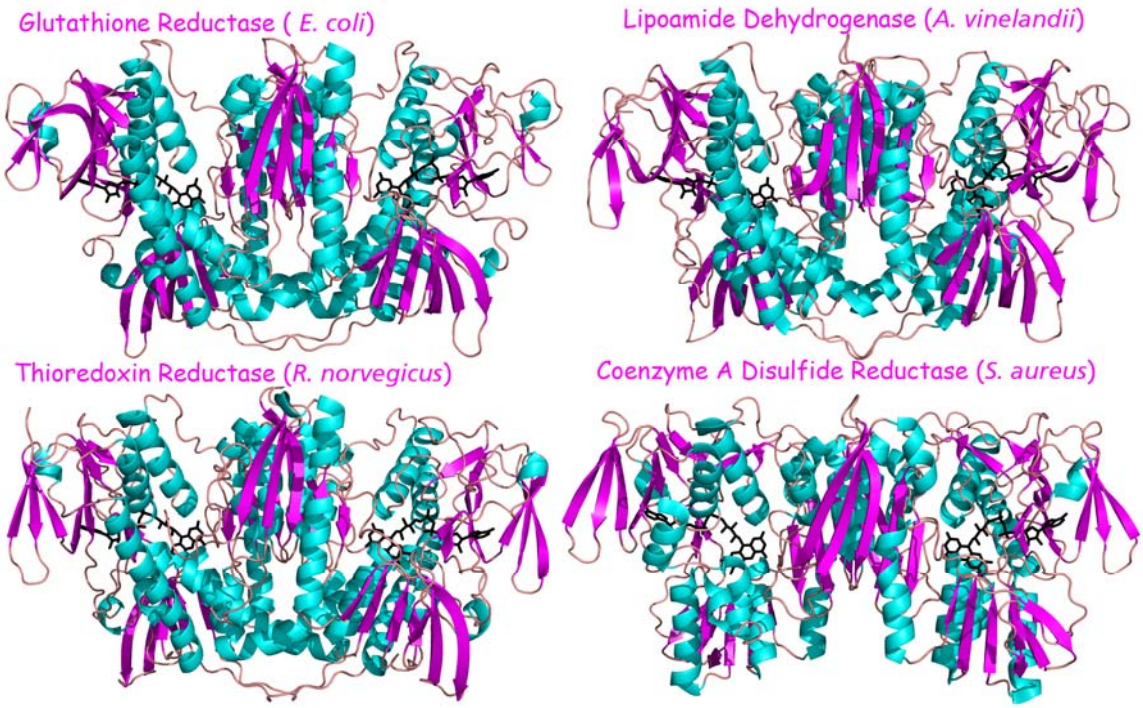

Figure 3.2: Crystal structures of Glutathione reducase (*Escherichia coli*) (PDB 1GRE), Lipoamide dehydrogenase (*Azotobacter vinelandii*) (PDB 3LAD), Thioredoxin reductase (*Rattus norvegicus*) (PDB 1H6V) and Coenzyme A disulfide reductase (*Staphylococcus aureus*) (PDB 1YQZ)

ion that is a part of the secondary structure or involved in the reaction mechanism. Although a metal binding site is clearly visible in 2-KPCC, its location is far removed from the substrate binding site where it could potentially stabilize the enolate intermediate. The geometry of this metal binding is octahedral with some distortion in the angles. The plane of the square bipyramid is formed by the carbonyl oxygens of Leu427, Val429, the gamma side chain oxygen of Ser450 and a water molecule. The corresponding angles are 78.77 º (427O-M-429O), 109.28 º (450O-M-429O), 92.96 º (450O-M-wat) and 81.09 º (wat-O-427O). The ligands perpendicular to the plane are Leu431O at 80.00 º and Ala447O at 94.83 º. The metal coordination results in essentially fixing the loop into place with the 3_{10} helix hooked up to the loop. This arrangement causes the side chain of Lys444 to extend out towards the exterior of the molecule. The Lys 444 side chain flips over a 180 º upon substrate binding as compared to native form. Since this occurs on the surface of the molecule, it is hard to assign any importance to the side chain conformational change. But there is little or no change of the amino acids in the vicinity of this lysine side chain on the surface of the molecule, which leads to a possibility that Lys444 is strategically placed in its position.

Upon substrate binding, the movement of the Lys444 side chain covers up a part of the subunit interface that is close to the potential CO_2 entry /exit site. In lieu of the positions of product acetone and CO_2 in the product bound state being channeled towards hydrophobic regions presumably for exit, the flipping over of the Lys444 side chain could be to block an alternative exit path. Also, it is conceivable that the absence of a metal coordination and hence fixing of the 18 amino acid loop would cause the loop to extend into the subunit interface, which in turn is likely to block the exit of the products.

Figure 3.3: Structure based sequence alignment of (top to bottom) 2-KPCC, Glutathione reductase, trypanothione reductase, lipamide dehydrogenase, mammalian thioredoxin reductase and mercuric reductase. The secondary structure on top is that of 2-KPCC. The secondary structure is color coded according to domains to match figures 3.10 and 3.11. Signature motif of the Rossman fold of the FAD domain (GXGXXG(X)17D/E is shown in maroon, the T(S)(X)5F(Y)hhGD(E) motif of oxidoreductases is shown in green, highly conserved ATG domain oohhhATG of DSORs is shown in orange, partially conserved D(X)6GXXP motif of Glutathione reductase like NADPH binding proteins is shown in violet and the His-Glu dyad sequence HXXXXE of DSORs is shown in blue. (h-hydrophobic, o-polar, X-any amino acid

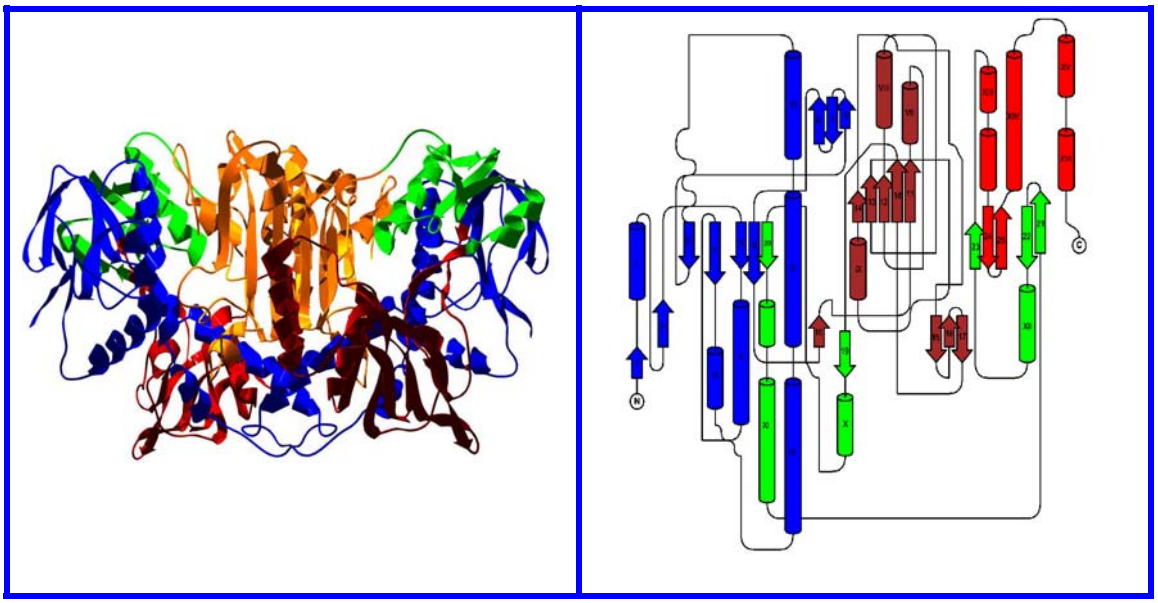

Figure3.4: The crystal structure and topology diagram of 2-KPCC color coded bydomain. FAD domain in blue, NADP domain in brown, central domain in green and diimerization domain in orange.

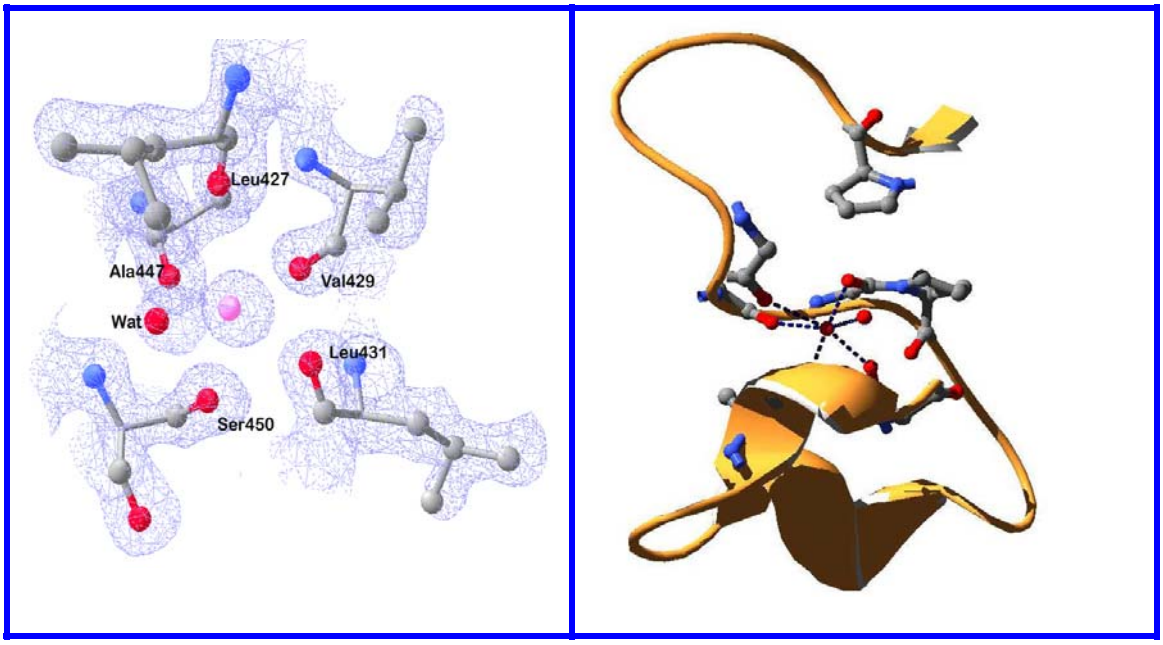

Figure 3.5: Electron density for a hexacoordinated metal ion contoured to 1 σ . Right: Position of the metal ion relative to the proline flanked insertion loop

Substrate Binding

A superimposition of the Cα atoms of the KCoM bound 2-KPCC on those of the native form (RMS=0.921) indicates considerable movement of the residues around the substrate binding site so as to encapsulate the substrate completely (Figure 3.7). A similar superposition with human glutathione reductase shows very little movement of the residues surrounding the substrate, the maximum displacement of 1.14 Å shown by Tyr114, such that the size and exposure of the substrate binding site stays essentially unchanged (Figure 3.6, right).

The substrate binding site of 2-KPCC, as in human glutathione reductase, occurs at the subunit interface with residues from both subunits forming the substrate binding environment. The residues contributed by the substrate binding subunit are from the FAD binding domain (α2, α6 and α11) while the residues from the other subunit are from the end of the central domain (proline flanked loop) and the interface domain (α13, α15 and α16). 2-ketopropyl CoM binds to the active site largely through hydrogen bonding of its sulfonate group to Arg 56 and Arg365 guanido groups. The carbonyl group of KCoM is hydrogen bonded to a water molecule (2.90 Å) and is within Van der Waals distance of Met140 S.

A comparison of KCoM bound and native 2-KPCC structures shows that substrate binding induces movements of side chains of active site residues with an overall effect of shielding the substrate ketopropyl moiety from charge from polar main chain or side chains of charged residues as hydrophobic groups close in on the leaving group (Figure 3.7). The substrate binding cavity is lined by Met (140,361), Ile (139), Phe (57,442,501), Pro (83), Val (88), and leu (431,502), the only charged residues being

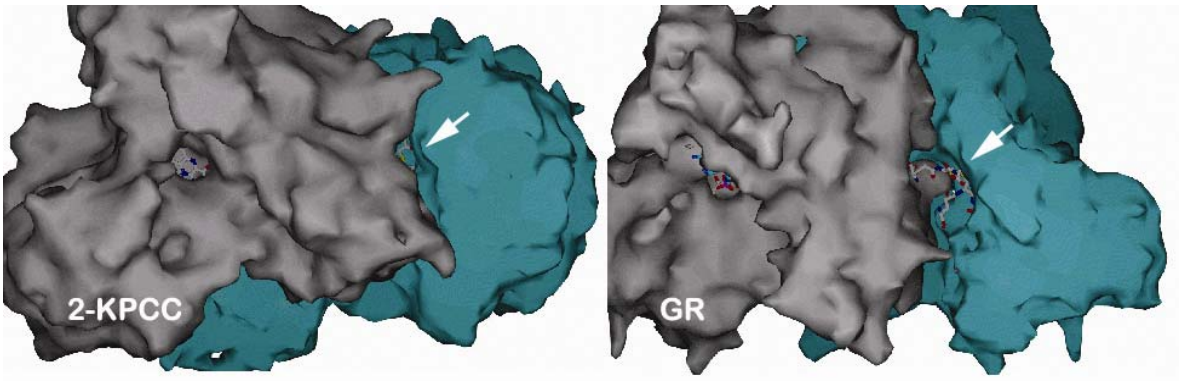

Figure 3.6: The substrate binding sites of 2-KPCC and GR reductase at the dimer interface.

Arg56 and Arg365. Met140 is present at a position that is a tyrosine in the DSORs presented here and is conserved in all DSORs except LAD where the equivalent residue is a valine in the structural alignment. The role of this tyrosine has been investigated in glutathione reductase, where its side chain rotates and translates by 1 Å to bring the group within hydrogen bonding distance of CysN and the substrate GSSG [237].

It has been proposed that this phenolate could promote the protonation of the second molecule of glutathione by the acid catalyst His467. Mutation of Tyr114 to Leu resulted in an enzyme with 14% of the catalytic activity demonstrating that the residue is involved but not essential for catalysis.

In 2-KPCC, the sulfur atom of Met140 moves 2.51 Å towards the substrate binding site on KCoM binding (Figure 3.7). The methyl group translates 1.66 Å and rotates 90 ° with respect to the CH_3-S plane in native to get closer to the leaving group of KCoM so that it contributes to the hydrophobic environment around the terminal CH_3 group of the latter. It does not, however, come close enough to the substrate to influence

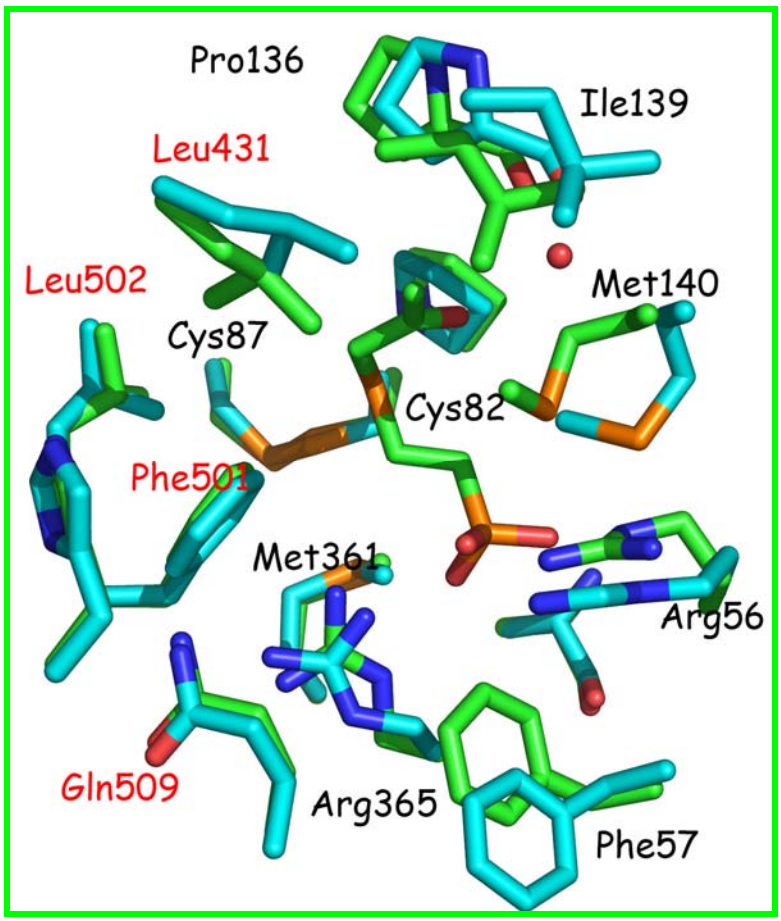

Figure 3.7: A superimposition of the ligand free 2-KPCC structure (cyan carbons) on 2-ketopropyl CoM bound structure (green carbons). Residues from the two subunits are labeled in black and red. The water molecule shown is present only in the substrate bound structure

catalysis in any way. Interestingly, four of the hydrophobic residues fall in the proline flanked loop between β23 and α13 which is either very short or absent in the other DSORs. It is notable that Met419 and Leu431 precede Pro420 and Pro432 that flank the beginning and end of the central infolding of this loop. Met438 and Phe442 from the beginning and end of α13 respectively and Met361 at the start of α11 are the other hydrophobic residues in the substrate binding environment. Phe501 is conspicuously present where a highly conserved histidine is present as part of the conserved HXXXXE sequence in the interface domain of the DSORs. It is positioned with the phenyl ring

facing the sulfur atom of the CoM part of the substrate, and moves away from the substrate binding site slightly, presumably to influence the hydrophobic pocket. The residue carboxy to Phe501, a *cis* Leu502, also moves away so that the side chain is farther from the benzyl ring of Phe501. The side chain rotates on binding of 2KCoM to change the χ^2 angle to from -160˚ to 64°. This increases the distance of closest approach between the two side chain groups- 3.40 Å between Leu502 Cδ2 and Phe501 Cε2 to 3.76 Å between Leu502 Cζ and Phe501 Cζ . The distance between the Cα of the two residues also increases from 2.88 Å to 2.92 Å The occurrence of non-proline *cis*-peptide bonds has been associated with steric strain in proteins [234], similar to the occurrence of residues with unfavourable Φ / Ψ angles and it has been speculated that the location of these *cis* peptide bonds is often a peculiar one with respect to the function of the molecule [235, 236]. Leu 502 is at an analogous position to a proline in the DSORs with the exception of mercuric reductase, which also has a leucine, adjacent to the histidine shown to be the catalytic acid that stabilizes the leaving group by protonation [42]. In all cases with a His-Pro pair in this sequence, the proline is *cis* to the His and has been shown to be essential for activity in lipoamide dehydrogenase, glutathione reductase and thioredoxin reductase. The leucine of the Tyr-Leu pair in mercuric reductase, however, is not *cis* to the Tyr, but the side chains of the two residues do stack as Phe 501-Leu 502 side chains in 2-KPCC do. The suggestion that these sites of strain are some kind of energy reservoir for the protein has been discussed [235, 236]. In the course of a chemical reaction or a conformational change, the energy that could be liberated by a conversion of a *cis* bond to a *trans* one could help drive the reaction towards the product. On substrate binding in

2-KPCC, however, there is no such change in the nature of this bond, the only change being that of a movement of Phe501 and Leu502 residues ~1 Å away from the active site.

It is noticeable that all residues contributed by the other subunit at the KCoM binding site of one subunit are hydrophobic. Met140 and Met361 are present just above the plane of the sulfonate moiety on the opposite sides of CoM and serve to shield the ketopropyl part of the substrate from the charge from sulfonate or the surrounding arginines. The sulfur of Met140 moves 2.51 Å and rotates 108º to get closer to the substrate while the CH_3 group rotates 90º with respect to the CH_3-S axis in native to point CH_3 towards the ketopropyl moiety of the substrate, hence contributing to the hydrophobic environment around the latter. Met419 methyl group points towards Leu431 in the native enzyme but is rotated 96.47º to constitute the environment of the ketopropyl moiety. Phenyl ring of Phe57 rotates 69.44º towards the sulfonate moiety, blocking further translation of the substrate so that the sulfonate is brought in correct proximity and orientation to hydrogen bond to Arg56 and Arg365 while holding the substrate thioether in proximity to the redox disulfide for electron transfer.

The Mixed Disulfide

The proposed mechanism of 2-ketopropyl CoM reduction and carboxylation assumes the formation of a mixed disulfide between the interchange thiol (Cys82) and Coenzyme M [68]. Crystal structure of 2-KPCC obtained on incubation with physiological product acetoacetate and CoM shows clear density for this mixed disulfide [209] (Figure 3.8). Mixed disulfides have also been shown to be formed during the mechanisms of thioredoxin reductase and glutathione reductase. A stable mixed

disulfide between Cys138 of *E. coli* thioredoxin reductase and Cys35 of its substrate thioredoxin has been characterized [51]. The carboxylate of Asp26 of the substrate thioredoxin deprotonates the thiol of Cys35 to facilitate its attack on Cys 138 of the enzyme thioredoxin reductase to form a Trx-TrxR mixed disulfide. [237]. A mixed disulfide has been shown to occur between glutathione and Cys58 of glutathione reductase in its 3 Å crystal structure, the covalently bound glutathione being the second to leave the GSSG binding site [238] (Figure 3.8) Mixed disulfide formed during catalysis by glutathione reductase from human erythrocytes is stable over a wide range of pH [33]. The proposed mechanism underscores the importance of His of the catalytic dyad in protonation of the first glutathione molecule through positioning of its proton to polarize the mixed disulfide bond. The interchange thiol hence becomes accessible for a nucleophilic attack by the charge transfer thiol.

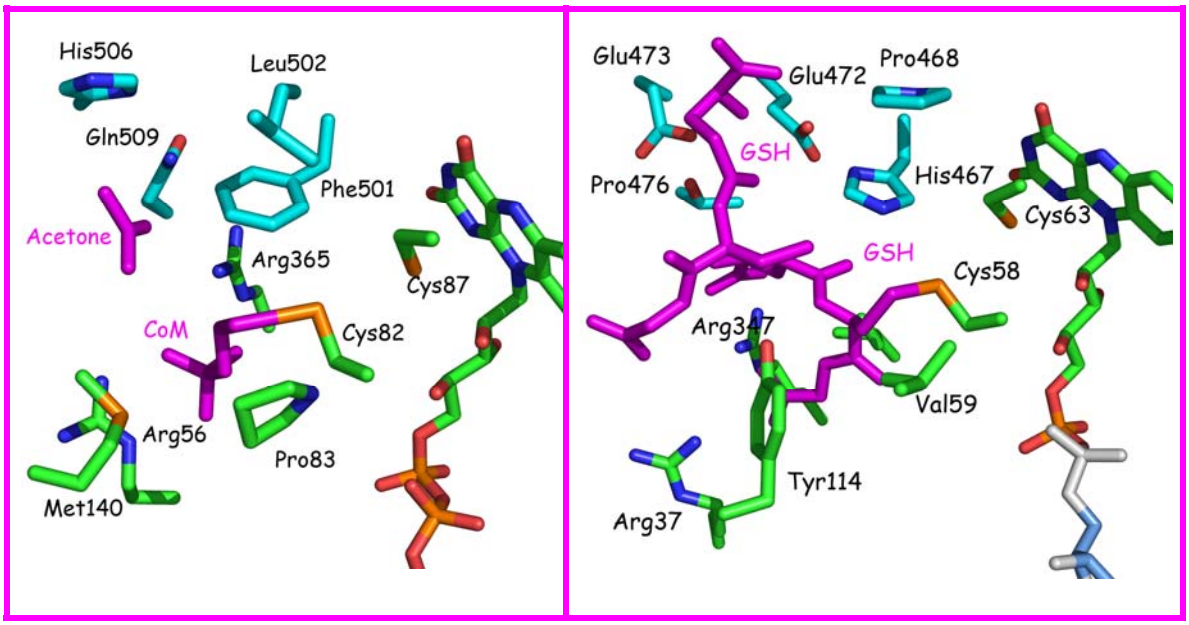

Figure 3.8: Positions of mixed disulfide and one of the products (acetone/GSH) shown in KPCC (left) and GR (right). Residues from the two subunits are identified through cyan and green carbons

The Catalytic Dyad

2-KPCC is different from the group 1 FDRs in not having the conserved HXXXXE sequence in the C-terminal region that occurs in the rest of the members. Instead it has an FLNPTH (residues 501-506) sequence whose involvement in catalysis is not clear from the substrate or the product bound structures. A comparison of the positioning of Phe501 and His 506 with that of His467 and Glu472 of the catalytic dyad of mammalian glutathione reductase shows quite similar placement of these residues in relation to the substrate C-S / S-S bonds as well as to the redox active cysteine disulfide (Chapter 2, Figure 2.4). A histidine to phenylalanine mutation in lipoamide dehydrogenase from *Azotobacter vinlandii* has been shown to render the enzyme almost completely inactive in both directions [239]. A histidine to pheylalanine as well as a histidine to tyrosine mutation results in a lowered pKa of the charge transfer thiol due to lowered influence of the interchange thiol on the former. This in turn is attributed to the enhanced interaction of the interchange thiol with a hydronium ion which is enhanced in an apolar environment. In the mixed disulfide bound structure of 2-KPCC, a water molecule is present in the proximity of the mixed disulfide and might have the role of initiating the cleavage of the mixed disulfide to release CoM. It can be speculated that the presence of a non-polar as opposed to a basic residue in the 2-KPCC substrate binding site is important for enhancing the interaction of the water molecule with the mixed disulfide once the ketopropl CoM moiety of the substrate has been released. The role of glutamate residue of the catalytic dyad in glutathione reductase [33] and lipoamide dehydrogenase [42] is to stabilize the histidine through hydrogen bonding resulting in a lowered pka of the latter. His506 in 2-KPCC is too far (10 Å) from the

active site redox active disulfide or the 2-ketopropyl CoM C-S linkage (8 Å) in the 2-KPCC crystal structure, thus unlikely to take part in substrate protonation. In 2-KPCC there are no other interactions that can be rationalized to supplant the role of the catalytic dyad in the DSORs and this we have attributed to be favorable in the context of the ability of the enzyme to discriminate and favor carboxylation over protonation [71].

Although decarboxylation of acetoacetate is a thermodynamically favorable reaction that occurs spontaneously in aqueous solutions, 2-KPCC catalyzes the reaction at a low rate (4.1 nmol acetone formed $.min^{-1}.mg^{-1}$ above the abiotic rate) which increases 77-fold when CoM is included in the assay [68] indicating that the formation and release of the mixed disulfide might be related to the decarboxylation and carboxylation processes respectively.

Product Binding and release

2-KPCC catalyzes the reverse reaction i.e. the conversion of acetoacetate to KCoM and CO_2 in the presence of CoM [68]. The trigonal planar electron density modeled as acetone exists adjacent to the CoM moiety of the mixed disulfide in the substrate binding site in a cavity that is occupied by a water molecule in the substrate bound state. The best fit of the acetone molecule to the density shows the carbonyl oxygen stabilized by hydrogen bonding to a water molecule and Nε2 of the side chain of Gln509 of the other subunit with the two methyl groups facing a part characteristically composed of non-polar residues (Figure 3.8). Gln509, although not a part of the FLNPTH sequence that corresponds to the conserved HXXXXE sequence of the DSORs, occurs close enough to suggest that interactions between the physiological product acetoacetate

and residues of the FLNPTH sequence are possible. A structure of 2-KPCC with a CoM disulfide bound to the active site was obtained on incubating 2-KPCC with coenzyme M [209]. The binding of a second sulfonate moiety in this structure is stabilized through interactions with His506 and Arg365. We have proposed that the product acetoacetate could get stabilized in a similar way. This would suggest that the presence of a Phe-His pair instead of the His-Glu pair of the catalytic dyad of other DSORs could also serve to stabilze and release products, albeit in a different manner.

There is good superimposition of residues of the substrate and product bound structures in the active site region showing no major changes of conformation accompanying the formation of acetone. The binding site for acetone in the product bound structure comprises of residues contributed by both subunits and lies close to the surface so that the molecule is visible from the surface of the molecule. The residues lining the pocket with acetone at the bottom appear suited to channel the exit of acetone. From the structural information obtained from the CoM disulfide bound structure, it is possible that a wider opening of this channel occurs to release acetoacetate. This can only be established, however, with the enzyme captured with acetoacetate bound to the active site.

FAD Binding Domain

As shown in figure 3.3 and 3.9B, the FAD-binding domain forms at the N-terminus from regions of peptide chain that are not contiguous. The N-terminus, as compared to other DSOR members, has a 40 amino acid extension. There is an 18 amino acid N-terminus extension in glutathione reductase which has been shown to not have

any influence on the catalytic activity of the enzyme [240]. An all atom superimposition of the native and substrate bound crystal structures of 2-KPCC (RMSD=0.92), however, shows a movement of this N-terminus region by 3 Å towards the substrate so as to constrict the substrate binding cavity. It is concluded that this region has a role to play in holding the substrate in place once it is bound at the active site, effectively closing the site to further influx/efflux [71]. The FAD-binding domain consists of a single Rossman fold and a β meander [241, 242] formed from non-contiguous regions of the peptide chain (Figure 3.9 B). The central region of parallel β sheets is formed by β3, β4, β5, β9 and β20 with α2 and α11 being the helices on its side while β6, β7 and β8 form the β meander of antiparallel β sheets. β20 and α11 occur in the central domain, separated from the FAD binding domain by the NADP binding domain. As in glutathione reductase, the central domain interconnects the other three domains by forming interactions with regions within them [243]. The signature motif of the Rossman fold, $GXGXXG(X)_{17}D/E$ [242, 244-246] (Figure3.2, maroon box) is well conserved in all DSORs and occurs in α2 and β4 of 2-KPCC. The 11 amino acid segment T(S)XXXXXF(Y)hhGD(E) (X=any amino acid, h=hydrophobic amino acid) , another highly conserved motif in oxidoreductases first identified from studies of rubredoxin reductase [247], occurs in β20 and its flanking loops (Figure 3.3, green box). The ATG domain oohhhATG (o=polar or charged residue), highly conserved in all other DSOR members, occurs at the end of β7 of the FAD domain as KNLILAVG (Figure3.3, orange box). The partially conserved motif $D(X)_6GXXP$ [248] has been observed to occur in the Glutathione reductase like NADPH binding proteins at the interface of the FAD and NADPH binding domains. As part of the FAD domain of 2-KPCC is formed by the first

half of the central domain, this motif occurs at the junction where the NAD domain ends and the central domain begins encompassing β18 and β19 (Figure3.3, purple box).

The structure of the substrate bound 2-KPCC determined to 1.55 Å shows clear density for FAD (Figure 3.9 A) so that a detailed analysis of interactions of surrounding residues with the cofactor is possible. FAD binds to each monomer in an extended conformation with the isoalloxazine ring occupying a cavity in the centre of the monomer with the rest of the molecule extending into the protein. The isoalloxazine ring divides the active center into two parts: the *re* side of the ring faces the NADP molecule while the redox active disulfide is present towards the *si* face. The adenine moiety points towards the FAD fold while the isoalloxazine ring points away from it (Figure 3.9 B).

The formation of a flavin C(4a)-thiol adduct has been shown by absorption spectroscopy [27]. The substrate used for these studies, 1,3 -propanedithiol, when added to the enzyme along with $NADP^+$ showed the appearance of a band with a maximum at 580nm within 5.6ms. By analogy with similar studies on Lipoamide dehydrogenase [216, 249], it was concluded that this is due to the formation of a charge transfer complex between FAD and the proximal cysteine thiolate with $NADP^+$ bound. A new band with absorption maxima at 402 nm, representing the flavin C(4a)-thiol adduct by analogy with Lipoamide dehydrogenase and mercuric ion reductase [217], was observed as the reaction progressed further. The two bands (A_{max}=402nm and A_{max}=580nm) were also observed on the addition of NADPH to the enzyme in the absence of 1,3-propanedithiol, representing the covalent adduct and charge transfer complexes respectively.

The mixed disulfide bound structure of 2-KPCC shows a movement of the proximal cysteine sulfur ~0.1 Å towards the isoalloxazine ring as compared to that of the

substrate bound structure (Figure 3.10). In both structures, the proximal cysteine thiol is approximately the same distance from C4a and C10a of the isoalloxazine ring. The charge transfer complex has been shown to form in the presence as well as absence of $NADP^+$ and the presence of NADPH [27]. The condition appears to be the presence of a mixed disulfide between the substrate and the distal cysteine thiol. The distance between proximal cysteine thiolate and isoalloxazine C4a and C10a atoms, (~3.4 Å) probably represents the charge transfer complex in the mixed disulfide and $NADP^+$ bound structure and probably represents the stable form of the two electron reduced form EH2. Reduction to the EH4 form is very hard to achieve [27]. Even in the presence of 40-fold molar excess of NADPH or 16-fold molar excess of dithionite, a small amount of semiquinone remains. A ^{13}C-NMR study of *A. vinelandii* lipoamide dehydrogenase and erythrocyte glutathione reductase at the Eox, EH2 and EH4 levels, shows that the flavin in the EH2 forms of the two enzymes is strongly polarized and that higher π-electron density is stabilized at the C4a position in glutathione reductase than in lipoamide dehydrogenase [250]. Complete reduction of EH2 to EH4 form of these enzymes can occur with dithionite. The extinction coefficient of the charge transfer species of lipoamide dehydrogenase and glutathione reductase decrease as the pH is lowered due to the protonation of the proximal thiol [251, 252].

The formation of flavin C4a-thiol adduct occurs under turnover conditions in 2-KPCC. This species has been observed in mercuric ion reductase at low pH [219] and in a blocked mutant [217], in thioredoxin reductase with FAD substituted by 1-deaza-FAD [218] and in a covalently modified lipoamide dehydrogenase [216]. In all cases, the protonated state of the proximal cysteine thiol is thought to be the factor that determines

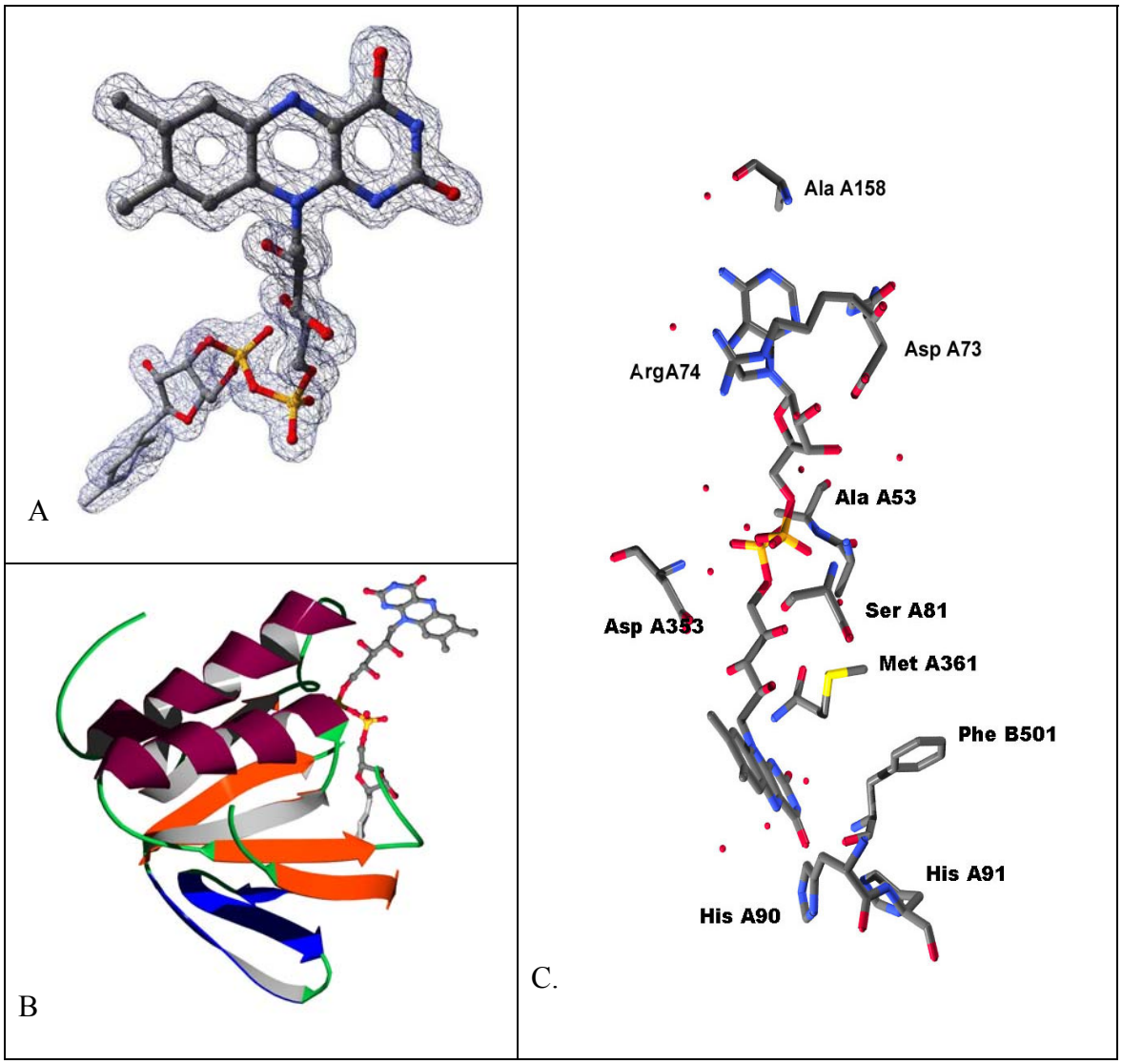

Figure 3.9: A. Electron density around FAD molecule in KPCC contoured to 1 σ . B. FAD binding domain of KPCC color coded to match the secondary structure in the structure based sequence alignment of figure 3.2. **C**. Residues withing 3.5 Å of the FAD molecule in 2-KPCC

the formation of the C4a-thiolate adduct. Lower pH, raised pKa of the proximal thiol and the presence of $NADP^+$, cause the accumulation of the C4a-thiolate adduct, while a higher pH favors the formation of the charge transfer complex. The C4a-thiolate adduct in case of 2-KPCC was observed at pH 7.0, but not at pH 9.0. There was however, no intentional attempt to keep the proximal thiol protonated to achieve this. In case of

thioredoxin reductase, glutathione reductase and lipoamide dehydrogenase, the presence of a proton donor that would protonate this thiol, forms an integral part of this mechanism. Mercuric reductase, however, like 2-KPCC, does not have a catalytic acid residue in close proximity to the proximal thiol. In wild type mercuric reductase [219], the formation of the adduct was observed at a low pH (5.0) although the completion of formation was ~30%. The same effect was achieved to a higher completion with a change in the pKa of the proximal thiol. This can be carried over to the case of 2-KPCC to speculate that the pKa of this cysteine, due to the different environment of the active site, might be on the higher side as compared to the other DSORs, so that a covalent adduct was observed without modifications. The speculation would however be stringent upon the similar absorption spectroscopy experiments conducted with the physiological substrate 2-ketopropyl coenzyme M.

Although the primary sequence of 2-KPCC shows the conservation of all motifs known to be present in the flavin disulfide oxidoreductases (Figure 3.3), the interactions of the FAD molecule differ compared to the group 1 FDRs (Table 3.2). In 2-KPCC, the oxygen on C4 of the isoalloxazine ring, O4, hydrogen bonds with the Nε of His90 and His91 while N3 and N5 of the ring each interact with a water molecule . The interactions of N3, O4 and N5 are invariably with a histidine and a lysine respectively in group 1 FDRs. This histidine interacting with N3 in the group 1FDRs belongs to the catalytic dyad of the conserved HXXXXE motif on the other subunit.

A phenylalanine residue is present at this position in the NAD-dependent group 3 FDR NADH peroxidase that hydrogen bonds to N3 through its main chain carbonyl oxygen. 2-KPCC, though NADP dependent, also has a phenylalanine at this position.

The histidine residue of the His-Glu catalytic dyad acts as the general acid for catalyzing the oxidative half of the overall reduction of R-S-S-R substrates [42, 195] in glutathione reductase, lipoamide reductase and mammalian thioredoxin reductase. Mutations of the His or Glu in glutathione reductase and dihydrolipoamide reductase have been shown to cause an accumulation of the transiently reduced intermediate $FADH_2 \cdot NADP^+$ [36, 195, 253] due to impaired transfer of electrons to the redox disulfide from $FADH_2$.

Histidine of this catalytic dyad has been assigned several roles through mutational studies of the residues (His and Glu) of the catalytic dyad in lipoamide dehydrogenase [42]. Aside from protonating the leaving group during catalysis, it plays an important role in maintaining the redox potential of the active site to avoid over reduction by NAD as well as facilitating internal electron transfer between the two redox centers in the reductive half of the reaction. The residues in 2KPCC that correspond to this catalytic dyad of the HXXXXE motif of DSORs in the multiple sequence to structure alignment (Figure 3.2) are Phe501and His506, which are present in the vicinity of the isoalloxazine ring (Figure 3.10 C). Resonance Raman spectral studies in yeast glutathione reductase have shown that the hydrogen bonding between the isoalloxazine ring and the surrounding atoms influences the redox potential of the flavin [254]. Due to the difference in the interactions of the ring with the surrounding protein environment as compared to the other DSORs, the redox potential of flavin in 2-KPCC can be rationalized to suit electron transfer to a substrate that differs from the conventional –S-S-containing DSOR substrates in an environment that needs to be hydrophobic for preferential carboxylation over protonation of the enolacetone intermediate.

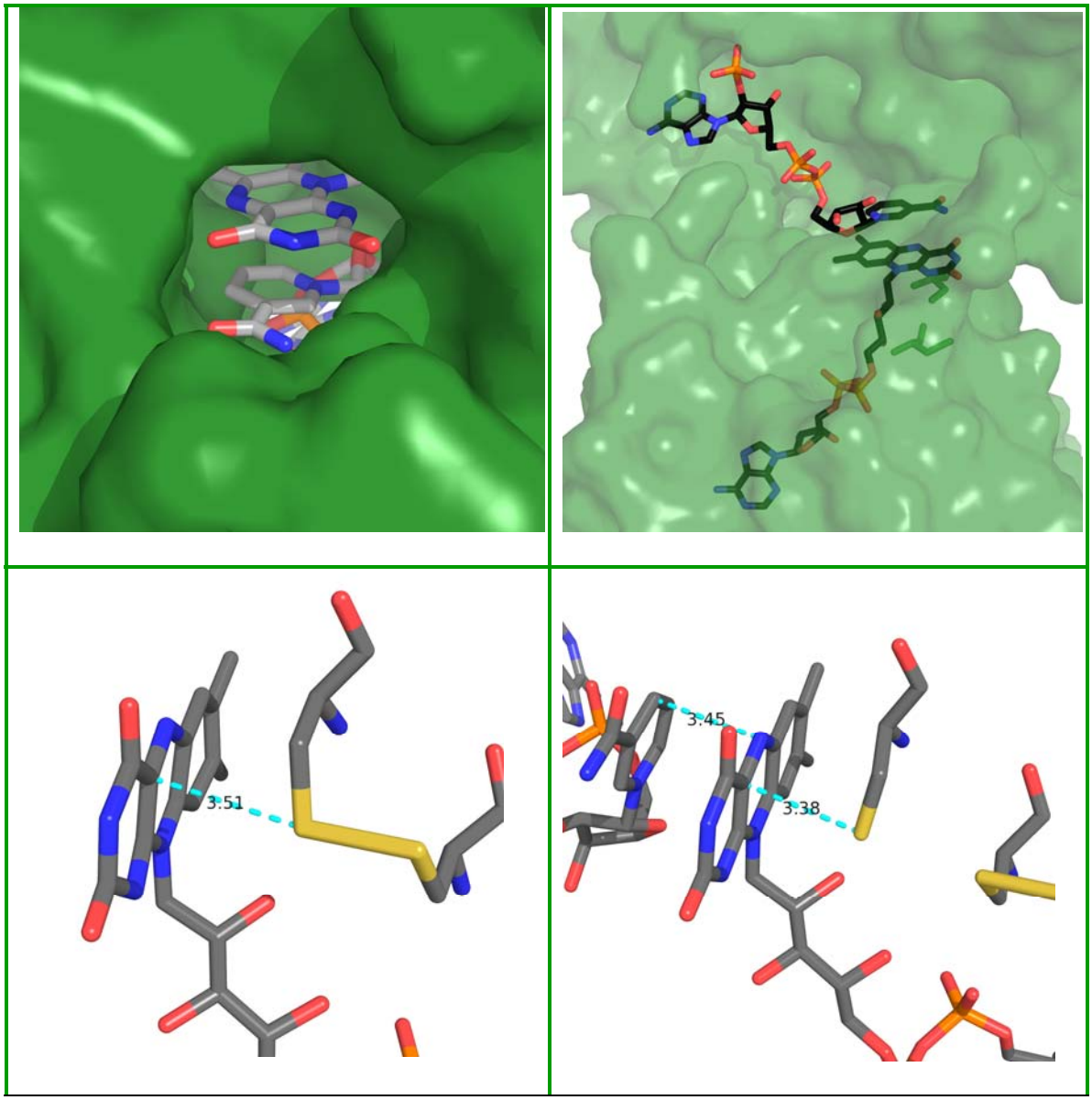

Figure 3.10: Top left: Central hole in a 2-KPCC monomer showing the isoalloxazine and pyridine rings stacked on each other. Top right: Side view of transparent surface of 2-KPCC monomer showing the extended binding of NADP+ and FAD. The redox active cysteines are shown in green. Bottom: The distances between the proximal cysteine (Cys87) sulfur atom and C4a of the flavin isoalloxazine ring (left) and the same in addition to the nicotinamide C4 and isoalloxazine N5 distance.

Table3.2. Interactions of FAD with the protein residues in structurally characterized disulfide oxidoreductases. 3GRS: Human glutathione reductase, 1NPX: NADH peroxidase (*Enterococcus faecalis*),1FEC:Trypanothione reductase (*Crithidia fasciculata*), 1H6V:mammalian thioredoxin reductase (*Rattus norvegicus*), 3LAD: Dihydrolipoamide dehydrogenase (*Aztobacter vinelandii*), mer A: mercuric reductase. Numbering of atoms follows protein data bank convention..Van der Waals interactions and C…H hydrogen bonds have been excluded

	3GRS	1NPX	1FEC	1H6V	3LAD	merA	2KPCC
Isoalloxazine							
N1	----	A 299 N		T 343 Oγ1	----	----	----
N3	H 467 O	F 424 O	H 460 O	H 472 O	H450 O	----	F501O
N5	K 66 Nζ	w	K 59 Nζ	K 67 Nζ	----	----	w
N10	---	C 42 Oδ2	Y 197 O	---	---	----	---
O2	w	A 299N, w	T334 N, w	T 343 N	A326 N	----	w,w,M361 N
O4	K 66Nζ	w	K 59Nζ w	K 67 Nζ	K57 Nζ	K216Nζ	H90Nε2,H91 N
Ribitol							
O2*	---	---	---	R 293 O	---	----	D 353 Oδ1
O3*	D 331 Oδ	D 281 Oδ	D 326Oδ1	D 34 Oδ1	---	D472Oδ2,D4	w
O4*	---	---	---	S22Oγ,T34	---	T 206 Oγ1	---
Phosphate (FMP)							
O1P	G31N, w	S110Oγ,G11N	G 14N, w	G 23 N	G 14N	G 179 N, A 1	D353, w
O2P	D33N, w	D 281N, w	D 326 N ,	D 34 N	D 318N, w	D 472 N	w,A53 N,A54 N
Phosphate (Adenine)							
AO1	T 57Oγ1	R132 NH1, w	S 13N,T 5(	T 58 Oγ1	T 47 N	---	A 53,w
AO2	w	S 9 Oγ	T Oγ1,w	S 22 N,S 22	T 47 Oγ1	T 206 N	S 81Oε,w ,w
Ribose							
AO2*	E 50 Oε2,	E32 Oε2	D34 Oδ1,w	F 43 O	E 33 Oε1	---	D 73Oδ, w
AO3*	E 50Oε1,w	E 32Oε1,E 32	D34 Oδ2	-----	E 33Oε2	E 199Oε1,E 1	D 73Oδ, w
AO4*	-----	-----	-----	D42 Oδ1	-----	-----	-----
Adenine							
N1	A 13 N	I 79 N	G 126 N	G 132 N	G 121 N	S 280 N	A 158N
N3	--	K 33N	---	F 43 N	---	---	R 74 N
N6	A 13 O	I 79 O	G 126 O	G132 O	G121 O	S 438Oγ,S 28	w, w
N7	----	N 247 Oδ1	w	---	---	---	w

Interactions of ribitol, pyrophosphate and ribose moieties in 2-KPCC are quite similar to those of the FDRs (Table 3.2). There is, however, a stacking of Arg74 on the adenine ring not present in the DSORs examined here (Figure 3.10 C). This is one of the

features that have been observed to result in preferential binding of $NADP^+$ over NAD^+ by pyridine dinucleotide binding proteins [255]. In a large scale data mining of the PDB to analyze molecular determinants for recognition of adenine moiety of ATP by proteins [256], cation-π interactions between a lysine or arginine and adenine bases were found to exist in 59% of the protein adenylate complexes. The most remarkable feature of cation-π interactions was found to be their large strength of interaction ranging from -8.01 to -16.10 kcal / mol. A stacking of arginine above / below the adenine ring facilitates multiple modes of intermolecular interactions namely cation – π and π – π stacking between guanidinium and adenine base. Arg74 in 2-KPCC stacks above the adenine ring and also hydrogen bonds to the N3 of the adenine ring resulting in stabilization of the latter. There is a similar stacking of a lysine on the adenine ring of FAD in NADH peroxidase, a group 3 FDR. The conserved GXGXXG (X)17D / E sequence motif occurs between the first β sheet and α helix of the Rossman fold of the FAD domain (Figure 3.2, maroon). In 2-KPCC, the conserved Asp residue from this motif hydrogen bonds to 2*O of ribose as in other FDRs. The redox active disulfide occurs on α helices that constitute an excursion before the secondary structure returns to being a part of the FAD fold, which is also the case in human glutathione reductase [242]. These helices are far removed from the FAD molecule, but occur on the dimer interface where they form intimate contacts with regions of the other subunit. The redox active cysteines are a part of highly conserved amino acid sequence, GGTCV/LNVGCV/IP on the first of these helices. The corresponding sequence in 2-KPCC is GGSCPHNACVP several of which form contacts with residues from the other subunit. The helix extends along the *si* side of the isoalloxazine ring placing the SH groups of the charge transfer cysteine (Cys87)

close to C4a for electron transfer and the imidazole rings of His90 and His91 towards the top to stabilize the anionic FAD formed during electron transfer. The Ser / Thr residues preceding CysN in 2-KPCC as in all other DSORs, hydrogen bonds to the phosphate of AMP. The last β sheet and second α helix of the FAD binding domain are contributed by the central domain where the conserved T(S)xxxxxF(Y)hhGD(E) motif of the dinucleotide containing proteins encompasses the last β sheet and its flanking pentapeptides (Figure 3.3). The highly conserved aspartate of this sequence hydrogen bonds with the ribitol and phosphate of flavin monophosphate.

NADP(H) Binding

The NADP domain is similar to the FAD domain and consists of a single βαβαβ Rossman fold motif followed by a β meander more typical of the FAD domains instead of a second βαβαβ Rossman fold motif (Figure 3.11 B). The central open twisted parallel β sheets of the Rossman fold are β12, β13 and β14 flanked by α 8 and α9 on one side and the β meander formed by β15, β16 and β17 on the other. The finger print motif GXGXXG/AXE highly conserved in the dinucleotide binding proteins is conserved in 2-KPCC as in all DSOR members (Figure 3.3). It occurs in the loop connecting β12 and α8. This motif binds the pyrophosphate moiety of NADP in NADP binding proteins and mutations within the sequence generally render the enzyme inactive [31, 35, 257]. In 2-KPCC, as in mammalian thioredoxin reductase and some mercuric reductases (*Shigella flexneri*, *Thiobacillus ferrioxidans*), a serine occurs instead of the second glycine in the GXGXXG/A motif.

The structure of 2-KPCC with NADP(H) and mixed disulfed bound has been determined at a resolution of 2 Å [209]. NADP binds in an extended conformation with the nicotinamide moiety stacked on the isoalloxazine ring and the rest of the molecule extending into the NADP binding domain on the surface of the protein molecule (Figure 3.10 Top). The nicotinamide ring is stacked over the central ring of the isoalloxazine ring such that the C4N of NADP is 4 Å from C4a of isoalloxazine. A lysine residue (Lys224) from within the conserved GXGXXG sequence between β12 and α8 of the β12-α8- β13 Rossman fold occurs on the *re*-face of nicotinamide ring (Figure 3.12, Bottom). In the absence of NADP, it is hydrogen bonded to Glu360, Asp 389 and a water molecule (Figure 3.13) . When NADP binds, additional interactions occur between the Nz of Lys 224 and the main chain O of Phe390 as well as N2N of the carboxyamide of the nicotinamide ring. Lys 224 is stacked on the latter and probably serves to stabilize it as well as protect it from solvent access in the oxidized enzyme (Figure 3.13). A tyrosine residue is present at an equivalent position in glutathione reductase (Figure 3.12 Top), mammalian thioredoxin reductase, trypanothione reductase, adrenoredoxin and mercuric reductase, in each of which except mercuric reductase, it has been shown to block the NADP-binding site in the absence of the latter. In human GR, this conserved tyrosine assists the His-Glu pair in the general acid base catalysis [258]. This conserved Tyr moves aside to accommodate the nicotinamide ring in the presence of $NADP^+$ as part of conformational changes in the NADP domain on NADP binding. In *E. coli* glutathione reductase, this Tyr residue (Tyr 177, Figure 3.12) was changed to a Phe, Ser and Gly by site directed mutagenesis [259]. The Y177F mutant showed very slight changes compared to the wild type, the Y177S and Y177G mutants showed a marked decrease in

the turnover numbers and an alteration in reaction kinetics that could be explained by ordered sequential mechanism as opposed to ping-pong in the wild type. This was attributed to the slower rate of reduction of FAD by NADPH. In *E. coli* thioredoxin reductase which lacks an interface domain, the NADP domain has been shown to rotate 67º to allow NADPH to react with isoalloxazine ring [54]. Adrenodoxin reductase shows a less dramatic displacement of 2.5 Å of a part of NADP domain relative to the FAD binding domain on NADP binding [260]. In other DSORs, a tyrosine conserved in the GXGYXG/A occupies the space on the *si* side of FAD and moves aside when NADP binds. In 2-KPCC however, Lys224 stays in the same position and conformation on NADP binding in the space between the lysine and the isoalloxazine which otherwise is filled with water molecules.

The binding of NADP in 2-KPCC is accompanied by displacements in the NADP domain centered in the GXSXXA motif on the loop between β12 and α8. The largest change occurs on Ser223 where the Cα of this residue moves by 1.75 Å away from the site where the 2' PO_4 of NADP binds (Figure 3.13). This results in an overall displacement of the side chain OH group of Ser223 by 3.48 Å away from this site. This movement is transmitted to the residues on the N-side of Ser223 such that the Gly222 and Gly 221 move about an Å away from the 2'PO_4 binding site. This displacement, however is not transmitted to the residues carboxy to Ser223. Lys224, as stated earlier, remains largely fixed in its position. It seems to act as a hinge across which motion is

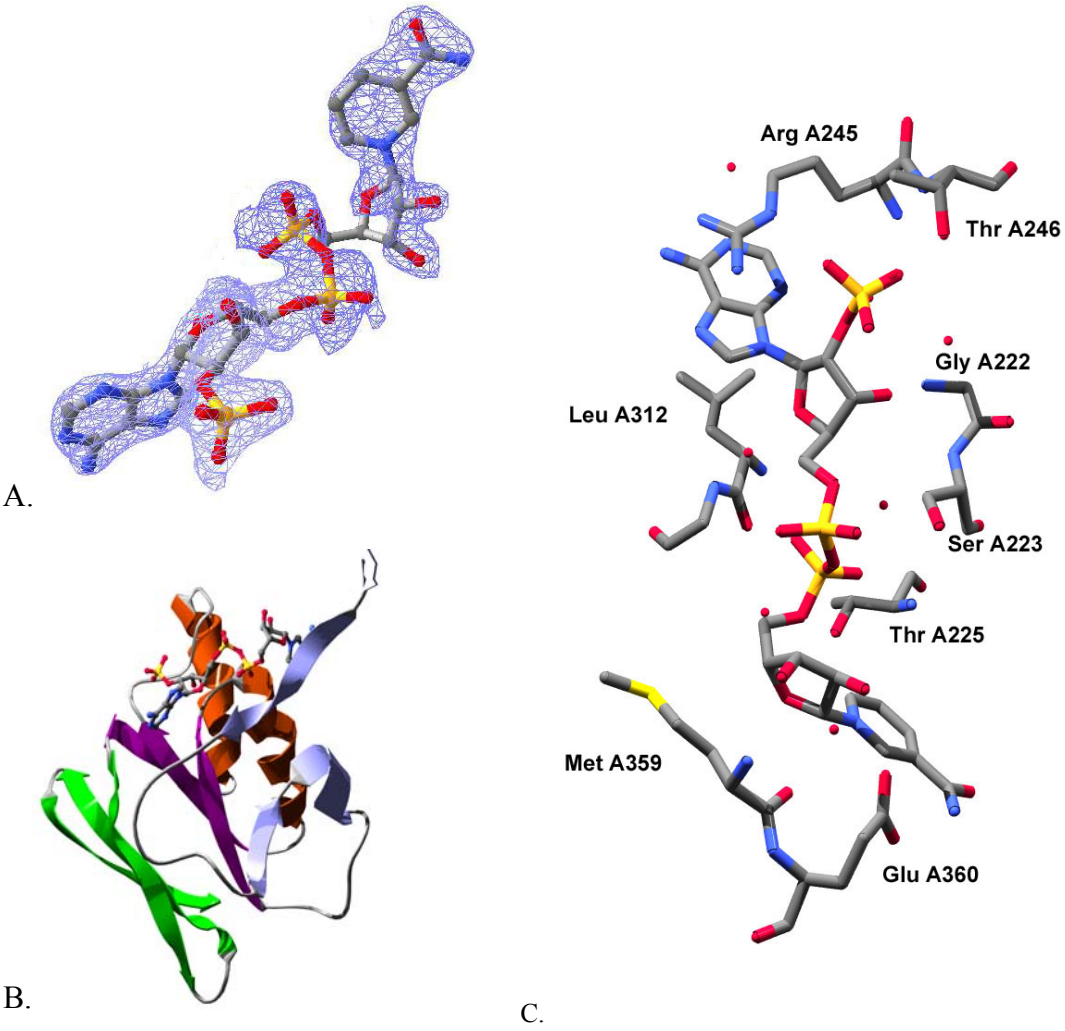

Figure 3.11 : A: Electron density around NADP molecule contoured to 1 σ. B. The NADP domain of KPCC, color coded to match the structure based sequence alignment shown in figure 3.2 C. The residues of the NADP binding site including water molecules involved in non-covalent interactions with NADP

communicated to the next few residues of the motif due to the outward displacement of Ser223. This causes Thr225 to move forward to enter into Van der Waals interaction with C5N of nicotinamide. This motion, however, is discernible only in one of the subunits.

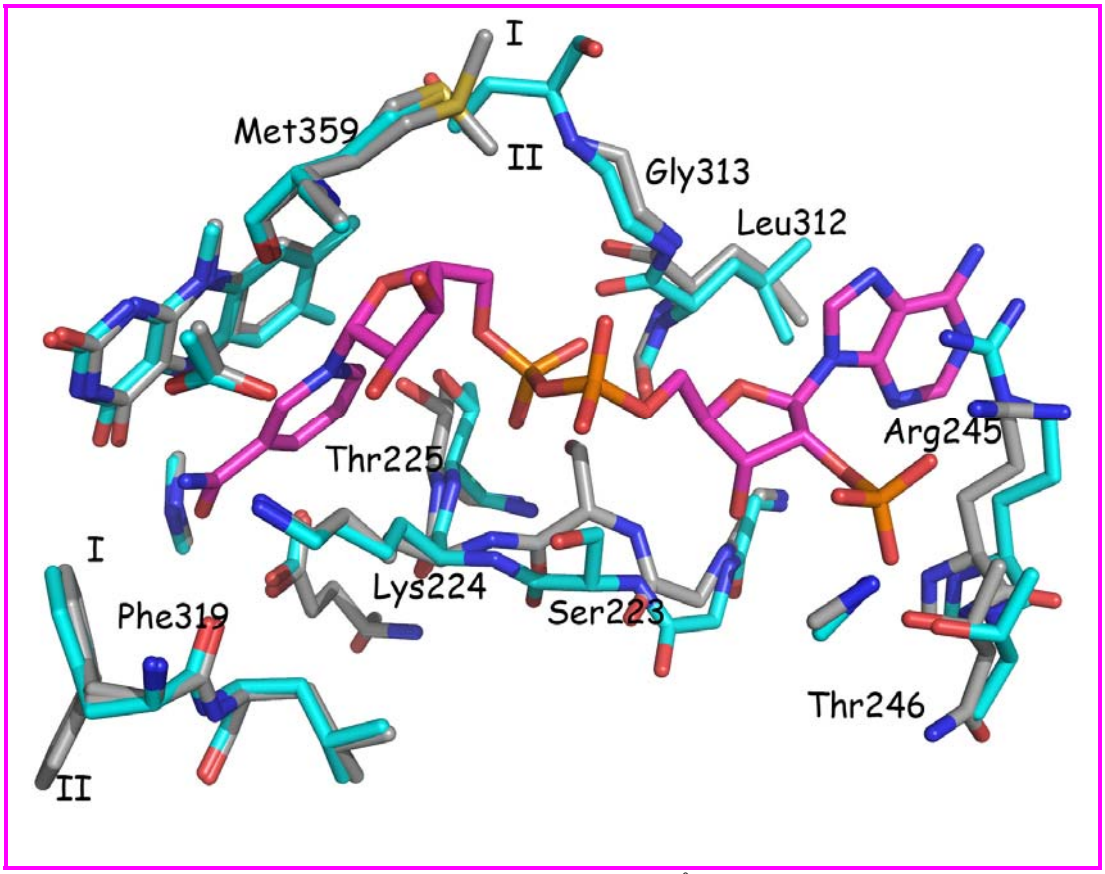

Figure 3.13 A superimposition (RMS=0.237) of the 1.51 Å substrate bound 2-KPCC structure (gray carbons) on the mixed disulfide structure (cyan carbons) showing the residues in the NADP binding region. Only the residues that move on NADP binding are labeled. The NADP molecule is shown with magenta carbon atoms. I and II in case of Met 359 and Phe 319 represent two alternate conformations of the side chain discernible in the high resolution substrate bound structure.

Another prominent change in the amino acid side chain conformation occurs at the end of the first Rossman fold between β13 and α9. All NADP dependent oxidoreductases have a conserved arginine in this loop region except lipoamide dehydrogenase that utilizes NAD^+ instead of $NADP^+$ and has an alanine instead. This arginine forms a stacking interaction with the adenine moiety of $NADP^+$ and hydrogen bonds to the phosphomonester, and is considered to be a determinant of the specificity of

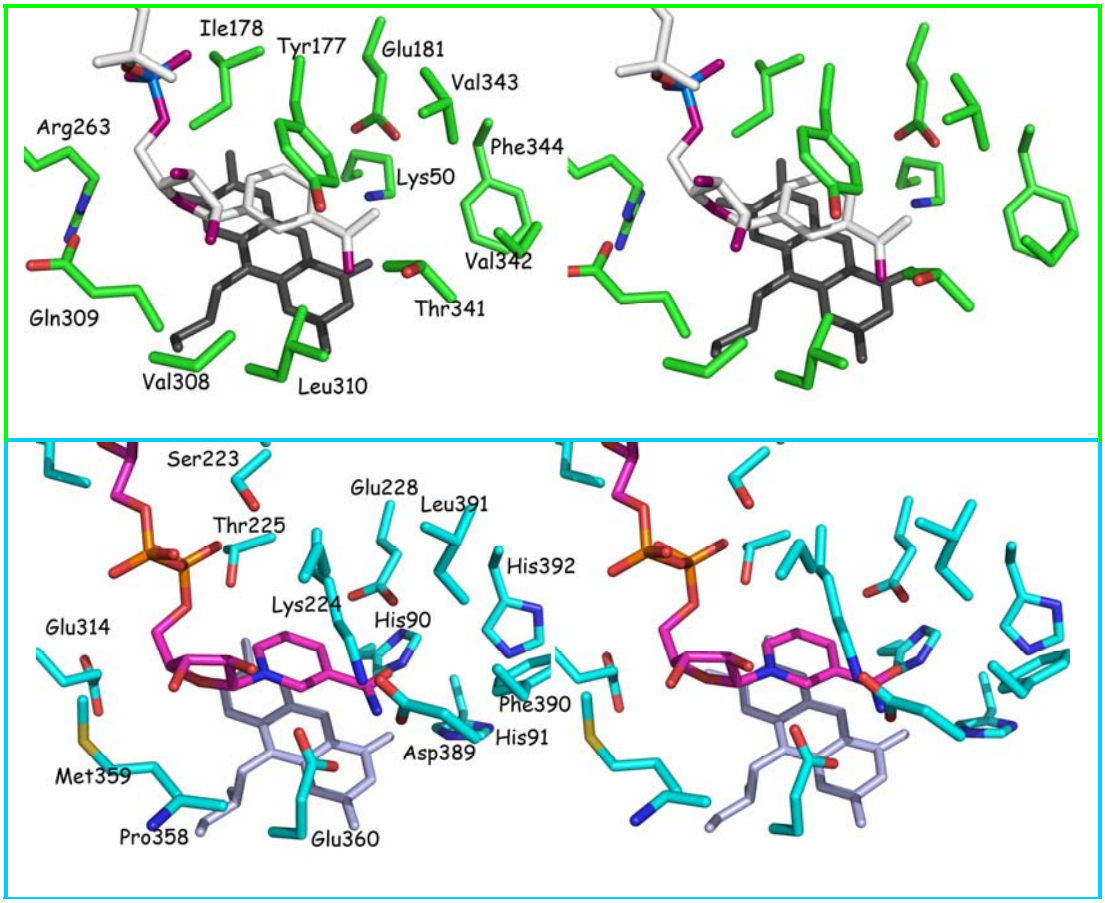

Figure 3.12 Top: Wall eyed stereo of the NADP binding site of *E.coli* glutathione reductase. FAD is shown in black and NADP in white and purple. Bottom: Wall eyed stereo of the NADP binding site in 2-KPCC. FAD is shown in gray and NADP is shown in pink.

these enzymes for $NADP^+$ as opposed to NAD^+ [255]. In 2-KPCC, Arg245 rotates about 99 º towards the adenine ring to stack on to it (Figure 3.13), stabilizing the latter. In this conformation, NH_1, NH_2 and Nε of its side chain form hydrogen bonds with the 2' phosphate and N6 of adenine and water as compared to a single hydrogen bond to a water molecule in the conformation when $NADP^+$ is absent.

As with other $NADP^+$ dependent DSORs most of the interactions of $NADP^+$ occur with the 2'phosphate of the adenine ribose (Table 3.3) with residues within the NADP binding domain and a few from the central domain. A majority of these in turn come

Table 3.3. Interactions of NAD/NADP with the protein in disulfide oxidoreductases. Numbering of atoms follows Protein Data Bank convention.1GRA:Gutathione reductase (*Homo sapiens*), 1TYP: Trypanothione reductase (*Crithidia fasciculata*), 1H6V: Thioredoxin reductase (*Rattus norvegicus*), 1LVL: Dihydrolipoamide dehydrogenase (*Pseudomonas putida)*

	1GRA	1TYP	1H6V	1LVL	2KPCC
Nicotinamide					
NN7				R 226O, w	E 228 Oε1
NO7					E 360Oε1, K 224 Nz
Ribose					
NO2*		Y198 Oγ		M311O, Y181Oγ	E360Oε2, w
NO3*			E 341 Oε2	Tyr181 Og,w	M359N, w
Phosphate (Nicotinamide)					
NO1			R 166NH2, V 299N	A263 O	T 225 N, w
NO2					L 312 O
Phosphate (Adenine)					
AO1	w,w,w				w
AO2	w, w, w, w				
AP	w				
Ribose					
AO2*					w
AO3*	w	w, G196N	S 199N	E 201 Oε1	S223N,G222N,w
AO4*	A 195N				
2' Phosphate					
AOP1	R 218NH2,R 224NH2	Y 221 Oγ	R 226 Nε		w
AOP2	R218 Nε, w	R228 NH2	R 221 NH1		R 245 NH2, R245 Nε, w
AOP3	R 224 Nε, w, w		R221NH1, S222 Oγ		T 246N,T 246Oγ, w
Adenine					
AN3	w				w
AN6	w				R 245 NH1
AN7	w				w
AN9			R 221NH1		
stacking	R 218	R 222	R 221	R 226	R 245

from the Rossman folds of the domain. The GXGXXG/A motif as shown above plays a major role in interacting with and stabilizing NADP bound state of the enzyme. The importance of the conserved glycines in NADP binding has been investigated in the case

of glutathione reductase [261-263]. The first glycine of this fingerprint motif is conserved in all DSORs and is responsible for the tight turn of the main chain at the end of the first β chain. The role of the second glycine had been assumed to be more functional than structural in these studies. Mutations where this second glycine was changed to serine in glutathione reductase showed that the enzyme still retained 19% of the activity [263]. 2-KPCC and mammalian thioredoxin reductase both have a serine in this position.

Conclusion

2-KPCC has structural and 30% sequence similarity to the FAD containing NADP dependent oxidoreductases that catalyze the reductive cleavage of disulfide / metal ion substrates. Although most of the conserved sequence motifs of dinucleotide binding proteins also occur in 2-KPCC, certain differences in interactions are notable as compared to other disulfide oxidoreductases. It can be rationalized that these differences are present such that the reduction potentials of FAD / NADP / the redox active disulfide cysteines are optimized for electron transfer to a thioether linkage of the substrate. Marked differences in the active site residues, highly conserved in other DSORs, specifically the active site catalytic histidine and glutamate, indicates the presence of a mechanism adapted to a preferential carboxylation over the protonation as occurs in the DSORs. There are no proton donating residues close to the substrate to stabilize the proposed enolate intermediate other than a histidine-glutamate pair stabilized water molecule. The product, acetone, is stabilized by hydrogen bonding to a glutamine side chain amide NH and in CO_2 depleted conditions, this group might be the proton donor to

the acetone molecule. The distinct hydrophobicity of the active site region is maintained in both the substrate and product bound forms suggesting an effort on the part of the enzyme to keep the environment conducive to CO_2 entry while blocking the entry of protons. .A multiple sequence to structure alignment of 2-KPCC with other DSOR members shows good alignment of the secondary structure elements (Fig.1). The residues between the redox active cysteines are hNVG in GR, TrxR, TR and LAD, while in 2-KPCC these are PHNA. The His residue of this sequence hydrogen bonds to another histidine residue (His 137) which in turn hydrogen bonds to a water molecule that presumably stabilizes the enolate intermediate. The fingerprint motif GXGXXG/A of the Rossman fold [264] in the NAD binding domain occurs as GXSXXA, a feature 2-KPCC shares with mammalian thioredoxin reductase. Also, while the rest of group 1 and group 2 FDRs have a conserved HXXXXE region (Figure 1, blue box) in the interface domain, the sequence is FLNPTH in the same region, a characteristic that distinguishes 2-KPCC from all other known DSORs, since histidine and glutamate of this sequence are involved in catalysis in the rest of the oxidoreductases [30].

CO-CRYSTAL STRUCTURES OF 2-KPCC WITH SUBSTRATE AND PRODUCT ANALOGS

Introduction

The crystal structures of 2-ketopropyl coenzyme M oxidoreductase / carboxylase have been determined in the native, substrate bound, mixed disulfide and coenzyme M disulfide bound states. These states, besides the native, have been obtained by incubation of the enzyme with the physiological substrate (2-ketopropyl coenzyme M), product (acetoacetate) and cofactor (coenzyme M) respectively. Several substrate analogs have been used for co-crystallization in order to test dependence of substrate binding on chain length. These included carboxylic acids of chains varying from C6 to C8 containing a carbonyl group on the last but one carbon atom, and no sulfur atoms. All attempts to capture the enzyme with the product acetoacetate bound resulted in acetoacetate getting turned over. An acetoacetate analog that has been shown to be a competitive inhibitor of acetoacetate carboxylase [265] was therefore used for co-crystallization in the presence as well as the absence of coenzyme M. A putative mechanism based inhibitor length as the substrate was also designed, with an oxime group replacing the carbonyl group with the aim of displacing the His-coordinated water molecule.

Experimental Procedures

Substrate and Product Analogs

The compound 6-oxoheptanoic acid, 4-oxohexanoic acid (5-oxohexanoic acid was not available) and 7-oxooctanoic acid were obtained from Sigma-Aldrich. Oxopropyl phosphonate was obtained from Germany and its synthesis has since then been

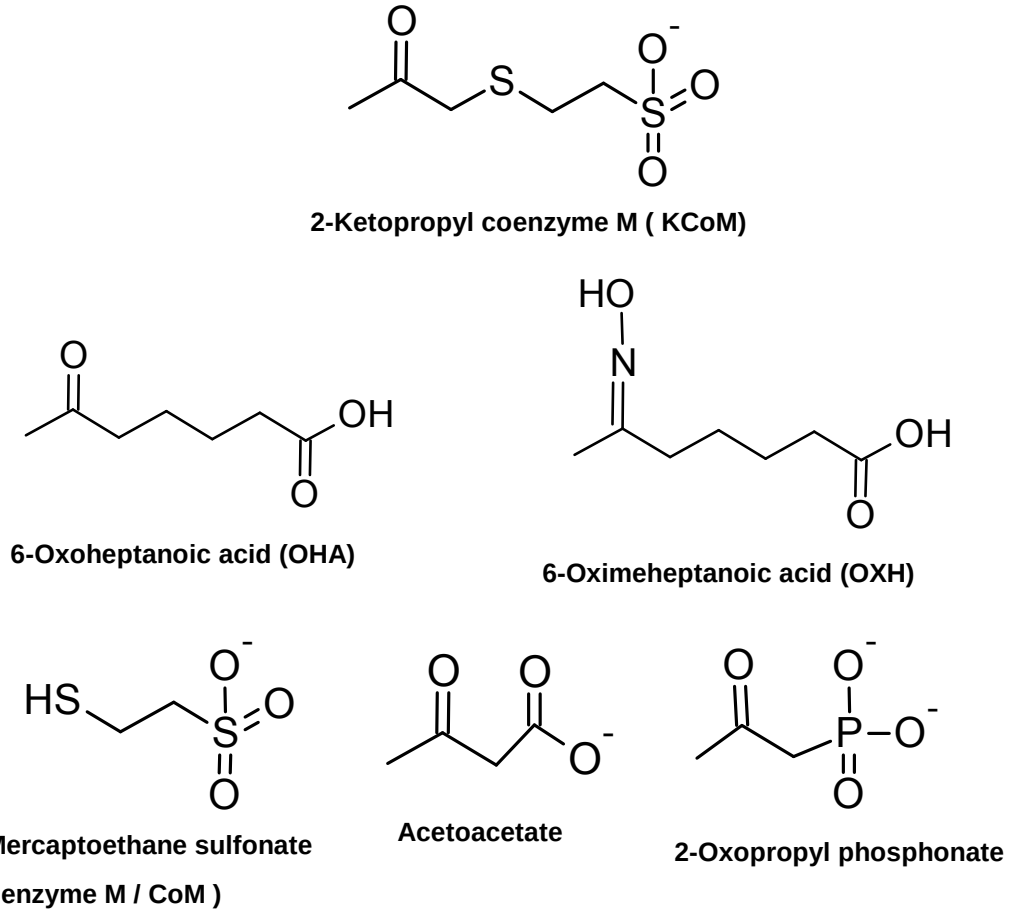

Figure 4.1: The substrate (KCoM) and its analogs (OHA and OXH). The product (acetoacetate) and its analog (OPP). A sketch of coenzyme M is also shown.

discontinued. 6-oxime heptanoic acid was obtained by the oxidation of 6-oxoheptanoic acid with hydroxylamine. A mixture of 6-oxoheptanoic acid dissolved in dioxane and hydroxylamine was refluxed for 4h and cooled. Dioxane and water were removed and the residue was taken up in ether and washed with water. The ether extracts were dried using $MgSO_4$ and evaporated to yield oxime. The compound was verified with ^1H NMR and mass spectroscopy.

Crystallization

Co-crystallization of 2-KPCC was carried out as described previously [71] with varying concentrations of PEG4000. The protein (~0.2mM) was incubated with 30mM of the analog (OPP or OHA) for 10 minutes, with subsequent incubation with 5mM NADPH in case of oxopropyl phosphonate before setting up for crystallization by the hanging drop method. The setups were done both with and without 10 mM coenzyme M.

2-KPCC crystals of good diffraction quality were obtained with 6-oxoheptanoic acid, 6-oximeheptanoic acid + coenzyme M, oxopropyl phosphonate and oxopropyl phosphonate+coenzyme M in crystallization conditions that had 25.5 % PEG4000. The crystals obtained were isomorphous with those obtained with the substrate 2-ketopropyl coenzyme M [71].

Data good to 2.4 Å on crystals incubated with OPP only was collected at home (Chemistry and Biochemistry, Montana State University) on a RigakuIV detector. Data collection on crystals obtained with OHA, 6-oxime heptanoic acid and OPP+CoM was collected at SSRL. All of the latter diffracted to better that 2 Å resolution. Data obtained from OHA co-crystals was processed with MOSFLM [197] in and with HKL2000 [266] for the rest. The previously determined substrate bound structure was used as a model for molecular replacement for all of the different data sets obtained and refined with REFMAC [224]. Data and refinement statistics are given in Table 4.1. Figures were generated with CHEMSKETCH [203] and PyMOL[267].

Results and Discussion

6-Oxoheptanoic Acid (OHA)

The structure of OHA bound 2-KPCC has been determined to 1.95 Å. OHA binds to the substrate binding site through interactions with the same residues, Arg365 and Arg56 as KCoM does. The density for OHA is quite clear and shows the molecule oriented in a similar position as KCoM except for the ketopropyl moiety which is rotated away towards the alternate anion binding site (Figure 4.2, Right). The position of the

Table 4.1 Data and refinement statistics for the substrate and product analogs : OHA: 6-oxoheptanoic acid, OXH: 6-oxime heptanoic acid, OPP: 2-oxopropyl phosphonate

Data statistics

	OHA	OXH	OPP	OPPCoM
Program	MOSFLM/SCALA	MOSFLM/SCALA	HKL2000	MOSFLM/SCALA
Space group	$P2_1$	$P2_1$	$P2_1$	$P2_1$
Cell parameters (Å)	a=88.2 b=60.1 c=105.3 β = 102.4°	a=88.2 b=60.2 c=105.6 β = 102.4°	a=87.9 b=60.2 c=105.3 β = 102.5 °	a=87.7 b=59.3 c=102.4 β = 99.7 °
Resolution (Å)	52 -1.95	38 – 1.50	50 - 2.44	50 – 1.70
Total number of observations	199578	275760	75161	419363
Number of unique reflections	123077	164050	65658	111669
Av I/σ I	9.1(3.0)	13.0 (3.9)	18.9 (5.2)	19.9 (9.5)
Average Redundancy	2.8	2.6	2.1	3.8
%completeness	91.3(95.0)	94.9 (94.9)	89.9 (92.1)	97.3 (85.2)
R_{sym}	0.112(0.41)	0.046(0.27)	0.05(0.15)	0.06 (0.10)

Refinement Statistics

Program used	REFMAC	REFMAC	CNS	REFMAC
Resolution range (Å)	51.4 – 1.95	38-1.50	50 – 2.5	8 -1.7
R_{free}(R_{cryst})	0.20 (0.16)	0.25 (0.21)	0.25 (0.21)	0.20 (0.17)
r.m.s.d				
bond lengths (Å)	0.010	0.010	0.006	0.010
bond angles (°)	1.6	1.4	1.3	1.5

keto-propyl group, as in case of KCoM, is not clear. The current orientation is based upon the presence of a water molecule that is 2.64 Å from the carbonyl oxygen and is held in its place by interaction with the backbone carbonyl of Ala430. It is noticeable that in this position, the ketopropyl moiety faces the region formed by the cis-proline flanked loop that so distinctly stands out in the structure based sequence alignment of 2-KPCC with the DSORs (Chapter3, Figure 3.2). The His137 oriented water molecule is quite far away from any of the atoms of the ketopropyl moiety since the latter is rotated a 180° apparently along the C3-C4 bond compared to its position in the KCoM bound state .

The alternate anion binding site is occupied by two water molecules. These water molecules are held at this site through hydrogen bonding with the side chain NH group of Gln509 and the backbone carbonyl of Gln143. The density for these water molecules is disordered in the plane formed by His506 on the left and OHA on the right. OHA binds to the substrate binding site in a manner similar to that of the substrate 2-ketopropyl coenzyme M. Hydrogen bonding between the carboxyl group oxygen atoms and Arg56 and Arg365 hold OHA in place. The binding of OHA at the substrate binding site occurs in the same way as that of KCoM and hence is comparable. The ketopropyl moiety however is rotated away from the site where a His stabilized water molecule is postulated to stabilize the enolate intermediate during its formation after the nucleophilic attack of the cysteine thiol. The rotation of ketopropyl group does not affect the nature of enolate stabilization as it might occur in this position as the keto group is quite close (2.64 Å) to a water molecule.

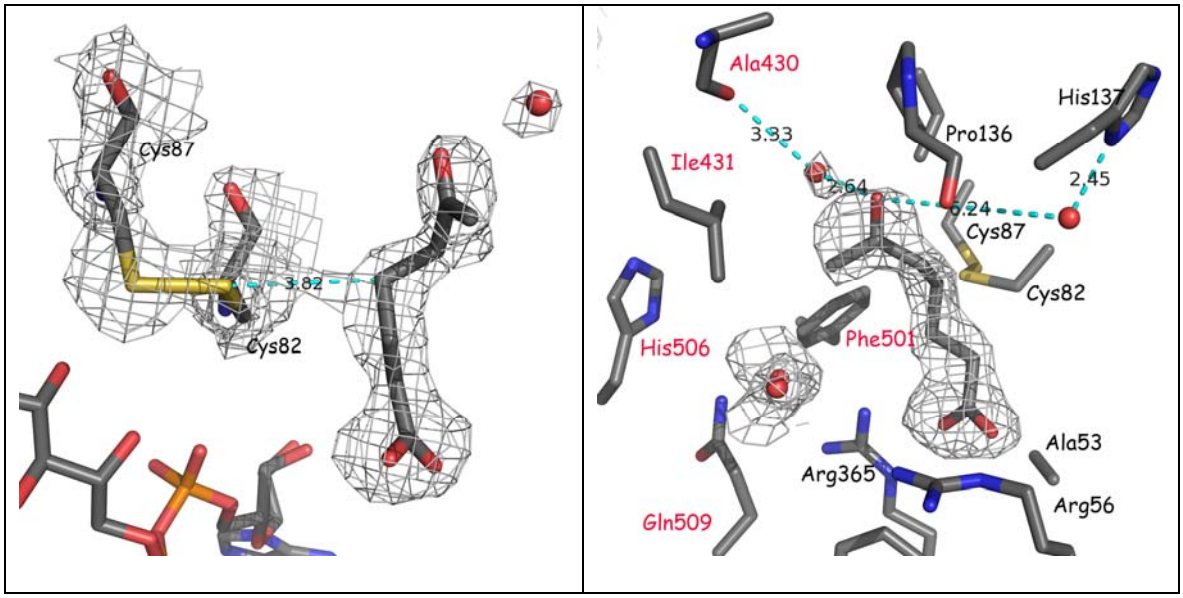

Figure 4.2: *2Fo-Fc* maps showing electron density around a bound OHA molecule and relevant surrounding protein residues and solvent molecules. Residues of different subunits are labeled in different colors

This water molecule is stabilized by the carbonyl group of Ala 430 which is a part of the *cis*-proline flanked loop of 2-KPCC. It can be rationalized that the proximity of the cysteine thiol serves to hold the C3-C4 bond of OHA rigid so that it acts as a pivot around which the ketopropyl moiety is capable of rotation. The corresponding bond in the KCoM molecule would be the C-S bond, which in the absence of reduction of cysteine disulfide by NADPH would get stabilized by the proximity of the cysteine disulfide, and would act as a pivot in a similar fashion as mentioned for OHA. If the developing charge on the product acetoacetate is indeed stabilized at the alternate anion binding site as proposed [209], a rotation of the ketopropyl moiety might be a requirement to place the whole product at the adjacent alternate anion binding site. It has been shown through ^{14}C exchange experiments that the decarboxylation of acetoacetate also occurs through the formation of an enolate intermediate, which in the presence of

coenzyme M results in the formation of KCoM [68]. As the enolate is formed at this site, the Ala430 stabilized water molecule likely serves to stabilize it in the same manner that

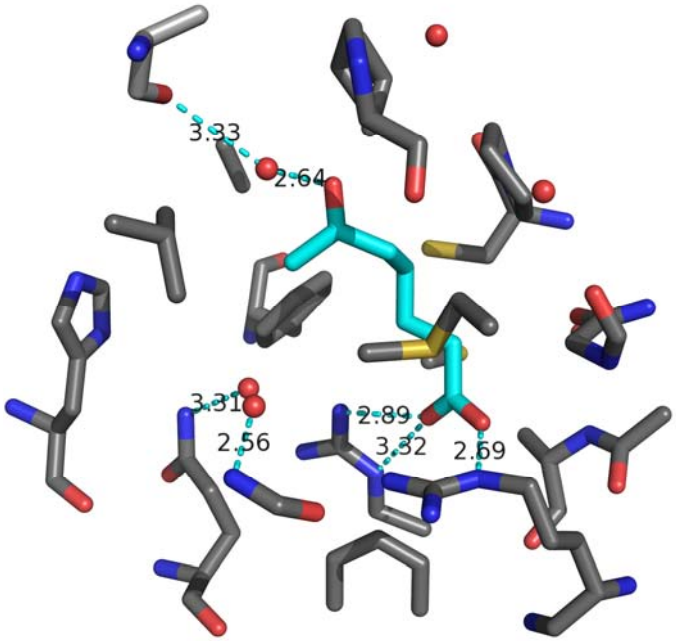

Figure 4.3**:** Relevant interactions of OHA with the surrounding residues. The interactions of the two water molecules at the alternate anion binding site are also shown

His137 oriented water molecule is proposed to stabilize the enolate at the other site. The enzyme seems to employ low barrier hydrogen bonds [268] with ordered solvent molecules for stabilization of enolate.

It is noticeable that the residues forming the loop coordinate the metal ion with their backbone carbonyls while their hydrophobic side chains face the proposed CO_2 binding pocket. The opposite case occurs in case of Ala430 which hydrogen bonds to the water molecule seen stabilizing the carbonyl group of OHA. This suggests a role for the *cis*-proline flanked loop in the mechanism of carboxylation / decarboxylation.

Co-crystals of 2-KPCC+oxime+coenzyme M+$NADP^+$

The crystals obtained on incubation with oxime, coenzyme M and $NADP^+$ were good diffraction quality. Examination of the *Fo-Fc* maps showed that the density was not consistent with an oxime and a coenzyme M molecule (Figure 4.4).

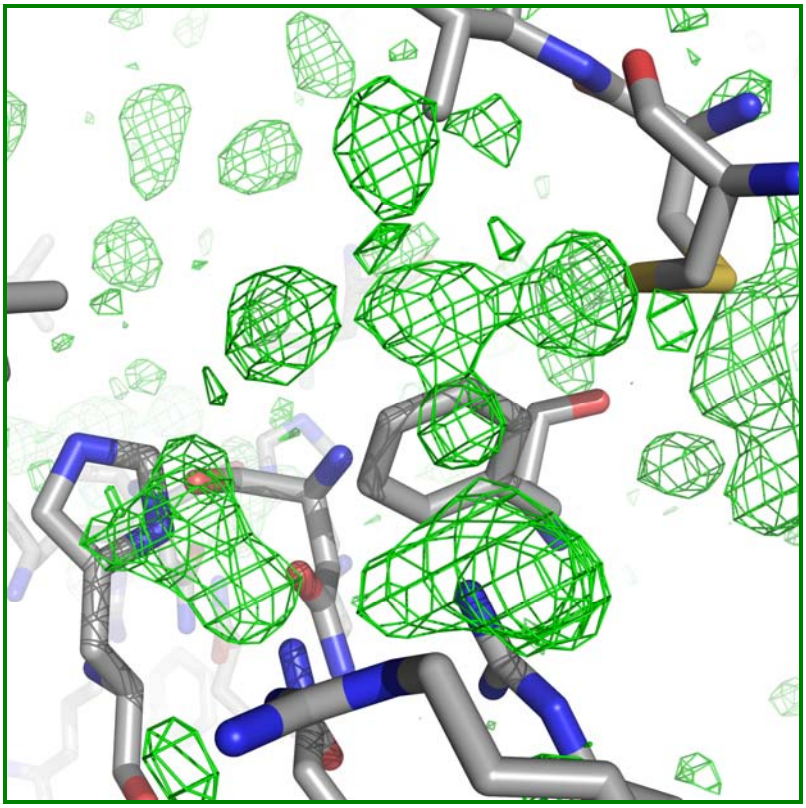

Figure 4.4: The *Fo-Fc* maps obtained for the OXH co-crystallized 2-KPCC. The electron density at the active site is contoured to 3 σ.

The density at the active site in this structure is consistent with a coenzyme M disulfide. In comparison with the earlier structure of 2-KPCC obtained on incubation with coenzyme M only, the density in the two appears to be very similar. Since the K_i of OXH for 2-KPCC was not determined, its binding capacity could not be compared to coenzyme M. OXH was found to inhibit the rate of oxidation of NADH to NADP and

was assumed to be an inhibitor of the mechanism. It was also used in excess (50 mM) as compared to coenzyme M (5 mM) during crystallization setups. OXH either yields to coenzyme M or doesn't bind at the active site at all. This provides a clue for future crystallization studies that the substrate analogs need to be used preferentially without coenzyme M.

Oxopropyl phosphonate+coenzyme M+$NADP^+$ bound structure of 2-KPCC

The structure obtained by incubation of 2-KPCC with OPP+coenzyme M+$NADP^+$ shows density at the substrate and the anion binding sites that could be

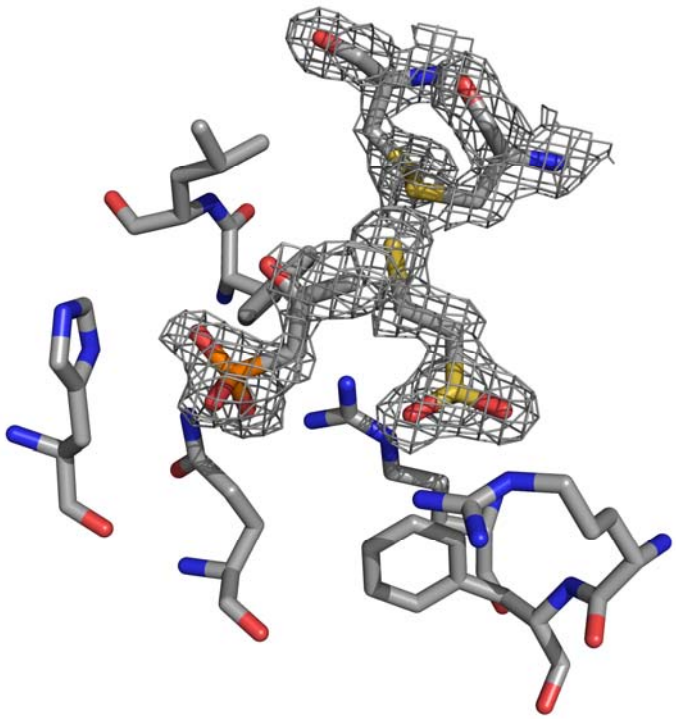

Figure 4.5 Electron density from a 2*Fo-Fc* map contoured to 1 σ in the OPP+CoM structure.

consistent with a coenzyme M disulfide or a coenzyme M at the substrate binding site and an OPP molecule at the alternate anion binding site (Figure 4.5). Since OPP is very similar in structure to CoM, it is not easily distinguishable from the latter. The density at the alternate anion binding site is, however, more consistent with an OPP than CoM because of some density visible for the carbonyl group. A 2*Fo-Fc* map contoured to 4σ shows good electron density around the two sulfur atoms of coenzyme which is comparable to the peaks due to sulfur atoms on the protein sulfur atoms in the active site

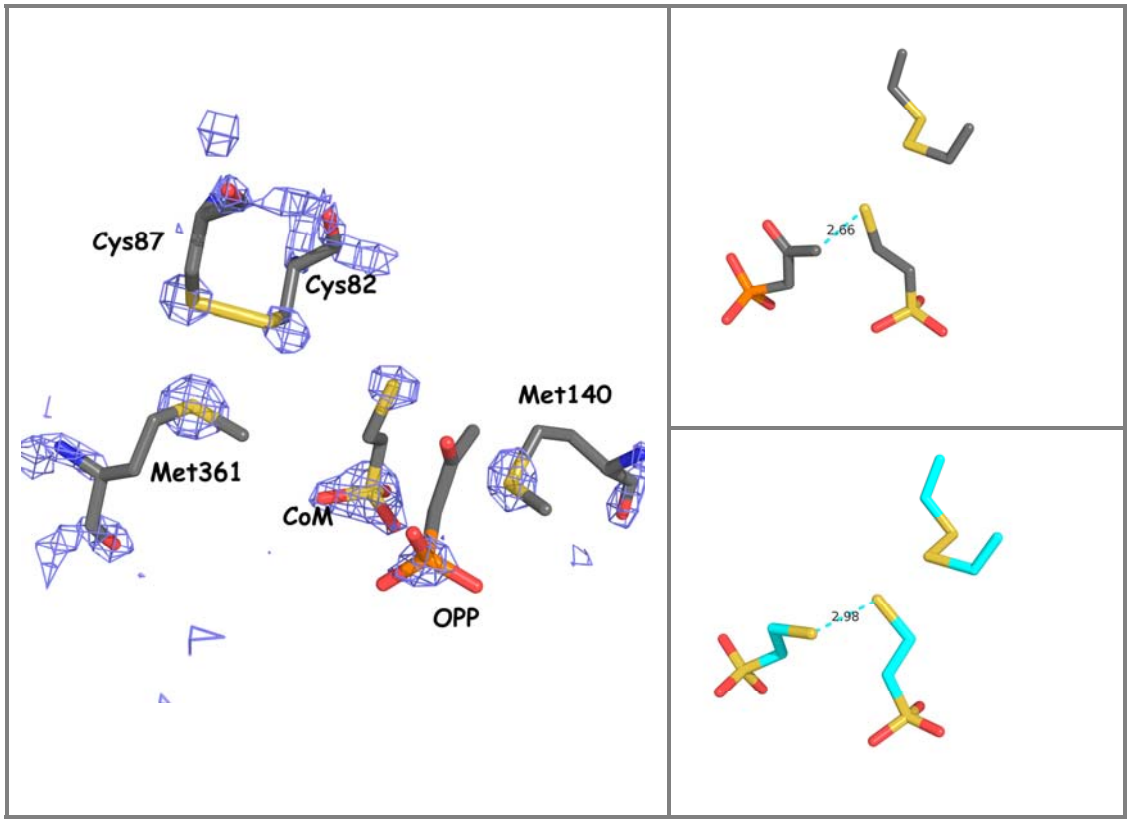

Figure 4.7*:* Left: 2*Fo-Fc* maps of the OPP+CoM+NADP+ structure contoured to 4.0 σ . Right: The distances between the putative C-S atoms in an OPP-CoM bound structure (top) and S-S atoms in the CoM-CoM disulfide bound structure.

(Figure 4.7, left). There is also difference density where the sulfonate / phosphonate bind. Phosphorous atoms would be expected to yield peaks similar to sulfur atoms, since

they differ by just one electron from sulfur. There is however no peak where a second sulfur atom would be present had this molecule at the alternate anion binding site been coenzyme M.

A comparison of distances with the coenzyme M disulfide obtained by co-crystallization with coenzyme M only provides further support for the identity of the molecule at the alternate anion binding site as an OPP. The S-S distance in a coenzyme M disulfide bound structure is 2.98 Å (Figure 4.7, Bottom right). The distance between the atom fit into the density at the thiolate position of the coenzyme M of the alternate anion binding site and the thiolate of the coenzyme M at the substrate binding site is 2.66 Å. The latter being shorter is more consistent with a C-S bond than with an S-S bond. Therefore it can be rationalized, that the molecule bound at the alternate anion binding site is an OPP molecule rather than another coenzyme M.

It can hence be concluded that the alternate anion binding site is indeed the site where an acetoacetate molecule binds in the presence of coenzyme M.

Oxopropyl Phosphonate Bound Structure of 2-KPCC

The structure obtained by incubation of 2-KPCC with OPP only showed density consistent with an OPP molecule at the sustrate binding site. The oxopropyl part of OPP could not be modeled unambiguously (Figure 4.8). The binding of OPP which is an acetoacetate (product) analog at the KCoM (substate) binding site points to the latter as the primary binding site for anions. In view of the fact that acetoacetate decarboxylation is increased 77-fold compared to the non-biological rate in the presence of coenzyme M [68], it can be concluded that decarboxylation site is the alternate anion binding site. In

order for the enzyme to decarboxylate, the acetoacetate molecule will have to be bound at the alternate anion binding site which cannot occur in the absence of coenzyme M. There is also an almost trigonal planar electron density at the alternate anion binding site seen in this structure. This density can only be explained as an acetate molecule from the crystallization buffer.

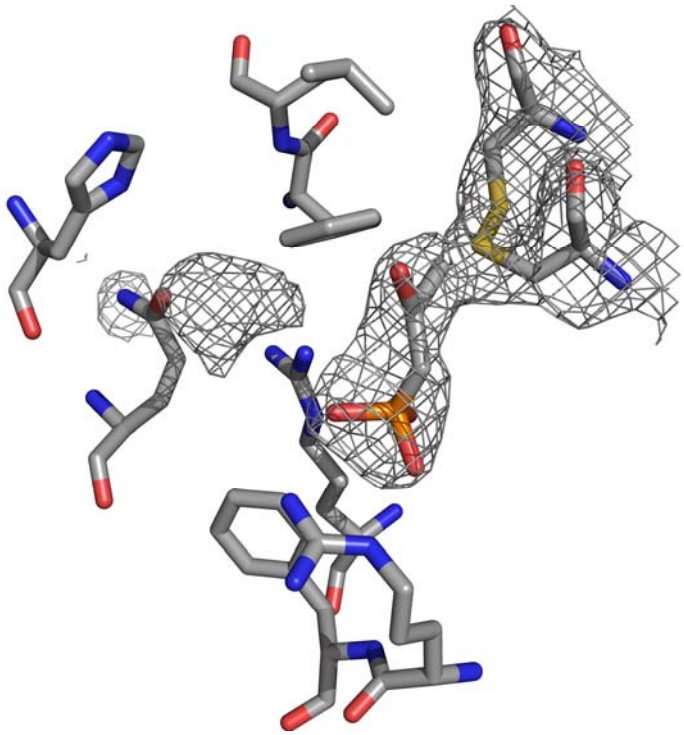

Figure 4.8: 2 *Fo-Fc* map showing electron density at the substrate binding site contoured to 1 σ.

Conclusion

2-KPCC can be co-crystallized with a number of compounds that serve as non-hydrolyzable substrate or product analogs. It crystallizes in the same space group as well as in the same crystallization condition as the previously determined substrate bound structure and is an ideal candidate for this kind of experimentation. The crystals obtained

are high diffraction quality with most co-crystals diffracting to 2 Å or higher resolution. Substrate analog bound structure of 2-KPCC reveals an alternate site for enolate stabilization with the ketoproyl moiety being able to rotate around the C-S (thiol) bond of coenzyme M. The substrate binding site is revealed as the primary anion binding site, where a single anionic molecule will prefer to bind. In using analogs isoelectronic with coenzyme M, the identity of the ligands bound at the active site cannot be established unequivocally as analog+CoM or CoM-CoM. A role for the cis-proline loop in avoiding carboxylation in this alternate positon is suggested.

DISTINCT SITES FOR CARBOXYLATION AND DECARBOXYLATIO IN 2- KPCC

Introduction

Autotrophs carry out carbon dioxide fixation by three major pathways: the Calvin cycle, the acetyl-CoA pathway and the reductive tricarboxylic acid pathway. These involve the CO_2 fixing enzymes rubisco, carbon monoxide dehydrogenase, pyruvate synthase, phosphoenolpyruvate carboxylase, α-ketoglutarate synthase and isocitrate dehydrogenase [269]. The acetyl CoA pathway is found in methanogenic archaea, some sulfate-reducing bacteria and in facultative heterotrophs that synthesize acetic acid from CO_2 during fermentation [270]. The acetyl CoA pathways in methanogenic archaea differ from that in bacteria in several aspects, one of them being the utilization of cofactors not commonly found in bacteria or eukarya. One such cofactor is coenzyme M (2-mercaptoethane sulfonic acid) that serves as a C1 carrier during methanogenesis [271].

Coenzyme M is also utilized in the epoxide carboxylation pathway during the aerobic metabolism of short chain alkenes in *Xanthobacter autotrophicus* Py2, [24] where it is conjugated to a short chain epoxide for subsequent reductive carboxylation to yield β-keto acids [19]. In the metabolism of propylene epoxide in *X. autotrophicus* Py2, the reversible carboxylation of CoM conjugated substrate ketopropyl coenzyme M (KCoM) is carried out by the enzyme 2-ketopropyl coenzyme M oxidoreductase/ carboxylase (2-KPCC), to yield acetoacetate as product [68]. 2-KPCC is an NADP-dependent carboxylase that reductively cleaves and carboxylates a thioether substrate. Pyruvate dehydrogenase carries out a similar reaction, utilizing thiamin pyrophosphate as a coenzyme, which is not required by 2-KPCC.

2-KPCC mechanism involves the catalytic acid stabilization of an enolate intermediate [68], formed by delocalization of charge on a carbanion into the adjacent carbonyl group. The role of the catalytic acid is fulfilled by a histidine bound ordered water molecule [71]. The reverse reaction, decarboxylation of acetoacetate in the presence of CoM to form KCoM, also occurs through the formation of an enolate intermediate [68]. Stabilization of a carbanion by delocalization into an adjacent carbonyl or imine that has been polarized by coordination to a Lewis acid is widely used in the catalysis of decarboxylation, isomerization and aldol reactions [268, 272]. Other mechanisms involve the participation of pyridoxal phosphate or thiamin pyrophosphate to provide an electron sink. 2-KPCC is devoid of these coenzymes and its crystal structure [71] reveals the absence of a nearby lysine residue, supporting the earlier observation of the absence of the formation of Schiff's base during decrboxylation.

Here we present a structure of 2-KPCC with a bicarbonate molecule and CO_2 molecule bound at relevant sites in relation to previously determined structures to elucidate the mechanism of carboxylation and decarboxylation by this enzyme. 2-KPCC bears structural and functional homology to the disulfide oxidoreductases family of enzymes which catalyze the reductive cleavage of a disulfide substrate followed by subsequent protonation of leaving groups. 2-KPCC catalyzes a similar reaction and has been shown to protonate the leaving groups only in the absence of CO_2. In the presence of CO_2, protonation to form acetone, is negligible.

Experimental Procedures

2-KPCC was purified according to the method described previously [20]. The crystals for this study were obtained by incubating purified 2-KPCC (~30 mg/ ml) with acetoacetate, coenzyme M and NADPH added in that order for 10 minutes prior to addition of an equal amount of precipitating solution of 0.1M ammonium acetate, 0.085 M sodium citrate pH 5.6, 25% PEG 4000 and 30 % glycerol. This mixture was set up for hanging drop crystallization over the precipitating solution. The crystals obtained were of the same morphology as the ones obtained with the substrate and acetoacetate + coenzymeM + NADPH. They belong to the monoclinic space group with one dimmer per asymmetric unit with the cell dimensions: a=88.5Å, b=59.8Å, c=105.5 Å and β =102.3°. Data was collected at SSRL beamline 9-1 equipped with a mar345 imaging plate detector (marUSA Inc.) with 1° oscillation.

Data was processed with MOSFLM [273] and scale with SCALA of the CCP4 suite [197]. The substrate bound crystal structure of 2-KPCC (a=88.0Å , b=60.1 Å , c=105.6, β = 102.5°) (1MO9) with one dimer per asymmetric unit was used as a model for molecular replacement. The structure was refined with REFMAC of the CCP4 suite [197] with simutaneous viewing of 2 *Fo-Fc* and *Fo-Fc* maps and model building in COOT [197]. The structure was refined to the resolution of 1.92 Å with 5% of reflections selected randomly for R_{free}. The data and refinement statistics for this structure are given in Table 5.1.

Results and Discussion

In our earlier structures [209] we had identified an alternate anion binding site adjacent to the KCoM binding site, where the carboxylate moiety of acetoacetate was proposed to get stabilized. The current structure shows bicarbonate as the immediate product of decarboxylation, which has equilibrated with water and CO_2, with concomitant formation of KCoM (Figure5.1, top and center right). The cysteine sulfurs

Table5.1: Data collection and refinement statistics obtained for the crystal structure obtained with acetoacetate, coenzyme M and $NADP^+$.

Data Collection Statistics	
resolution (Å)	1.88
no. of observed reflections	227604
no. of unique reflections	83,625
R_{merge} (%)	9.3(56.6)
completeness (%)	95.1(97.0)
I/σ	5.5(1.5)
Refinement Statistics	
resolution range (Å)	8.00-1.92
R_{cryst}	0.1704
R_{free}	0.2218
no. non-hydrogen atoms	9314
protein	8054
cofactor/substrate	137
solvent	1123
r.m.s.d. from target values	
bond lengths (Å)	0.016
bond Angles (deg)	1.5
average B factors (Å^2)	22.81
Protein	20.58
FAD	18.77
NAP	36.04
KPC	30.15
BCT	30.67
Solvent	33.35

are in the reduced state, with the cysteine distal to FAD 2.74 Å from the CoM sulfur atom. This can be rationalized to be a transient state in which there is partial breakage of the S(Cys)-S(CoM) bond and partial formation of the C(enolate)-S(CoM) bond.

We had identified a hydrophobic channel leading up to a hydrophobic pocket in the vicinity of the substrate binding site of 2-KPCC in our earlier work [209]. The current structure shows density consistent with a CO_2 molecule in the same region (Figure5.1 center, right). A superimposition of the current structure on the KCoM bound structure places this CO_2 molecule strategically to attack KCoM in this orientation (Figure 5.1, bottom). Although an enolate intermediate has not been captured as such, the presence of a His oriented water molecule within hydrogen bonding distance of the carbonyl oxygen of KCoM implies that the stabilization of enolate and attack by CO_2 molecule occur at this site. After covalent attachment to the ketopropyl moiety as a carboxylate, the acetoacetate molecule would then orient to place the latter at the alternate anion binding site. With acetaoacetate arising from the reaction, or externally added, bound in this fashion, the decarboxylation reaction is bound to occur at this same site. However, the site of decarboxylation, in addition to being richly supplied with waters interacting with residues from the other subunit, is 4.67 Å away from the hydrophobic pocket (Figure5.1 top and bottom right). It is rational to conclude that decarboxylation would be favored by the destabilizing interactions between water and the carboxylate group, resulting in the formation of enolate and a bicarbonate. This physically separates the site for carboxylation from decarboxylation. A slight rotation of the enolate moiety to position the carbanion for attack by the sulfur of coenzyme M to form the C-S bond can also be assumed.

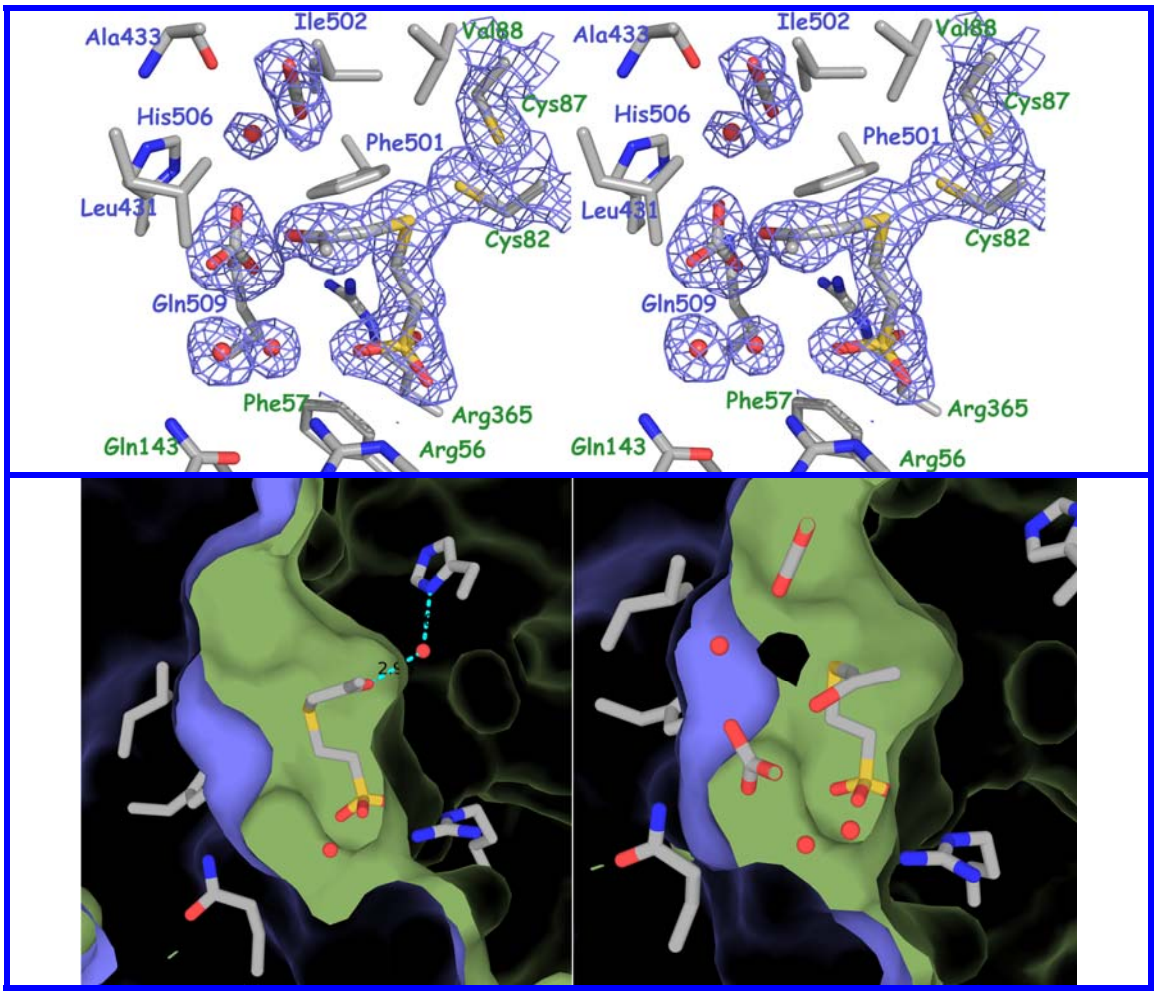

Figure 5.1: Top- Stereo view of the active site of 2-KPCC showing electron density caround 2-ketopropyl coenzyme M, bicarbonate and carbon dioxide and water molecules contoured to 1σ. Residues contributed by the two subunits are labeled in different colors. Bottom (Left)-Surface rendering of the 2-ketopropyl coenzyme M bound structure of 2-KPCC. The dark areas of the two subunits (blue and green) represent the space inside the protein, the bright area represents the substrate binding pocket. Positions of the substrate binding residues, His137, His137 bound water molecule, the water molecule at the anion binding site and residues corresponding to the catalytic dyad are shown. Bottom (Right): Surface rendering of the bicarbonate bound crystal structure of 2-KPCC. Dark and light areas represent the same features as the figure on left. Positions of the bicarbonate molecule with surrounding waters, the CO_2 molecule and the product of the reverse reaction, 2-ketopropyl coenzyme M are shown along with positions of the relevant residues.

The presence of water molecules at the alternate anion binding site in all crystal structures of 2-KPCC examined so far point to their importance in the reaction mechanism. This, in addition to other hydrogen bonding interactions, implies that the trigonal planar density observed at this site belongs to a charged molecule, capable of

electrostatic interactions through all three apical atoms. Based upon the above and the decarboxylation reaction mechanism [68], it can be concluded that the trigonal planar density at the alternate anion binding site belongs to a bicarbonate molecule and not to an acetone or an acetate from the buffer. The bicarbonate molecule at this site is 2.61 Å away from a water molecule which in turn is 2.67 Å away from the CO_2, according to the reaction:

$$HCO^-_3 + H^+ \rightleftharpoons H_2O + CO_2$$

The presence of water molecules so close to the bicarbonate also ensures that the bicarbonate formed will break down into water and carbon dioxide [274]. In a recently published structure of a β-carbonic anhydrase from *Haemophilus influenzae*, a bicarbonate was found bound at a noncatalytic site [275]. The authors have noted the presence of two water molecules in positions to form multiple hydrogen bonds with the oxygen atoms the bicarbonate ion and protein functional groups (PDB 2ESF, 2A8D), which are also seen in β-carbonic anhydrase structures from *Pisum sativum* [276] and *Porphyridium purpureum* [277]. The bicarbonate at the alternate binding site of 2-KPCC shares the presence of these two water molecules, although the interactions with the side chain residues of the protein are not as numerous. There is only one interaction (3.06 Å) with the amide nitrogen of Gln509, which forms a part of the alternate anion binding site along with the Phe501 and His 506 of the other subunit. Since a mixture of CO_2 and HCO_3^- were used as carbonate species during the kinetic studies on 2-KPCC, the active form of the substrate could not be determined beyond speculation. [209] [68]. The current work determines the CO_2 molecule, and not HCO_3^- as the cosubstrate for carboxylation.

A few examples of cofactor free decarboxylation reactions are available in literature. These include orotidine monophosphate (OMP) decarboxylase, which presumably facilitates decarboxylation through destabilizing electrostatic interactions between an active site aspartate and the substrate carboxylate [278], [279]. Another such decarboxylase is Uroporphyrinogen III Decarboxylase, which has been proposed to act by protonating a pyrrole ring on uroporphyrinogen so that it can act as an electron sink, thereby enabling decarboxylation[280].

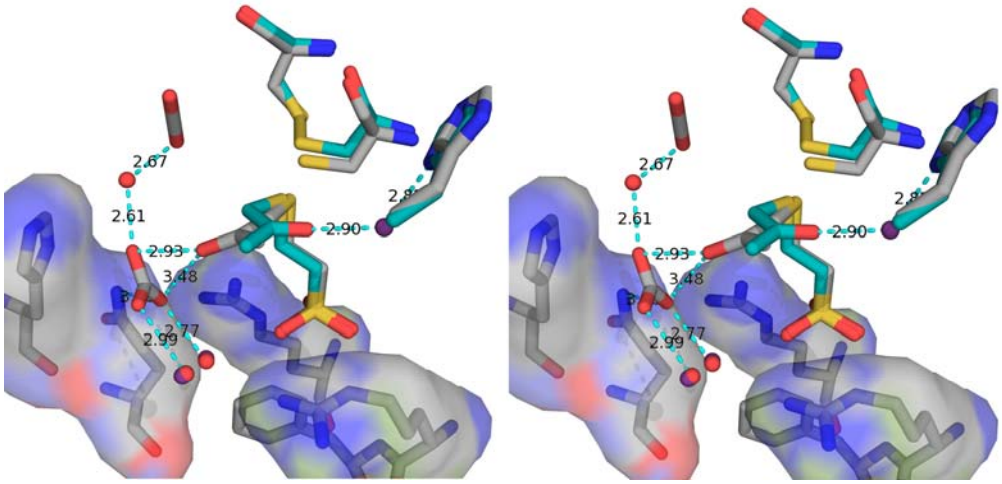

Figure 5.2: A superimposition of the bicarbonate bound structure (gray) on the substrate bound structure (cyan). The two anion binding sites are shown as surface rendering colored according to nature of amino acids, blue for basic and red for acidic moieties. All figures were generated with PyMOL.

Taking into consideration the above, the presented structure along with the earlier ligand and native structures of 2-KPCC, complete the picture regarding the mechanism of the enzyme (Figure 5.3). The substrate gets into the active site through an open channel formed by the walls of the two subunits of the dimer, which closes on substrate binding. The CO_2 channel opens on substrate binding, CO_2 enters to bind in the hydrophobic

pocket strategically positioned to electrophilically attack C1 of ketopropyl group of KCoM. This is accomplished by a nucleophilic attack of the redox active distal cysteine thiol on the C1-S bond resulting in a mixed disulfide, stabilization of the enolate by a histidine stabilized water molecule with concomitant attack of the CO_2 molecule on C1. The carboxylate hence generated orients toward the alternate binding site for stabilization, where it shares the charge on Arg365 with the sulfonate moiety of CoM . This is speculated to weaken the interactions holding the sulfonate of the mixed disulfide in place, initiating its release. The mixed disulfide bond is nucleophilically attacked by a water molecule, releasing CoM-SH as one of the products, while acetoacetate is released as the other bound state (not shown here, PDB code 2C3D). Figure was generated with ACD/ChemSketch and PyMOL.

The decarboxylation of acetoacetate by 2-KPCC has been found to not depend upon the redox active disulfide. [68]. The presented structure agrees with the proposed mechanism of decarboxylation, where after the loss of CO_2 as a bicarbonate, the resulting enol collapses with a concomitant electrophilic addition of CoM, which in the presence of $NADP^+$ allows KCoM to form. The orientation of CO_2 molecule with respect to the product KCoM would allow for an attack of CO_2 on KCoM, forming acetoacetate. This is in agreement with the $^{14}CO_2$ exchange with acetoacetate, where 14C was found to be incorporated in the C1 position of acetoacetate [68]. A 77- fold increase in the rate of decarboxylation has been observed in the presence of 2-KPCC [68] . It can be concluded from the structures determined that CoM has a more structural than functional role to play in catalyzing decarboxylation. An analogue of acetoacetate and a known inhibitor of acetoacetate decarboxylase, oxopropyl phosphonate [265], was found bound to the

substrate binding site (data not shown) on cocrystallization in the absence of CoM. Binding at this site would not be conducive to decarboxylation as the charge on the carboxylate would get stabilized by the arginine residues that take part in KCoM binding.

Conclusion

The current structure of 2-KPCC obtained by incubating the enzyme with acetoacetate, coenzyme M and $NADP^+$, shows density consistent with the substrate 2-ketopropyl coenzyme M, a bicarbonate and a CO_2 molecule at the active site. The sequence in which the product and cofactors were added determined the nature of product formed. Addition of acetoacetate and coenzyme M results in the decarboxylation of acetoacetate at the alternate anion binding site and the concomitant combination of the release CO_2 with water molecules at this site to form a bicarbonate anion. The carbanion is stabilized as an enolate which attacks the coenzyme M thiolate sulfur in the presence of $NADP^+$ to form coenzyme M. The bicarbonate anion equilibrates with a water molecule and CO_2 gas such that the latter ends up in a hydrophobic pocket at the base of a hydrophobic channel. It has been shown that in the absence of $NADP^+$, the carboxyl group exchanges with the exogenously added $^{14}CO_2$ [68] to yield ^{14}C labeled acetoacetate with the 14C incorporated in the carboxyl group. In the presence of $NADP^+$, however, a coenzyme M adds to the enolate intermediate to form 2 KCoM [68], which is consistent with the structure obtained. It can be concluded that the two processes of carboxylation and decarboxylation occur at two different sites in the active site : carboxylation occurs at the end of a hydrophobic channel where a CO_2 molecule is in proximity with the C-S

linkage of the substrate molecule, decarboxylation occurs at the alternate anion binding site where CO_2 is lost as a bicarbonate anion.

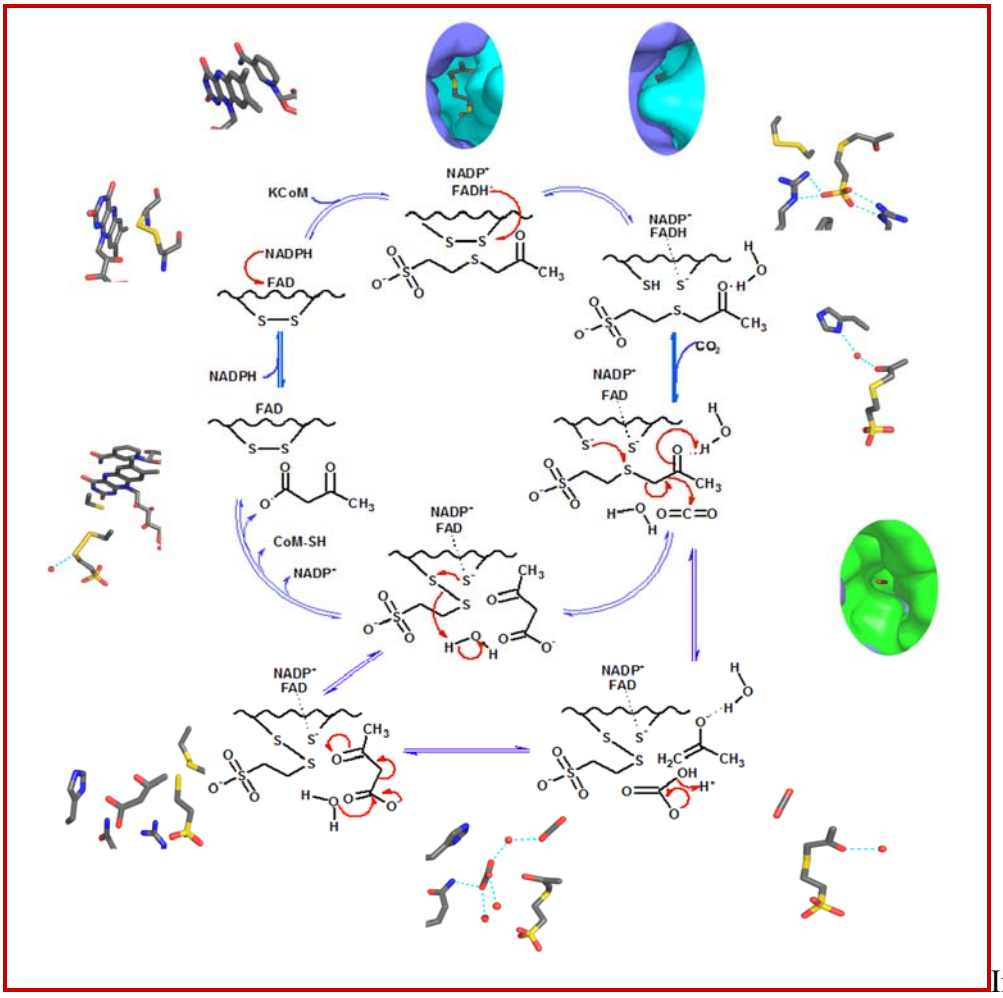

In

Figure 5.3: The reaction mechanism of 2-KPCC derived from the previously proposed mechanism and crystal structures The active site state for a particular step as seen in the crystal structure accompanies the relevant step where applicable. The acetoacetate bound state shows a modeled acetoacetate molecule in the active binding site based upon the coenzyme M disulfide

sum, we have determined that the processes of carboxylation and decarboxylation by 2-KPCC are physically separated from each other. Decarboxylation of an acetoacetate molecule that is bound at an anion binding site would cause the introduction of a non-polar molecule into a charged environment. This is prevented by the formation of a

carbonic acid as soon as decarboxylation occurs. The equilibration of carbonic acid, bicarbonate and CO_2 and water occurs with some movement such that the non-polar CO_2 moelcule ends up into a hydrophobic pocket.

HIGH RESOLUTION (1.39 Å) X-RAY CRYSTALLOGRAPHIC REFINEMENT OF THE [FE FE] - HYDROGENASE (*CP*I) FROM *CLOSTRIDIUM PASTEURIANUM* AND PARALLEL ATOMIC RESOLUTION REFINEMENT OF THE ACTIVE SITE H-CLUSTER BY DENSITY FUNCTIONAL THEORY

Introduction

Hydrogen metabolism is found in almost all taxonomic groups of prokaryotes, in some anaerobic microbial eukaryotes and in unicellular green algae. The reaction

$2\ H^+ + 2\ e^- \leftrightarrow H_2$

is catalyzed by metalloenzymes known as hydrogenases . There are three main classes of hydrogenases, the [FeFe]-hydrogenases, the [NiFe]-hydrogenases and the iron-sulphur cluster free hydrogenases (Hmd) with an iron containing co-factor [76] [281]. Crystal structures of the [FeFe] hydrogenase from *Clostridium pasteurianum Cp*I {Peters, 1998 #122} and *Desulfovibrio desulfuricans* (*Dd*ase) {Nicolet, 1999 #120} have been determined. These show that the active site in the [FeFe] hydrogenases is formed by a 6Fe cluster that consists of a 2Fe cluster bridged though a protein cysteinyl sulfur atom to a [4Fe-4S] cubane. The Fe atoms of the 2Fe cluster are bridged through a dithiolate ligand the composition of which could not be determined through the crystal structures. Density consistent with three atoms between the two sulfur atoms could either be a propane or a dimethylamine. The latter has been favoured as the central nitrogen atom could possibly serve as a proton donor during the production of H_2. In *Cp*I structure, a site on the Fe atom of the 2Fe cluster distal from the [4Fe-4S] cubane is occupied by a water molecule. This site was proposed to be the site where protons come together with electrons to form a hydride ion. No density has been observed at this site in Ddase

structure which was determined in the reduced form as opposed to the CpI structure which was that of the oxidized enzyme. The presence / absence of water molecule was attributed to the oxidation state of the enzyme. Two terminal CO and CN^- ligands coordinate to both iron atoms in *trans*- arrangement in addition to a bridging CO ligand between two Fe atoms. A CO inhibited state of *Cp*I was also captured that showed the exogenously added carbon monoxide bound to the site occupied by the terminal water molecule in the previous structure [176]. Carbon monoxide binding and inhibition were also investigated by electron paramagnetic resonance (EPR) spectroscopy in solution and in crystals of structurally described states of *Cp*I [177]. The EPR spectrum of CO-treated, dithionite reduced *Cp*I in solution indicated not only oxidation of the H cluster upon formation of the CO bound species but also partial oxidation of iron-sulfur complement of the enzyme. This was proposed to be indicative of slow proton reduction in the presence of dithionite despite the presence of CO, suggesting that CO is a competitive rather than an irreversible inhibitor. The EPR spectra of crystals of CO inhibited *Cp*I was indistinguishable from the inhibitory signal obtained for the CO inhibited enzyme in solution, showing that CO bound structure of *Cp*I was in fact an inhibited state of the enzyme. Activity is restored to the enzyme on removal of CO, indicating that the site at which CO binds might be the site where a hydride binds during catalysis. The presence of two terminally coordinated CO ligands, two terminally coordinated CN^- ligands and a bridging CO is also supported by infrared spectra of *Cp*I [182]. Irradiation of the exogenously added CO bound form of the enzyme results in the loss of the exogenously added CO ligand at 6-14 K, and the loss of bridging character of CO and loss of one of the CO ligands other than the exogenously added CO at >20K. It has been argued, based

on theoretical treatment of the IR data obtained for *Cp*I, that the current assignments of the CO and CN^- ligands in the CO inhibited structure of *Cp*I are inconsistent with the available IR data [283] and a DFT based model has been proposed showing the exogenously bound CO in a position close to the bridging CO instead of the vacant site as suggested by the crystal structure. These studies imply a mechanism more complex than a simple removal of a water molecule from the exchangeable site on the distal iron and binding of a hydride instead.

A potential electron transfer pathway has been proposed from clusters FS4C and FS2 on the protein surface to the H-cluster through covalent bonds, hydrogen bonding, and through space pathways amongst residues that constitute ligands to the clusters or are adjacent to these ligands. A potential mechanism for proton reduction by *Cp*I has also been proposed [143]. It was suggested that the terminal water ligand in the vicinity of the distal iron site of the 2Fe subcluster gets displaced upon reduction, with the subsequent generation of a hydride intermediate. A potential pathway for proton transfer exists from Cys299 to the protein surface involving two Glu residues (EXXX and EYYY), a Ser residue and a water molecule.

The assembly of the iron-sulfur framework of the active site of the H cluster that is capable of electrocatalysing proton reduction at a diffusion-controlled rate, was accomplished by Pickett and co-workers [284]. The environment provided by the protein for the cluster to function in is likely responsible for hydrogen production at biologically accessible reduction potential by hydrogenases, possibly by stabilizing one oxidation state over another and by tuning the redox potentials of the clusters. NH….S bonds between protein backbone and sulfurs of the coordinating cysteine thiols, presence of

polar side chains and solvent structure around the cluster have all been implicated in effecting the redox potential of iron sulfur clusters [285-287]. Here, the high resolution (1.39 Å) crystal structure of *Cp*I hydrogenase with the bond distances of the H-cluster determined within 0.04 Å accuracy, provides a model for setting up DFT optimizations to determine the composition of the bridging dithiolate ligand and its impact on the the mechanism of hydrogen production at the H-cluster.

Experimental Procedures

*Cp*I was purified from *Clostridium acetobutylicum* following the purification procedure as before [288]. Crystals of *Cp*I were obtained by the microcapillary batch diffusion method [289] in a precipitation solution of 25% polyethylene glycol 4000, 0.1M sodium acetate (pH 4.6), 0.1M sodium sulfate as described previously [143]. All manipulations were conducted in an anaerobic chamber under an atmosphere of 100% N_2 at room temperature. Crystals belonging to space group $P4_22_12$ with a=b=110.75 Å, c=103.54 Å and α=β=γ=90° were obtained in seven days. Data was collected at SSRL on a Q4 detector at a wavelength of 0.95364 Å, processed with MOSFLM [197] and scaled with SCALA [197] resulting in an overall R_{merge} of 0.081 using data up to a resolution of 1.39 Å .

The crystal parameters were very similar to those of the ones used earlier to solve the structure of *Cp*I, a=b=111.6 Å, c=103.8 Å, α=β=γ=90°, [143] so the latter could be utilized as a model for molecular replacement using the program AUTOMOLREP of the CCP4 suite [197]. Subsequent refinement was carried out with the program SHELXL [290] using conjugate gradient least squares (Konnert and Hendrickson 1980) and block

diagonal matrix least squares methods. Protein coordinates and isotropic B factors were refined using conjugate least squares method with protein bonds and angles restrained to target values from Engh & Huber (1998). Restraints for the iron-sulfur clusters were

Table 6.1 Data Collection parameters

	Space group		$P4_22_12$	
	Cell parameters		a=b=110.785Å α=β =γ =90.0°	c=103.57 Å
	Total observations		622,033	
	Independent reflections		121,060	
Resolution shell (Å)	Redundancy	Completeness	Avg $I/\sigma I$	R_{symm}
46.9-4.8	7.8	98.2	31.5	0.06
4.80-3.40	8.7	99.9	31.1	0.07
3.40-2.77	7.9	100.0	24.7	0.09
2.77-2.40	6.6	99.9	20.2	0.09
2.40-2.15	5.7	99.7	17.2	0.10
2.15-1.96	5.1	99.5	14.4	0.12
1.96-1.81	4.6	98.9	11.5	0.14
1.81-1.70	4.2	97.4	8.6	0.17
1.70-1.60	3.9	93.5	6.2	0.22
1.60-1.52	3.9	89.0	4.5	0.29
1.52-1.45	4.1	84.3	3.1	0.41
1.45-1.39	4.4	81.7	2.5	0.57
Overall	5.1	93.5	12.6	0.09

$$R_{symm}(I) = \Sigma_{hkl} \Sigma_i | I_i - \langle I \rangle | / \Sigma_{hkl} \Sigma_i I_i$$

generated using SHELXPRO [290] assuming the bridging dithiolate ligand to be ethyl dithiolate ether and anisotropic B-factors were switched on for subsequent steps of refinement resulting in a drop of 3% in R_{free}. *2Fo-Fc* and *Fo-Fc* maps were viewed in XTALVIEW [291] to fit the coordinates of protein side chain atoms and add alternate conformations where applicable. Hydrogen atoms were added as fixed atoms and another round of conjugated least squares refinement was carried out with the bond

distances for the H cluster adjusted to those obtained from a DFT energy minimization that included the protein environment of the cluster within 3.6 Å. A parallel refinement was done where only the iron sulfur clusters were refined anisotropically in order to maximize the data to parameter ration. This was done with three different bridging ligands in the H-subcluster, propane dithiolate, ethyl amine dithiolate and dithiolate ethyl ether. The coordinates of the H-subcluster were manually adjusted to DFT optimized values in XtalView and refined with the distances restrained to the same values. The resulting coordinates were used for the calculation of standard uncertainties in bond lengths and angles of the clusters. All restraints were switched off for calculation of standard uncertainties of individual clusters by full matrix BLOC'ed refinement.

Results and Discussion

Bond Distances and Angles

The structure of Fe only hydrogenase from *Clostridium pasteurianum* determined at atomic resolution allows for the determination of Fe-S and Fe-C bond distances within 0.04 Å accuracy (Table 6.3). The Fe-S bonds within this subcluster range from 2.28 Å to 2.39Å, the latter between the proximal Fe and Sγ of Cys503. The Fe-C distances of the bridging CO are within 1.91 Å and 1.97 Å from the proximal and distal irons respectively. The Fe and inorganic sulfur distances in the H cluster range from 2.25-2.38 Å with an almost constant value of standard uncertainty of ~0.008 Å. The Fe-Cys sulfur bonds range from 2.27-2.39 Å, the longest being between proximal Fe and Sγ503, while the shortest is between Sγ503 and Fe6 of the cubane. The Fe-Fe distance of the H-subcluster is 2.5641±0.0067.

Table 6.2: Progress of refinement of the previously published structure of *Cp*I as model against the 1.39 Å data with SHELXL. All reflections were included during the final step of refinement.

	Resolution (Å)	NA	NH	NW	NPar	NObs	*R*% (all)	R_{free} (all)	*R*% (>4 σ)	R_{free} (>4 σ)
Rigid body	2.5-46	4513	0	0	4522	22036	32.9	34.2	33.8	32.3
Coordinates, isotropic B-factors	1.45-10	4844	0	331	19377	102188	21.9	25.4	20.0	23.5
shelxwat	1.45-10	4940	0	427	19761	102188	20.4	24.3	18.5	22.4
AnisotropicB-values	1.45-10	4942	0	428	44477	102188	15.6	21.2	13.9	19.5
Rebuilding + wat + glycerols	1.45-10	5208	0	632	45646	102188	13.9	19.9	12.3	18.2
Includeall data+anisotropic	1.39-10	5208	0	632	46871	113858	14.1	20.1	12.1	18.0
Refine occupancies of split residues	1.39-10	5240	0	654	47045	113858	14.0	20.1	12.0	18.0
Add Hs	1.39-10	5251	4300	667	47219	113858	13.2	19.4	11.8	17.8
Final refinement	1.39-10	5251	4300	667	47219	119840	13.7	-	11.7	-

The standard uncertainties calculated for angles within the H cluster vary from 0.23° to 2.86°. The angles are similar whether refinement is done with C-O-C/C-N-C/C-C-C as the bridging ligand in the H-subcluster.

Comparison of H-cluster Geometry
with Synthetic Models

The first complete H cluster framework was synthesized by Pickett and coworkers in 200 [284] as $[Fe_4S_4(SCH_3)_3\{Fe_2(CH_3C(CH_2S)_3)(CO)_5\}]^{2-}$. The molecule lacks a bridging CO as seen in the *Cp*I H-subcluster and has only CO ligands on the H-subcluster and no CN^-. A DFT optimization of the *in silico* model of $[Fe_4S_4(SCH_3)_3\{Fe_2(CH_3C(CH_2S)_3)(CO)_5\}]^{2-}$ was done and the distances of this model

can be compared to the distances of H-cluster obtained during anisotropic refinement of the 1.39 Å structure of *Cp*I. Darensbourg and coworkers also synthesized structural and functional analogues of the H-cluster in 2004, called 1-PTA and 1-PTA_2 where PTA=1,3,5 –triaza-7-phosphaadamantane=$P(CH_2)_6N_3$, in which the 2Fe moiety with a bridging propane dithiol had CO ligands attached to one Fe atom while the other Fe atom attaches to one or two PTA molecules [184]. Earlier Rauchfuss group had prepared model complex $(Et_4N_2)[Fe_2[\mu\text{-}S_2(CH_2)_3](CN)_2(CO)_4]$ which reacts with protons to give substoichiometric amounts of dihydrogen [183]. Lucas De Gioia and coworkers have been able to obtain an isomer of $Fe_2(S_2C_2H_4)(\mu\text{-}CO)(CN)_2(PPh_3)_2\text{-}(CO)_2$, confirmed crystallographically to be having a semi bridging CO-ligand with Fe- μC bond lengths of 2.15 and 1.85 Å [292].

Wilson and coworkers have been able to crystallographically characterize a bridged and terminal hydride in monocations $[Fe_2(edt)(\mu\text{-}H)(CO)_2\text{-}(PMe_3)_4]PF_6([1H]PF_6)$ and $[Fe_2(edt)(\mu CO)(H)(CO)\text{-}(PMe_3)_4]PF_6([1H]PF_6)$ respectively [188] The Fe-Fe distance in the crystal structure H-subcluster is closest to that of a synthetic mimic of H-cluster with a hydride at the terminal position of distal Fe atom and a bridging CO between the two iron atoms [188]. The hydride in this structure binds at the position where a water molecule is seen in the crystal structure and had been proposed to be the site where a hydride might bind during catalysis [143]. This distance is 2.610 Å in the synthetic mimic that has a hydride in the bridging position [188] and 2.546 Å in another mimic with a bridging CO that has a CO,CN^- and a tertiary phosphine as ligands to each iron. The distances of the bridging CO in the crystal structures does not agree with that seen in any of the mimics compared here, The distance between the distal Fe and the

bridging CO carbon atom in the crystal structure, within standard deviations, is slightly longer than that between the proximal Fe and the bridging CO carbon. In the synthetic mimics, considering the position of the bound hydride atom as the basis for assigning proximal and distal iron atom equivalents, the distal Fe-C (O) distances are shorter than the proximal Fe-C (O) distances. In looking for the closest mimic, these distances agree most with the bridging hydride mimic, where the difference between the two distances is ~0.06 Å and could be considered as equivalent. The mimics containing a bridging CO, show much greater displacement of the bridging CO towards the distal iron, with this distance 0.672 Å shorter than the proximal Fe-C (O) distance in the mimic containing a terminal hydride and a bridging CO.

In comparison of the H-subcluster angles with similar mimics [284], the largest differences in the angles occur where the sulfur atoms bonded to the dithiolate bridging ligand are involved. The current structure was refined with C-O-C as the bridging ligand based upon our DFT optimized calculations. Other areas of differences involve the sulfur atom of the cysteine that bridges the 2Fe subcluster with the 4Fe-4S cubane. The fact that the structural similarity of the above mentioned model complexes does not translate into functional equivalence to Fe-only hydrogenases implies that the protein environment has a key role to play in the catalytic process. It has been observed [293] that the model complexes and the active site clusters of enzymes differ in the orientation of the two-edge-bridged square pyramids with the model complexes placing the open sites underneath the μ-[2Fe-2S] unit, while the binuclear active site has one square pyramid inverted with respect to the other. This state has been observed to occur as a “transition state” in the DFT calculations of the intramolecular CO-site exchange processes in (μ-

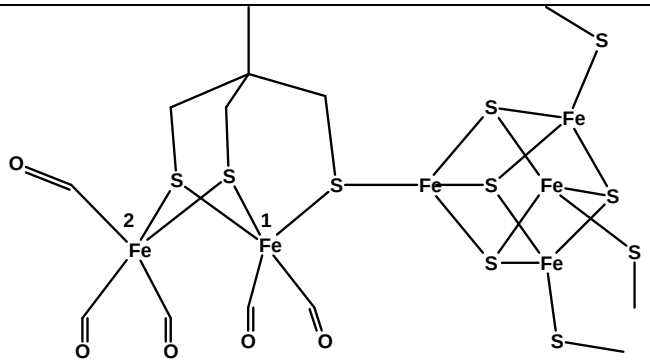

I. $Fe_4S_4(SCH_3)_3\{Fe_2(CH_3C(CH_2S)_3)(CO)_5\}]^{2-}$[284]

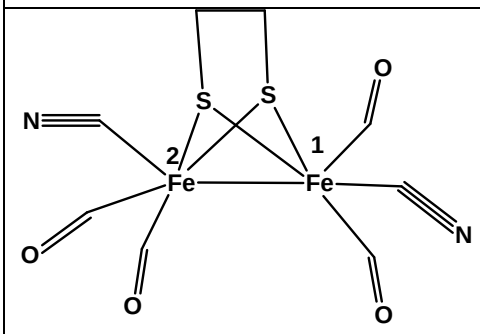

II. $Fe_2(S_2C_2H_4)(CN)_2(CO)_4]^{2-}$ [294]

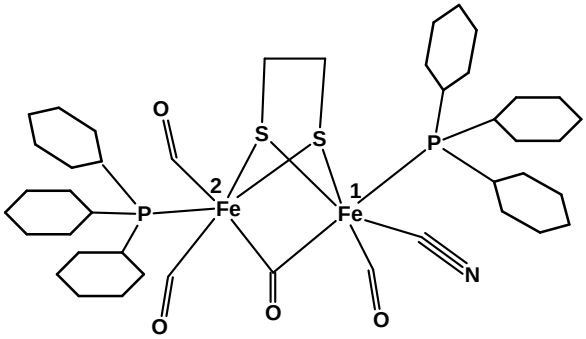

IV. $Fe_2(S_2C_2H_4)(\mu\text{-}CO)(CN)_2(PPh_3)_2(CO)_2$[292]

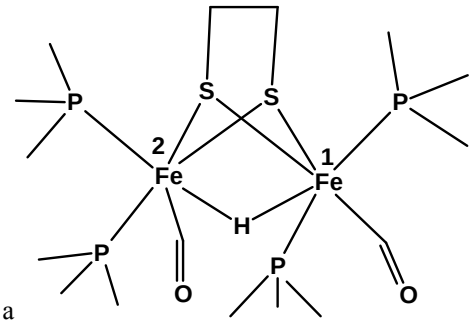

III a

$Fe_2(edt)(\mu\text{-}H)(CO)_2(PMe_3)_4]PF_6([1H]PF_6)$ [188]

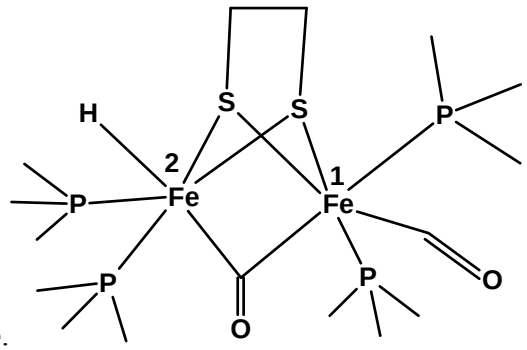

IIIb.

$Fe_2(edt)(\mu\text{-}CO)(H)_(CO)(PMe_3)_4]PF_6\alpha\text{-}[1H]PF_6)$

[188]

Figure 6.2: Sketches of the synthetic/DFT optimized H-cluster/H-subcluster mimics compared in Table 6.3

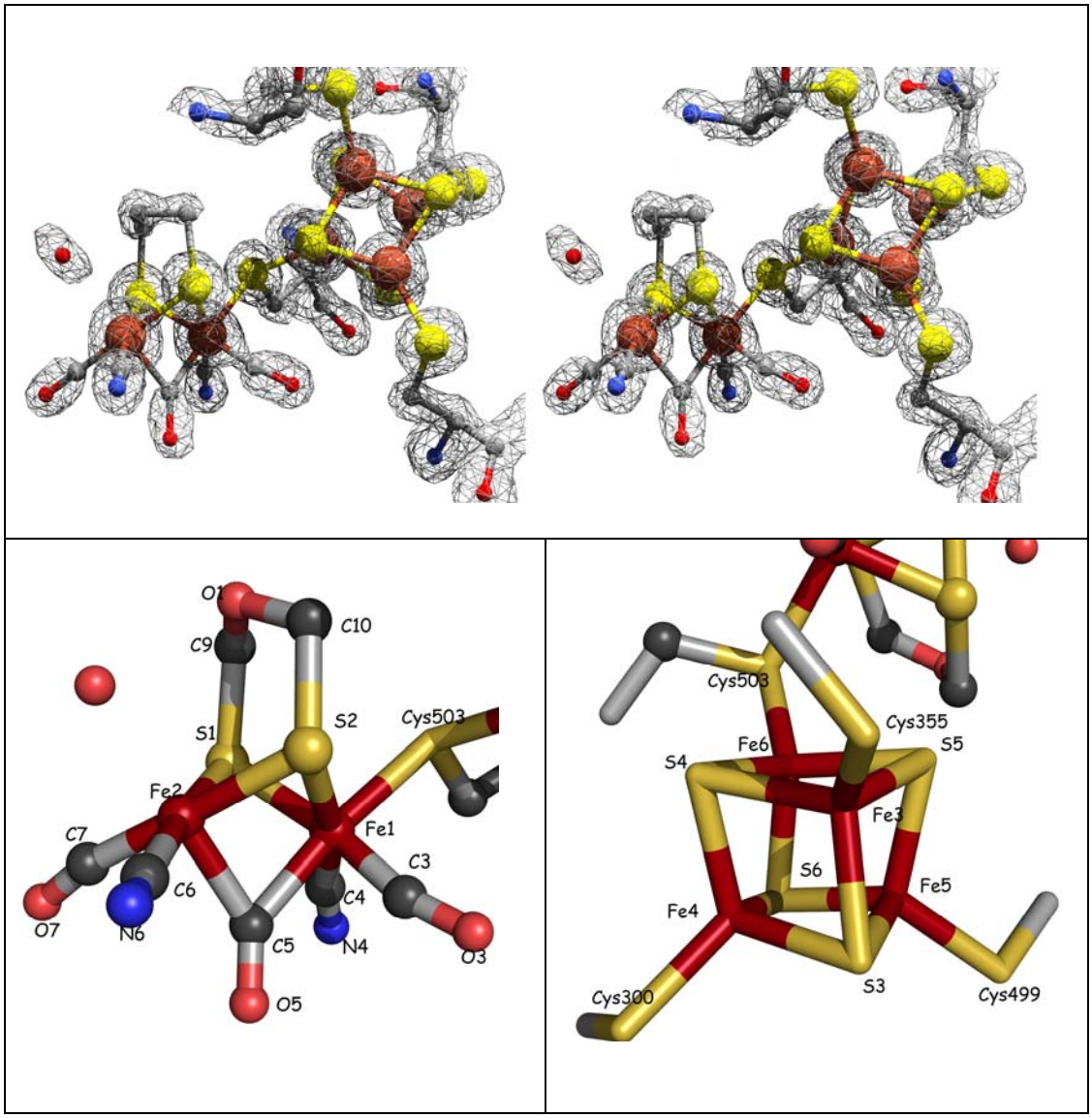

Figure 6.1 Stereo view of the electron density contoured to 1 σ around the atoms of the H cluster (Top). The central atom of the dithiolate bridging ligand is shown in magenta. The [FeFe] sub-cluster and the [4Fe-4S] subcluster showing the labeling of atoms as used in Table 6.3.

pdt)[Fe(CO)$_3$]$_2$ [295]. The holding in place of this higher energy conformation of the subcluster is attributed to interactions with the protein as well as to the stronger donation

of proximal iron to the bridging CO due to the presence of the bridging cysteine sulfur trans to the latter [293].

H-Cluster Coordination Sphere

The H cluster is housed in the active site domain formed by amino acid residues 210-574, which is the largest of the four domains of the protein [143]. The cavity in which the cluster exists is largely devoid of water, except for two water molecules, one at 2.36 Å from the distal Fe of the 2Fe subcluster relative to the [4Fe-4S] cubane that likely hydrogen bonds (2.55 Å) to the central atom of the dithiolate ligand refined as an oxygen. The other water molecule exists 3.75 Å from Cys 355 Sγ coordinating to the cubane and is held in position through hydrogen bonds to the amide nitrogen of Gly507. The 2Fe cluster is surrounded by primarily hydrophobic residues on the dithiolate side of the subcluster. The CN ligand on the distal Fe is at 2.28 Å and 2.77 Å from Nζ atom of the Lys358. The β, γ and ε hydrogens of Lys358 form hydrogen bonds with sulfurs of both the [FeFe] subcluster as well as that of cubane. The β and γ hydrogens also hydrogen bond with the oxygen of distal CO ligand. There are two methionine residues capping the [FeFe] subcluster on the top and bottom. In a sequence alignment of the Fe-only hydrogenases from *C. pasteurianum, D. desulfuricans*, *Chlamydomonas reinhardtii*, *Shewanella oneidensis* and *Thermatoga maritima*, both of these methionines are fully conserved. The bridging CO ligand of the 2Fe H-subcluster is in close contact with the sulfur atom of Met353. The other methionine, Met497 occurs directly above the bridging cysteine sulfur of Cys503. Interestingly, in the sequence alignment of Fe-only hydrogenases mentioned above, this residue is an alanine in all the organisms except *C.*

pasteurianum. All of the residues that are present in the immediate vicinity of the [FeFe] subcluster are fully conserved in all of the organisms mentioned above.

Table 6.3: A comparison of relevant bond distances within the 2Fe H-subcluster with select synthetic mimics (See Figure 6.2)

	CpI (1.39 Å) H-Cluster		I	II	III a	III b	IV
Fe-S		esds			μ H:⁻	axial H:⁻,μ-CO	μ-CO
Fe1-Fe2	2.5641	(0.007)			2.610	2.566	2.546
Fe2-H_2O	2.379	(0.038)					
$Fe_1 - S_1$	2.288	(0.010)	2.286	2.245			2.239
$Fe_1 - S_2$	2.300	(0.010)	2.285	2.244			2.256
$Fe_1 - S_{\gamma\ 503}$	2.391	(0.008)	2.312				
$Fe_2 - S_1$	2.320	(0.010)	2.315	2.265			2.268
$Fe_2 - S_2$	2.300	(0.010)	2.310	2.273			2.278
Fe – C							
$Fe_1 - C_3$	1.7326	(0.0151)	1.765				
$Fe_1 - C_4$	1.8402	(0.0150)		1.762			
$Fe_1 - C_5$ (H:⁻)	1.9109	(0.0150)		1.924	(1.65)	2.443	2.148
$Fe_2 - C_5$(H:⁻)	1.9705	(0.0146)			(1.61)	1.771	1.853
$Fe_2 - C_6$	1.8738	(0.0148)					
$Fe_2 - C_7$	1.7591	(0.0049)	1.776	1.944			

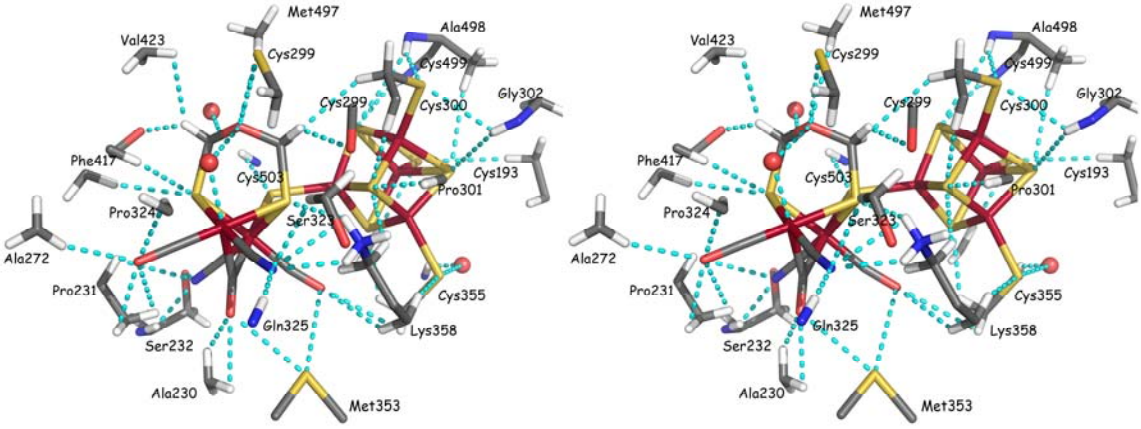

Figure 6.2 Stereo view of the interactions of H-cluster with the protein in CpI.

The nitrogen of the CN^- ligand on the proximal Fe forms a H-bond with the Oγ atom of Ser232 (2.81 Å) that could be a potential proton donor to the 2Fe H-subcluster. The [4Fe-4S] subcluster is covalently linked to the protein through four cysteines that are conserved in the organisms mentioned above. These cysteines are part of highly conserved sequences that consist of residues that form the cavity in which the cubane is contained. The backbones of these residues face the cubane to enter into several N-H….S contacts with the sulfur atoms of the cluster or the coordinating cysteines (Figure 6.2 A). The importance of hydrogen bonds between the amide hydrogen of the main chain and inorganic sulfur or cysteine Sγ atoms of the 4Fe-4S clusters are believed to stabilize the

Table 6.4 A list of the interactions shown in Figure 6.2.

H-cluster interactions with protein (Å)			
N6 - Hζ3 Lys358	2.28	N6 -Hβ1 Ser323	3.00
N6 - Hζ1 Lys358	2.77	Sγ Cys499 - Hα Gly506	2.93
Fe2-H2O	2.36	Sγ Cys499 - Hβ2 Cys193	3.30
S2 - H ζ 1 Lys358	3.14	S3 - Hβ3 Ala 498	3.09
N6 - HN Gln325	2.10	S4 - Hβ2 Cys 355	2.88
N4 - Oγ Ser232	2.81	O1 - Hε1 Met497	2.62
N4 - HN Ser232	2.34	S1 - Hβ2 Phe417	2.73
O1 - Sγ Cys299	3.45	O7- Hδ2 Pro231	2.94
O3 - Sδ Met353	3.52	O7- Hδ1 Pro 231	3.12
O5 - Sδ Met353	3.15	O5- Hβ1 Ala 230	2.78
O1 - Distal water	2.55	O5- Hβ2 Ala 230	2.41
Sγ Cys503 - HN Cys503	2.96	H9A - O Phe417	2.42
Sγ Cys355 - wat1	3.22	S5- Hε2 Lys358	3.14
Wat1 3.22 - HN Gly 507	2.20	Sγ Cys355 - Hγ1 Lys 358	2.77
Sγ Cys300 - HN Ala498	2.56	H10 - O Cys299	2.81
S6 - HN Cys499	2.65	H9A - wat2	2.61
S6 - HN Ala 498	3.20	S1- Hδ2 Phe 417	3.23
S3 - HN Gly302	3.53	O3 - Hγ2 Lys358	3.03
Sγ Cys300 - HN Gly302	2.98	O3 - Hβ1 Cys355	3.13
S5 - Hδ1 Pro391	2.63	S5 - Hα1 Cys300	2.95
O7- Hβ1 Ala 272	2.72	N4 - Hγ2 Pro231	3.34
O7- Hγ1 Pro324	2.94		

reduced form of the clusters by attenuating the charge density on the metal bound S atom. [285]. A serine side chain (Ser357) forms strong dipole interactions with Sγ of Cys355. In an alternate conformation the Oβ of Ser357 rotates away from the cubane to form a hydrogen bond (2.81 Å) with a water molecule which in turn is part of a network of hydrogen bonds leading to the exterior of the protein (Figure 6.3 Left). Two potential H^+ channel pathways can be identified, one leading from the water molecule liganded to distal iron to the exterior of the protein, and another originating at Lys357 and leading to the exterior (Figure 6.3 Right). The latter consists of residues that are highly conserved in the Fe-only hydrogenase from *D. desulfuricans* where in a similar manner they form a proton channel leading to and from the 2-Fe H-subcluster. A rapid influx of protons through these channels leading to the 2Fe H-subcluster would ensure a constant rate of H_2 production. In the [FeFe]-hydrogenase from *Desulfovibrio desulfuricans*, a cavity calculation [117] performed on the crystal structure using a 0.75 Å probe radius showed a single hydrophobic channel connecting the active site to the molecular surface [141]. The internal end of the channel faces the coordination site of distal iron atom which is vacant in the Ddase structure. As the radius of H_2 is about 1 Å, it was postulated that the entry of H_2 through this channel probably requires some protein flexibility. In *Cp*I, the binding site of distal iron coordinated water has been proposed to be the site where the formation of H_2 occurs [296].

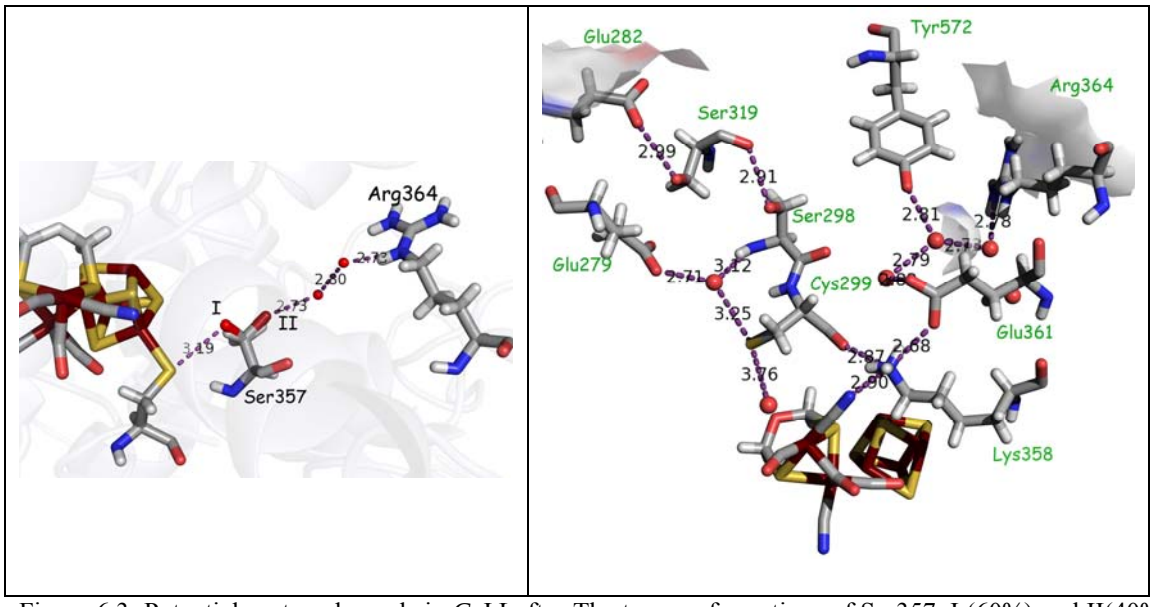

Figure 6.3 :Potential proton channels in *Cp*I.Left : The two conformations of Ser357, I (60%) and II(40%) making contact with the 4Fe-4S H-subcluster in conformation I and with the Arg364 on the protein surface in conformation II. Right**:** Two potential proton channel pathways originating from the water molecule at the distal iron and Lys358. The exterior of the protein is shown as a surface.

Previous studies have shown that the oxidation of H_2 by hydrogenases occurs by a heterolytic cleavage mechanism involving the formation of a hydride and a proton and assisted by a base [91]. In both *Dd*ase and *Cp*I (Lys 358, figure 6.3, right) , a conserved lysine residue that hydrogen bonds to the CN^- ligand on distal iron atom, is in a position to serve as a proton donor directly to the 2Fe H-subcluster. The acceptor has been proposed to be the CN^- ligand [141]. A third proton channel is identified in the current structure of *Cp*I that leads to the exterior of the proton (Figure 6.3 Left). This channel, however, leads to the [4Fe-4S] sub cluster through the movement of Ser357 side chain in two different conformations. In its major conformation, Ser357 side chain hydroxyl group forms dipole interactions with Cys355 Sγ that is one of the ligands to the [4Fe-4S] H-subcluster. This Cys355 Sγ also hydrogens bonds to a γH on Lys358. This strengthens the role of Lys358 as a proton donor, probably to the CN^- ligand on distal iron.

The proposed proton pathways shown lead to the exterior. It has been shown in the crystal structure of *Cp*I that two potential electron transfer pathways exist from the [2Fe-2S] cluster of the FS2 domain and the [4Fe-4S] cluster of the FS4C domain to the H-cluster through the [4Fe-4S] clusters of the FS4A-FS4B domains [143, 296]. The [2Fe-2S] cluster and the FS4C domain [4Fe-4S] cluster get reduced by electron donors as these occur on the surface. The reducing equivalents are then channeled through the clusters as shown in Figure 6.4. It is noticeable that the electron transfer pathways also lead to Sγ of Cys355 of the [4Fe-4S] H-subcluster. Cys355 Sγ hence might be a branching point where the protons are channeled towards the 2Fe subcluster through Lys358 while the electrons go through the [4Fe-4S] cluster itself.

The proton pathway leading to the 2Fe H-subcluster distal iron coordinated water molecule shows the proximity of Cys299 Sγ to this site where hydrogen formation has been proposed to occur. It is hence in a position to donate the proton directly to the hydride when it binds at this site. The yet unidentified dithiolate bridging ligand probably has a role to play in this transfer. The nature of amino acids at the exterior of the protein (Glu and Arg) can be used as a basis for speculating that the way in for protons is the pathway involving glutamate (pKa 4.25) at the exterior with the final proton donor to the active site being Cys299 (pKa 8.18). It can be assumed that during the reverse reaction, i.e. the production of protons, the pathway involving Lys358 (pKa 10.53, assuming it is not influenced too much by proximity to the cluster) is the preferred pathway for release of protons to the exterior.

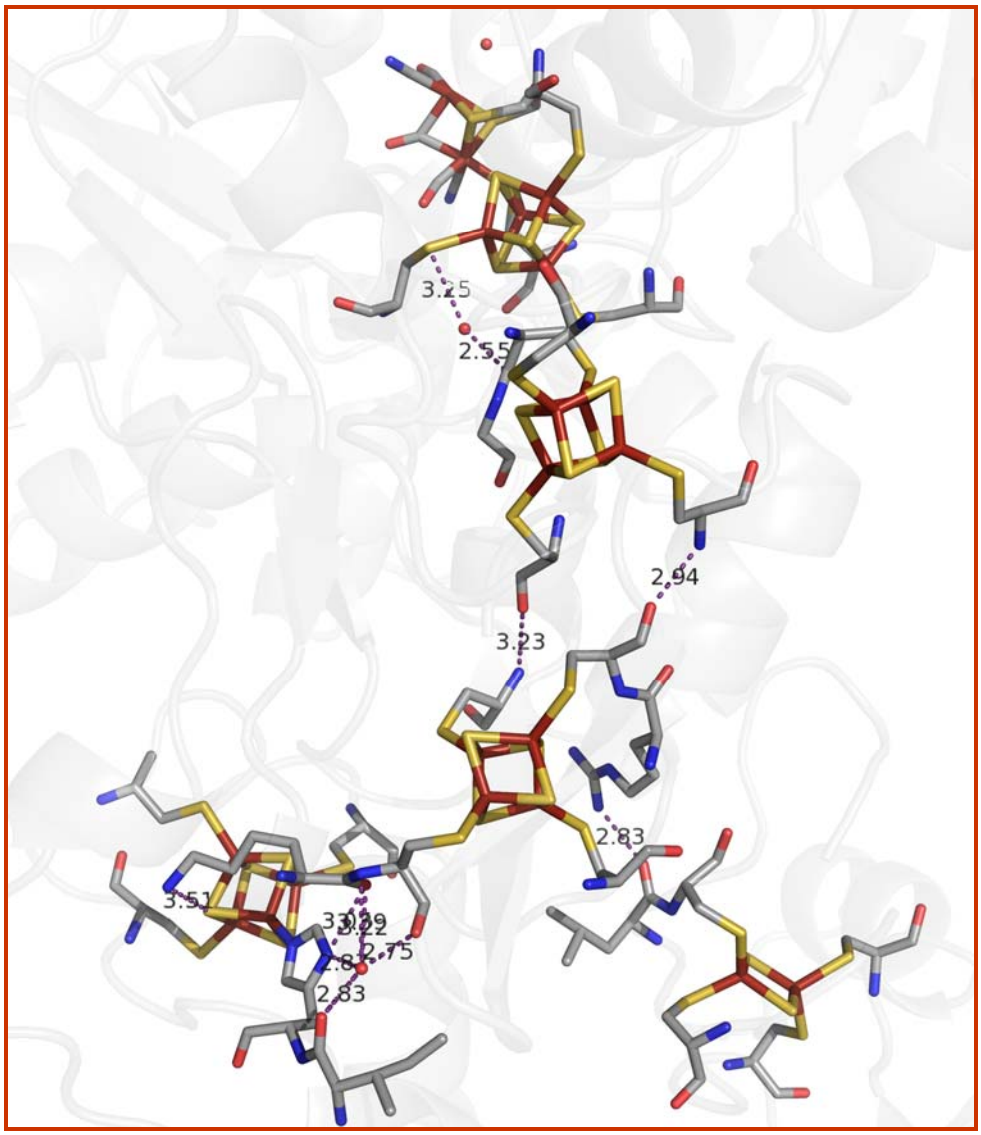

Figure 6.4: Two potential electron transfer pathways from the [2Fe-2S] and [4Fe-4S] clusters leading to the Cys355 Sγ of H-cluster.

Density Functional Optimization of the H-cluster

The identity of the dithiolate ligands bridging the two sulfur atoms of the 2Fe subcluster has been ambiguous. It has been speculated that this central ligand could be a propane dithiolate (PDT) or a dithiomethylamine (DTMA). A DTMA ligand has been

favoured because of the ability of the amine group to be able to donate a proton to a hydride ligand at the distal Fe site or accept proton from the coordinated dihydrogen. In order to resolve this, a DFT optimization of the 6Fe-6S H-cluster including residues from the protein within 3.8 Å of this cluster, was carried out. This was done with C-C-C, C-N-C, C-O-C, and C-S-C ligand compositions as the potential entities that bridge the two sulfur atoms of the 2Fe H-subcluster. Various protonated forms of the N bridgehead atom were considered. The unlikely C-S-C composition was also evaluated to validate that the optimizations with thioether moiety result in unreasonable structural changes in comparison to the high resolution crystal structure. Figure 1 shows the relative energy changes as a function of optimization cycles to the most accurate crystallographic structure (kJ/mol).

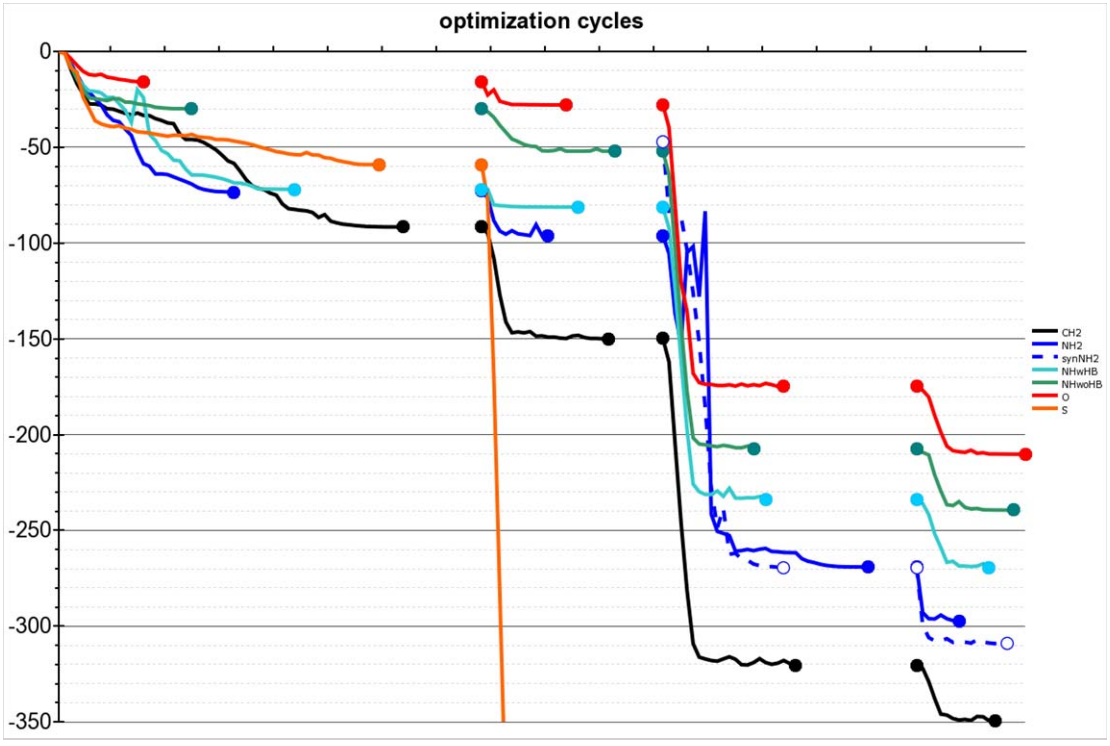

Figure 6.5: Gradual structural optimizations of a) distal water, b) distal water, bridgehead group, c) distal water, CH_2-X-CH_2 moiety, d) distal water, S-CH_2-X-CH_2-S moiety

Figure 6.4 clearly indicates that the experimental atomic positions are most consistent with the thioether composition as this stoichiometry shows the smallest energy change between the structurally optimized (atomic resolution geometry) and the experimentally observed geometry. The order of agreement decreases from O (red), NH (cyan and teal), NH_2^+ (blue), CH_2(black), and not unexpectedly S (orange). The latter already shows large structural changes and corresponding drop in the relative energies due to the much longer C-S distances and very different C-S-C angles than in the experimental structure. Interestingly, an experimentally non-observed conformation of the NH_2^+ group becomes more favourable (dashed blue line) where the bridgehead group points toward the bridging cysteine (Cys503) sulfur. As observed by ^{1}H NMR [297], the fused Fe-dicyclohexyldithiol ring is fluxional at room temperature, which implies that the protonated amine bridgehead is likely to turn away from the catalytically important distal iron site and actually acts as an inhibitor to the dihydrogen production and uptake.

Further optimization of the H-cluster and its protein environment maintains the same energetic preference once the Fe ions, diatomic ligands, 6Fe-6S cluster, 6Fe-6S cluster with four Scys links are optimized (Figure 6.5).

Changes of two selected structural parameters (distal Fe, distal water distance, Figure 6.6; and bridgehead group, distal water distance, Figure 6.7) as a function of optimization constraints also imply the preference of the thioether composition.

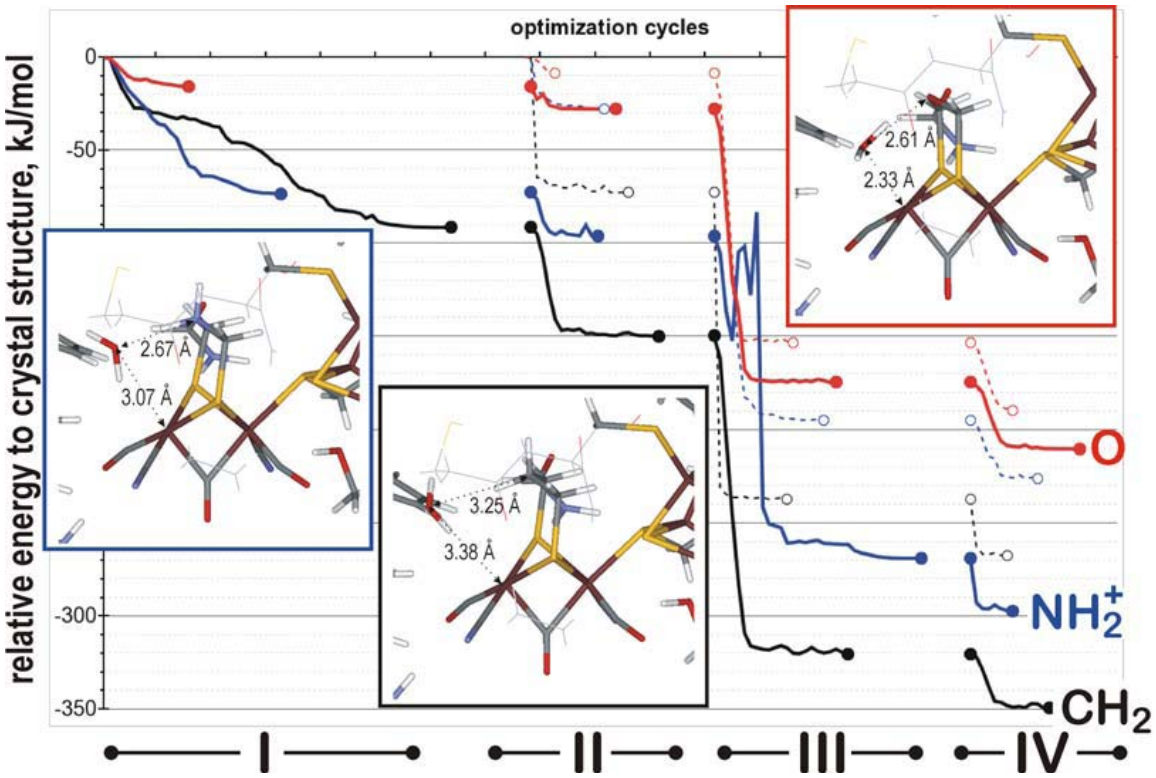

Figure 6.6: Energy stabilization upon sequential structural optimization of section I (distal water), II (I + γ-group), III (II+β-CH2), and IV (III+μS) of the dithiolate ligand of the H-cluster embedded in a 3.5 Å protein environment

Conclusion

The crystal structure of *Cp*I Fe-only hydrogenase refined at 1.39 Å anisotropically, provides more accurate atomic positions within the protein. The calculated standard uncertainties for the bond distances within the H-cluster show the accuracy to be within 0.04 Å. Two more proton channels in addition to the one proposed earlier are identified.

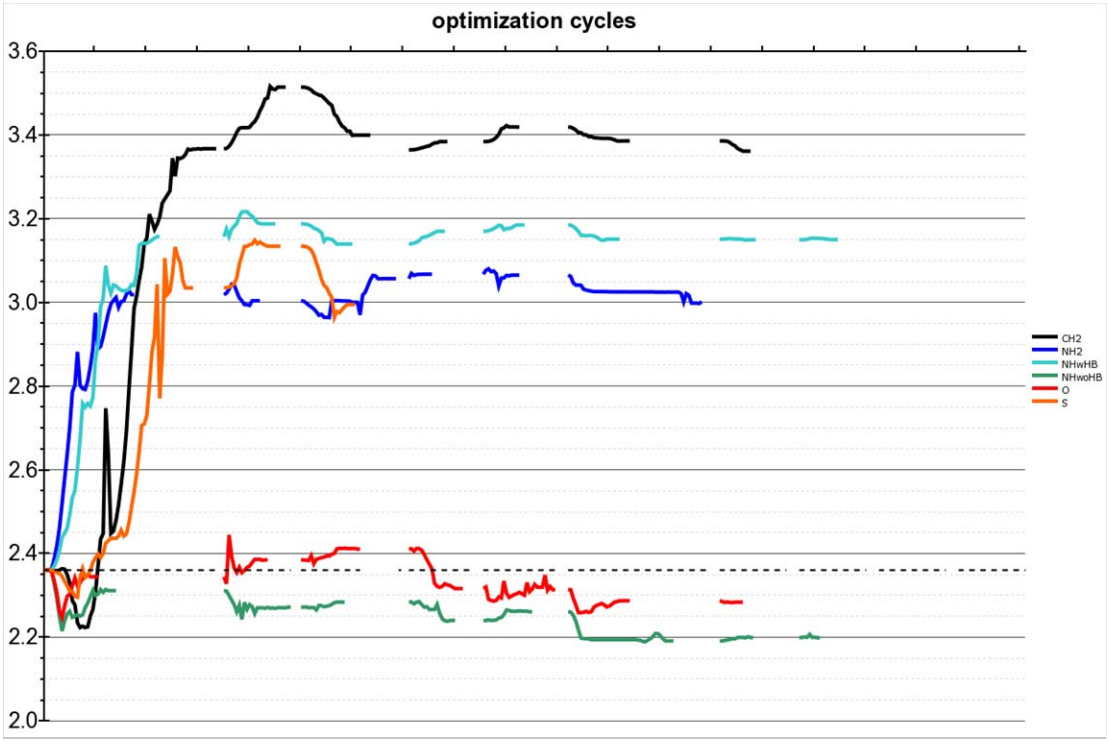

Figure 6.7: Change of distal iron and distal water distance in Å as a function of gradual structural optimizations of a) distal water, b) distal water, bridgehead group, c) distal water, CH_2-X-CH_2 moiety, d) distal water, S-CH_2-X-CH_2-S moiety, e) distal water Fe-S-CH_2-X-CH_2-S-Fe moiety; f) {Fe_2(S-CH_2-X-CH_2-S)$(CO)_3(CN)_2$}(OH_2); g) [Fe_4S_4]{Fe_2(S-CH_2-X-CH_2-S)$(CO)_3(CN)_2$}(OH_2);h)[Fe_4S_4]$(SEt)_4${Fe_2(S-CH_2-X-CH_2S)$(CO)_3(CN)_2(OH_2)$

The previously proposed channel probably serves to donate protons for hydrogen production while the now identified proton channels would serve to transfer protons out during H_2 oxidation. The coordinates of H-cluster atoms with its first coordination sphere interactions was taken as a model for a DFT optimization with various options for the dithiolate bridging ligand. The calculations indicate that energetically, the most favourable central atom for the bridging ligand is an oxygen and implies a role for the distal iron bonded water molecule. The possible composition of dithiomethylthioether ligand brings up an exciting new mechanistic role for the distal water molecule. Its

oxygen bridgegroup can conveniently anchor the distal water molecule that can be a flexible and versatile proton donor or acceptor for the distal iron. In addition the

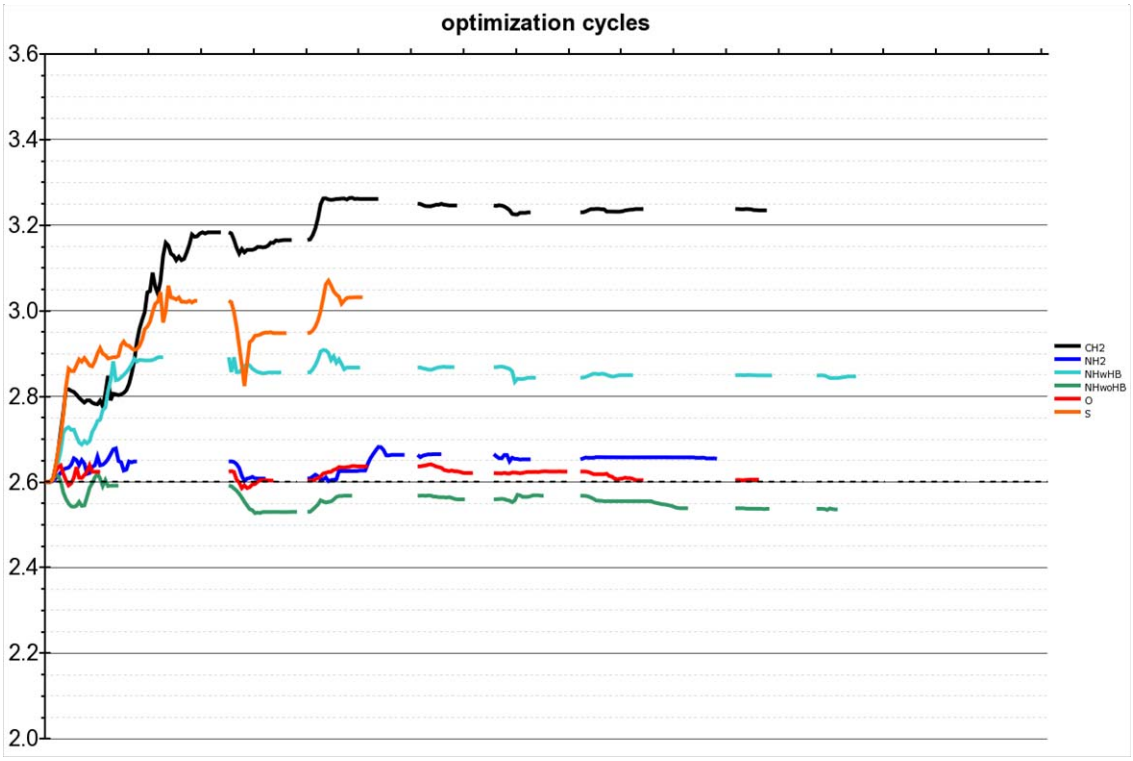

Figure 6.8: Change of bridgehead group and distal water distance in Å as a function of gradual structural optimizations of a) distal water, b) distal water, bridgehead group, c) distal water, CH_2-X-CH_2 moiety, d) distal water, S-CH_2-X-CH_2-S moiety, e) distal water Fe-S-CH_2-X-CH_2-S-Fe moiety; f) {Fe_2(S-CH_2-X-CH_2-S)$(CO)_3(CN)_2$}(OH_2); g) [Fe_4S_4]{Fe_2(S-CH_2-X-CH_2-S)$(CO)_3(CN)_2$}(OH_2); h)[Fe_4S_4]$(SEt)_4${Fe_2(S-CH_2-X-CH_2-S)$(CO)_3(CN)_2(OH_2)$}

sulfhydryl group of the nearby Cys299 residue connect the distal water molecule with the pool of water molecules for mediating the proton transfer from and to the active site. Comparison of the *Dd*ase and the *Cp*I H-cluster and the pool of water molecule suggest that even the distal water can be translocated between the active site and the pool of water molecules to allow for substrate (dihydrogen or hydride) binding.

CONCLUDING REMARKS

The enzyme 2-ketopropyl coenzyme M oxidoreductase / carboxylase (2-KPCC) catalyzes the NADPH dependent reductive cleavage of 2-ketopropyl coenzyme M (KCoM). The transfer of electrons from $NADP^+$ to KCoM occurs through a non-covalently bound FAD and a redox active cysteine disulfide, similar to the disulfide oxidoreductase (DSOR) family of enzymes. Although it shares ~30% sequence identity and bears the same secondary structure as some of the well known DSORs, it differs from the same in two aspects: one, it catalyzes the cleavage of a thioether C-S linkage as opposed to an S-S linkage by DSORs, two, it carboxylates one of the leaving groups and protonates the other, while DSORs protonate both leaving groups. The cleavage of KCoM and carboxylation occurs through the formation of an enolate intermediate which can undergo electrophilic attack by a CO_2 molecule to form acetoacetate or a H^+ to yield acetone. The enzyme discriminates between the two electrophiles and preferentially carboxylates the enolate intermediate rather than protonate it. The previously determined KCoM bound structure showed that KCoM binds in a distinctly hydrophobic site which is shielded from solvent by movements of the N- and C-terminii that accompanies substrate binding. This provides an environment conducive to carboxylation and prevents protonation of the enolate intermediate. The structure also showed that the keto group of KCoM is stabilized by a His oriented water molecule and likely serves to stabilize the enolate intermediate too. The NADPH dependent carboxylation catalyzed by some dehydrogenases (eg. Pyruvate dehydrogenase, isocitrate dehydrogenase, 6-phosphogluconate dehydrogenase) occurs by direct reduction of a keto group by

NADPH. In the pyruvate dehydrogenase catalyzed carboxylation of acetyl CoA, the cleavage of the C-S bond is mediated by thiamin pyrophosphate. The C-S cleavage by 2-KPCC is carried out by a cysteine thiol that is formed by electron transfer from NADPH via FAD to the redox disulfide.

The reverse reaction, decarboxylation of acetoacetate in the presence of coenzyme M, results in the formation of KCoM and is dependent on the presence of $NADP^+$. The decarboxylation also occurs through the formation of an enolate intermediate followed by its attack on the coenzyme M thiol of the mixed disulfide to form KCoM. It was however not clear from the available structures or the kinetic studies how the carboxylation / decarboxylation processes occur.

Co-crystallization studies of 2-KPCC with various catalytically relevant ligands were utilized to gain further insights into the mechanisms of the forward and reverse reactions. The crystallization of 2-KPCC was carried out by incubation of the protein with KCoM, acetoacetate, NADP(H), coenzyme M, analog 6-oxoheptanoic acid and product analog 2-oxopropyl phosphonate prior to crystallization. Reduced states for each form of crystal obtained were achieved by soaking the crystals in DTT before subjecting them to X-ray diffraction.

Crystals obtained with acetoacetate, $NADP^+$ and coenzyme M showed density consistent with a CO_2 molecule at the base of a hydrophobic channel in a hydrophobic pocket and a bicarbonate ion bound at an alternate anion binding site adjacent to the substrate binding site. In addition, there is formation of KCoM according to the reaction

$$CH_3COCH_2COO^- + CoM + NADP^+ \longrightarrow KCoM + NADPH + HCO_3^-$$

The alternate anion binding site where bicarbonate binds is capable of binding other anions as witnessed in the structure obtained by incubation with coenzyme M, showing a CoM-disulfide at the active site with the sulfonate moieties of the two CoM molecules bound at the substrate and alternate binding sites respectively. The coenzyme M sulfonate bound at the alternate anion binding site forms interactions with residues of the other subunit as well as one of the Arg residues at the substrate binding site. This suggests an overall weakening of interactions between the substrate binding site residues and the coenzyme M sulfonate moiety due to sharing of charge between two different anions. In co-crystallization of 2-KPCC with acetoacetate, the latter could never be captured bound as such. Since the addition of acetoacetate only did not yield good diffraction quality crystals and addition of CoM to the same resulted in acetoacetate turnover, an acetoacetate analog, OPP, was used as a substitute to gain insights into the nature of acetoacetate binding at the active site. In the absence of CoM, OPP binds at the substrate binding site through interactions of the carboxyl group with the Arg residues of the substrate binding site. This provides a structural basis for the close to abiotic rate of acetoacetate turnover by 2-KPCC in the absence of coenzyme M as shown during kinetic studies. This implies that 2-KPCC catalyzed decarboxylation cannot occur at the substrate binding site. In the structure obtained by incubation with OPP, coenzyme M and $NADP^+$, OPP was found to be bound at the alternate anion binding site while coenzyme M binds at the substrate binding site. This corroborates the assignment of the alternate anion binding site as acetoacetate binding site as well as the site where decarboxylation can occur. Decarboxylation of acetoacetate occurring at this site would favour the formation of a bicarbonate ion by immediate interaction of the cleaved CO_2

molecule with water molecules present at this site, and its stabilization therein. The bicarbonate ion, a water molecule and the CO_2 molecule occur within hydrogen bonding distances, suggesting a disproportionation occurring between the carbonate species such that each of them end up at sites suited to their nature. In the structure obtained from co-crystallization with the substrate analog 6-oxoheptanoic acid, the carbonyl group of the ketopropyl moiety of the analog was seen to be stabilized by a main chain carbonyl bound water molecule between the CO_2 and bicarbonate binding sites. This suggests the stabilization of the enolate intermediate at two different sites: the His137 stabilized water molecule on one subunit as shown in the KCoM bound structure and the Ala430 main chain carbonyl bound water molecule on the other subunit as shown in the OHA bound structure. This is in agreement with the kinetic studies on acetoacetate decarboxylation which showed that acetoacetate decarboxylation and subsequent attack by coenzyme M to form KCoM occurs through the formation of an enolate intermediate. If decarboxylation occurs at the alternate anion binding site as suggested by structural results, the enolate stabilization during the reverse reaction would occur by interaction with the Ala430 bound water molecule.

When the crystals obtained with acetoacetate, $NADP^+$ and CoM were reduced with DTT before subjection to X-ray diffraction, a mixed disulfide intermediate formed between CoM and redox active Cys82 were captured. In addition, density consistent with a trigonal planar molecule was captured at the alternate anion binding site, which was assigned to be an acetone molecule formed by protonation of the enolate intermediate. A water molecule within hydrogen bonding distance of the sulfur atom of the mixed disulfide suggested a mechanism for coenzyme M release in addition to the weakening of

interactions between the sulfonate group of coenzyme M and the substrate binding site. Free coenzyme M is then released by a nucleophilic attack of this water molecule on the mixed disulfide linkage.

The CO_2 binding site occurs at the end of a hydrophobic channel that opens into the active site. This hydrophobic channel is formed at the dimer interface by non-polar residues of both subunits. On superimposition of the CO_2 bound structure on the KCoM bound structure, CO_2 was found to occur in close proximity to the C-S linkage of KCoM, implying an attack of CO_2 on the enolate intermediate at this site to form acetoacetate. The carboxyl group of the latter would then orient towards the alternate anion binding site for product stabilization. The sharing of charge from Arg365 of the substrate binding site, between the carboxyl group and the sulfonate moieties would aid the release of coenzyme M as implied by the coenzyme M disulfide and OPP+CoM bound structures.

Most of the features of the mechanism have been elucidated by structures obtained in the above mentioned catalytically relevant forms. Although some of the structures mentioned above have been obtained in oxidized and reduced states, they do not provide relevant information about the electron transfer occurring from NADPH through FAD to the cysteine disulfide. The nature of product formed due to decarboxylation of acetoacetate clearly depends on the presence of $NADP^+$ as shown in the kinetic studies. Future co-crystallization studies will be directed at capturing an acetoacetate bound state, KCoM bound state in the presence of $NADP^+$ / NADPH, and NADPH only bound state.

The structural characterization of the above mentioned catalytically relevant states have provided important insights into the mechanism of carboxylation, decarboxylation,

intermediate formation and stabilization and product stabilization and release. This sets the stage for the design of site directed mutagenic experiments to verify the role of individual amino acid residues implicated by the structural studies to be involved in intermediate and product stabilization. These results also lay the groundwork for designing kinetic and spectroscopic analysis with the native and mutated enzyme to determine the NADP(H) dependence of the catalytic activities of 2-KPCC, role of metal ion in various catalytic activities and testing whether the enzyme has carobonic anhydrase like activity.

The active site of [FeFe] hydrogenase from *Clostridium pasteurianum* (*Cp*I) is the 6Fe H-cluster consisting of a 2Fe subcluster bridged to a [4Fe-4S] cubane through a protein cysteinytl sulfur bridge. The Fe atom distal to the cubane in the 2Fe subcluster is the site of reversible oxidation of H_2. The two Fe atoms of the same are bridged through a dithiolate ligand long accepted as dithiomethylamine. At a resolution of 1.39 Å, the anisotropic B-factors for all atoms of *Cp*I could be carried out resulting in a highly accurate model. The accuracy of positional assignment of individual atoms of the H-cluster could be determined by calculation of their estimated standard deviations with respect to energy optimized structures. The results showed that the assignment of atoms of the atoms of the H-cluster was accurate within 0.04 Å. This provided a reliable model for performing density functional theory calculations to determine the composition of the dithiolate ligand most energetically favoured and in agreement with the crystal structure. The orientation of this ligand as seen in the crystal structure agrees more with the assignment of this ligand as a dithiomethylether. According to this calculation, the orientation most favored energetically if this were a dithiomethylamine points in the

direction opposite to that shown by the crystal structure. The mechanism of H_2 formation at the distal Fe of the 2Fe H-subcluster hence suggests a role for Cys299 thiol group as the proton donor as opposed to proton donation by the nitrogen atom of the dithiomethylamine group. Dithiomethylether has been essentially as the ligand bridging the Fe atoms of the 2Fe H-subcluster for no clear reason. This study provides a strong basis for the next generation of H-cluster mimics and theoretical examination of dithiomethylether as an H-cluster ligand.

BIBLIOGRAPHY

1. Hopkins, A.L. and C.R. Groom, *The druggable genome.* Nat Rev Drug Discov, 2002. 1(9): p. 727-30.

2. Anderson, A.C., *The process of structure-based drug design.* Chem Biol, 2003. 10(9): p. 787-97.

3. Cleveland, C.C. and J.B. Yavitt, *Microbial Consumption of Atmospheric Isoprene in a Temperate Forest Soil.* Appl Environ Microbiol, 1998. 64(1): p. 172-177.

4. Hartmans, S., J.A. de Bont, and W. Harder, *Microbial metabolism of short-chain unsaturated hydrocarbons.* FEMS Microbiol Rev, 1989. 5(3): p. 235-64.

5. van Ginkel, C.G., H.G. Welten, and J.A. de Bont, *Oxidation of Gaseous and Volatile Hydrocarbons by Selected Alkene-Utilizing Bacteria.* Appl Environ Microbiol, 1987. 53(12): p. 2903-2907.

6. van Ginkel, C.G., De Bont JAM, *Isolation and characterization of alkene utilizing Xanthobacter spp.* Arch. Microbiol., 1986. 145: p. 403-407.

7. Miura, A.a.D., H, *Purification and characterization of the alkene monooxygenase from Nocardia corallina B-276.* Biosci. Biotechnol. Biochem., 1995. 59: p. 853-859.

8. Small, F.J. and S.A. Ensign, *Alkene monooxygenase from Xanthobacter strain Py2. Purification and characterization of a four-component system central to the bacterial metabolism of aliphatic alkenes.* J Biol Chem, 1997. 272(40): p. 24913-20.

9. Wade, D.R., S.C. Airy, and J.E. Sinsheimer, *Mutagenicity of aliphatic epoxides.* Mutat Res, 1978. 58(2-3): p. 217-23.

10. Guengerich, F.P., *Reactions and significance of cytochrome P-450 enzymes.* J Biol Chem, 1991. 266(16): p. 10019-22.

11. Guengerich, F.P. and D.C. Liebler, *Enzymatic activation of chemicals to toxic metabolites.* Crit Rev Toxicol, 1985. 14(3): p. 259-307.

12. Koskinen, M. and K. Plna, *Specific DNA adducts induced by some mono-substituted epoxides in vitro and in vivo.* Chem Biol Interact, 2000. 129(3): p. 209-29.

13. De Bont JAM, v.D.J., van Ginkel CG, *The metabolism of 1,2-propanediol by the propylene oxidizing bacterium Nocardia A60.* Biochim. Biophys. Acta, 1982. 714: p. 465– 70.

14. Hartmans, S., et al., *Metabolism of Styrene Oxide and 2-Phenylethanol in the Styrene-Degrading Xanthobacter Strain 124X.* Appl Environ Microbiol, 1989. 55(11): p. 2850-2855.

15. Small, F.J. and S.A. Ensign, *Carbon dioxide fixation in the metabolism of propylene and propylene oxide by Xanthobacter strain Py2.* J Bacteriol, 1995. 177(21): p. 6170-5.

16. Ensign, S.A., *Aliphatic and chlorinated alkenes and epoxides as inducers of alkene monooxygenase and epoxidase activities in Xanthobacter strain Py2.* Appl Environ Microbiol, 1996. 62(1): p. 61-6.

17. Ensign, S.A., M.R. Hyman, and D.J. Arp, *Cometabolic degradation of chlorinated alkenes by alkene monooxygenase in a propylene-grown Xanthobacter strain.* Appl Environ Microbiol, 1992. 58(9): p. 3038-46.

18. Small, F.J., J.K. Tilley, and S.A. Ensign, *Characterization of a New Pathway for Epichlorohydrin Degradation by Whole Cells of Xanthobacter Strain Py2.* Appl Environ Microbiol, 1995. 61(4): p. 1507-1513.

19. Ensign, S.A., et al., *New roles for CO2 in the microbial metabolism of aliphatic epoxides and ketones.* Arch. Microbiol, 1998. 169(3): p. 179-87.

20. Allen, J.R. and S.A. Ensign, *Characterization of three protein components required for functional reconstitution of the epoxide carboxylase multienzyme complex from Xanthobacter strain Py2.* J. Bacteriol, 1997. 179(10): p. 3110-5.

21. Gallagher, S.C., R. Cammack, and H. Dalton, *Alkene monooxygenase from Nocardia corallina B-276 is a member of the class of dinuclear iron proteins capable of stereospecific epoxygenation reactions.* Eur J Biochem, 1997. 247(2): p. 635-41.

22. Allen, J.R. and S.A. Ensign, *Purification to homogeneity and reconstitution of the individual components of the epoxide carboxylase multiprotein enzyme complex from Xanthobacter strain Py2.* J Biol Chem, 1997. 272(51): p. 32121-8.

23. Allen, J.R. and S.A. Ensign, *Two short-chain dehydrogenases confer stereoselectivity for enantiomers of epoxypropane in the multiprotein epoxide carboxylating systems of Xanthobacter strain Py2 and Nocardia corallina B276.* Biochemistry, 1999. 38(1): p. 247-56.

24. Allen, J.R., et al., *A role for coenzyme M (2-mercaptoethanesulfonic acid) in a bacterial pathway of aliphatic epoxide carboxylation.* Proc Natl Acad Sci U S A, 1999. 96(15): p. 8432-7.

25. Swaving, J., et al., *A novel type of pyridine nucleotide-disulfide oxidoreductase is essential for NAD+- and NADPH-dependent degradation of epoxyalkanes by Xanthobacter strain Py2.* J. Bacteriol, 1996. 178(22): p. 6644-6.

26. Swaving, J., et al., *Complementation of Xanthobacter Py2 mutants defective in epoxyalkane degradation, and expression and nucleotide sequence of the complementing DNA fragment.* Microbiology, 1995. 141 (Pt 2): p. 477-84.

27. Westphal, A.H., et al., *Purification and characterization of a flavoprotein involved in the degradation of epoxyalkanes by Xanthobacter Py2.* Eur J Biochem, 1998. 257(1): p. 160-8.

28. Pai, E., *Variations on a theme: the family of FAD-dependent NAD(P)H-(disulfide)-oxidoreductases* Curr. Opin. Struct. Biol., 1991. 1: p. 796-803.

29. Ghisla, S. and V. Massey, *Mechanisms of flavoprotein-catalyzed reactions.* Eur J Biochem, 1989. 181(1): p. 1-17.

30. Williams, C.J., *Lipoamide dehydrogenase, glutathione reductase, thioredoxin reductase and mercuric ion reductase: A family of Flavoenzyme Transhydrogenases*. Vol. 3. 1992, Boca Raton, FL: CRC Press.

31. Schulz, G.E., et al., *The structure of the flavoenzyme glutathione reductase.* Nature, 1978. 273(5658): p. 120-4.

32. Karplus, P.A. and G.E. Schulz, *Refined structure of glutathione reductase at 1.54 A resolution.* J Mol Biol, 1987. 195(3): p. 701-29.

33. Karplus, P.A. and G.E. Schulz, *Substrate binding and catalysis by glutathione reductase as derived from refined enzyme: substrate crystal structures at 2 A resolution.* J Mol Biol, 1989. 210(1): p. 163-80.

34. Pai, E.F., P.A. Karplus, and G.E. Schulz, *Crystallographic analysis of the binding of NADPH, NADPH fragments, and NADPH analogues to glutathione reductase.* Biochemistry, 1988. 27(12): p. 4465-74.

35. Pai, E.F. and G.E. Schulz, *The catalytic mechanism of glutathione reductase as derived from x-ray diffraction analyses of reaction intermediates.* J Biol Chem, 1983. 258(3): p. 1752-7.

36. Rietveld, P., et al., *Reductive and oxidative half-reactions of glutathione reductase from Escherichia coli.* Biochemistry, 1994. 33(46): p. 13888-95.

37. Worthington, D.J. and M.A. Rosemeyer, *Glutathione reductase from human erythrocytes. Catalytic properties and aggregation.* Eur J Biochem, 1976. 67(1): p. 231-8.

38. Pinto, M.C., A.M. Mata, and J. Lopez-Barea, *Reversible inactivation of Saccharomyces cerevisiae glutathione reductase under reducing conditions.* Arch Biochem Biophys, 1984. 228(1): p. 1-12.

39. Pinto, M.C., A.M. Mata, and J. Lopez-Barea, *The redox interconversion mechanism of Saccharomyces cerevisiae glutathione reductase.* Eur J Biochem, 1985. 151(2): p. 275-81.

40. Lopez-Barea, J. and C.Y. Lee, *Mouse-liver glutathione reductase. Purification, kinetics, and regulation.* Eur J Biochem, 1979. 98(2): p. 487-99.

41. Williams, C.H., Jr., *Lipoamide Dehydrogenase, Glutathione Reductase, Thioredoxin Reducatse, and Mercuric Ion Reductase:A Family of FlaVoenzyme Transhydrogenases* Ed. F. Muller. Vol. Vol. 3. 1992, Boca Raton, FL: CRC Press.

42. Benen, J., et al., *Lipoamide dehydrogenase from Azotobacter vinelandii: site-directed mutagenesis of the His450-Glu455 diad. Kinetics of wild-type and mutated enzymes.* Eur J Biochem, 1992. 207(2): p. 487-97.

43. Fairlamb, A.H., et al., *Trypanothione: a novel bis(glutathionyl)spermidine cofactor for glutathione reductase in trypanosomatids.* Science, 1985. 227(4693): p. 1485-7.

44. Bond, C.S., et al., *Crystal structure of Trypanosoma cruzi trypanothione reductase in complex with trypanothione, and the structure-based discovery of new natural product inhibitors.* Structure, 1999. 7(1): p. 81-9.

45. Schirmer, R.H., Muller, JG and Krauth-Siegel,RL, Angew. Chem. Intl. Ed. Engl., 1995. 34(141-154).

46. Williams, C.H., et al., *Thioredoxin reductase two modes of catalysis have evolved.* Eur J Biochem, 2000. 267(20): p. 6110-7.

47. Bauer, H., et al., *The mechanism of high Mr thioredoxin reductase from Drosophila melanogaster.* J Biol Chem, 2003. 278(35): p. 33020-8.

48. Gasdaska, J.R., et al., *Regulation of human thioredoxin reductase expression and activity by 3'-untranslated region selenocysteine insertion sequence and mRNA instability elements.* J Biol Chem, 1999. 274(36): p. 25379-85.

49. Gilberger, T.W., et al., *The role of the C-terminus for catalysis of the large thioredoxin reductase from Plasmodium falciparum.* FEBS Lett, 1998. 425(3): p. 407-10.

50. Prongay, A.J., D.R. Engelke, and C.H. Williams, Jr., *Characterization of two active site mutations of thioredoxin reductase from Escherichia coli.* J Biol Chem, 1989. 264(5): p. 2656-64.

51. Veine, D.M., et al., *Formation and properties of mixed disulfides between thioredoxin reductase from Escherichia coli and thioredoxin: evidence that cysteine-138 functions to initiate dithiol-disulfide interchange and to accept the reducing equivalent from reduced flavin.* Protein Sci, 1998. 7(6): p. 1441-50.

52. Mulrooney, S.B. and C.H. Williams, Jr., *Potential active-site base of thioredoxin reductase from Escherichia coli: examination of histidine245 and aspartate139 by site-directed mutagenesis.* Biochemistry, 1994. 33(11): p. 3148-54.

53. Waksman, G., et al., *Crystal structure of Escherichia coli thioredoxin reductase refined at 2 A resolution. Implications for a large conformational change during catalysis.* J Mol Biol, 1994. 236(3): p. 800-16.

54. Lennon, B.W., C.H. Williams, Jr., and M.L. Ludwig, *Twists in catalysis: alternating conformations of Escherichia coli thioredoxin reductase.* Science, 2000. 289(5482): p. 1190-4.

55. Stricks, W., et al., *Experimental study of the polarographic cancer test and of the sulfhydryl titration for the differentiation between normal, cancerous and other pathological sera.* J Lancet, 1953. 73(8): p. 328-35.

56. Brown, N.L., et al., *Nucleotide sequence of a gene from the Pseudomonas transposon Tn501 encoding mercuric reductase.* Biochemistry, 1983. 22(17): p. 4089-95.

57. Moore, M.J. and C.T. Walsh, *Mutagenesis of the N- and C-terminal cysteine pairs of Tn501 mercuric ion reductase: consequences for bacterial detoxification of mercurials.* Biochemistry, 1989. 28(3): p. 1183-94.

58. Moore, M.J., S.M. Miller, and C.T. Walsh, *C-terminal cysteines of Tn501 mercuric ion reductase.* Biochemistry, 1992. 31(6): p. 1677-85.

59. Engst, S. and S.M. Miller, *Rapid reduction of Hg(II) by mercuric ion reductase does not require the conserved C-terminal cysteine pair using HgBr2 as the substrate.* Biochemistry, 1998. 37(33): p. 11496-507.

60. Engst, S. and S.M. Miller, *Alternative routes for entry of HgX2 into the active site of mercuric ion reductase depend on the nature of the X ligands.* Biochemistry, 1999. 38(12): p. 3519-29.

61. Argyrou, A. and J.S. Blanchard, *Flavoprotein disulfide reductases: advances in chemistry and function.* Prog Nucleic Acid Res Mol Biol, 2004. 78: p. 89-142.

62. Summers, A.O., *Organization, expression, and evolution of genes for mercury resistance.* Annu Rev Microbiol, 1986. 40: p. 607-34.

63. Miller, S.M., et al., *Communication between the active sites in dimeric mercuric ion reductase: an alternating sites hypothesis for catalysis.* Biochemistry, 1991. 30(10): p. 2600-12.

64. Armstrong, F.A., *Hydrogenases: active site puzzles and progress.* Curr Opin Chem Biol, 2004. 8(2): p. 133-40.

65. Newton, G.L., et al., *Distribution of thiols in microorganisms: mycothiol is a major thiol in most actinomycetes.* J Bacteriol, 1996. 178(7): p. 1990-5.

66. delCardayre, S.B., et al., *Coenzyme A disulfide reductase, the primary low molecular weight disulfide reductase from Staphylococcus aureus. Purification and characterization of the native enzyme.* J Biol Chem, 1998. 273(10): p. 5744-51.

67. Claiborne, A., et al., *Structural, redox, and mechanistic parameters for cysteine-sulfenic acid function in catalysis and regulation.* Adv Protein Chem, 2001. 58: p. 215-76.

68. Clark, D.D., J.R. Allen, and S.A. Ensign, *Characterization of five catalytic activities associated with the NADPH:2-ketopropyl-coenzyme M [2-(2-ketopropylthio)ethanesulfonate] oxidoreductase/carboxylase of the Xanthobacter strain Py2 epoxide carboxylase system.* Biochemistry, 2000. 39(6): p. 1294-304.

69. Allen, J.R. and S.A. Ensign, *Carboxylation of epoxides to beta-keto acids in cell extracts of Xanthobacter strain Py2.* J Bacteriol, 1996. 178(5): p. 1469-72.

70. Ensign, S.A. and J.R. Allen, *Aliphatic epoxide carboxylation.* Annu Rev Biochem, 2003. 72: p. 55-76.

71. Nocek, B., et al., *Structural basis for CO2 fixation by a novel member of the disulfide oxidoreductase family of enzymes, 2-ketopropyl-coenzyme M oxidoreductase/carboxylase.* Biochemistry, 2002. 41(43): p. 12907-13.

72. Matthews, R.G. and C.W. Goulding, *Enzyme-catalyzed methyl transfers to thiols: the role of zinc.* Curr Opin Chem Biol, 1997. 1(3): p. 332-9.

73. Cleland, W.W., et al., *Mechanism of Rubisco: The Carbamate as General Base.* Chem Rev, 1998. 98(2): p. 549-562.

74. Walsh, C., *Enzymatic Reaction Mechanisms*. 1979: W.H Freeman and Company.

75. Stephenson, M. and L.H. Stickland, *Hydrogenase: The reduction of sulphate to sulphide by molecular hydrogen.* Biochem J, 1931. 25(1): p. 215-20.

76. Vignais, P.M., B. Billoud, and J. Meyer, *Classification and phylogeny of hydrogenases.* FEMS Microbiol Rev, 2001. 25(4): p. 455-501.

77. Shima, S., et al., *The cofactor of the iron-sulfur cluster free hydrogenase hmd: structure of the light-inactivation product.* Angew Chem Int Ed Engl, 2004. 43(19): p. 2547-51.

78. Schnackenberg, J., R. Schulz, and H. Senger, *Characterization and purification of a hydrogenase from the eukaryotic green alga Scenedesmus obliquus.* FEBS Lett, 1993. 327(1): p. 21-4.

79. Zinn, T., et al., *Evidence for nickel in the soluble hydrogenase from the unicellular green alga Scenedesmus obliquus.* Z Naturforsch [C], 1994. 49(1-2): p. 33-8.

80. Wunschiers, R., H. Senger, and R. Schulz, *Electron pathways involved in H(2)-metabolism in the green alga Scenedesmus obliquus.* Biochim Biophys Acta, 2001. 1503(3): p. 271-8.

81. Florin, L., A. Tsokoglou, and T. Happe, *A novel type of iron hydrogenase in the green alga Scenedesmus obliquus is linked to the photosynthetic electron transport chain.* J Biol Chem, 2001. 276(9): p. 6125-32.

82. Blokesch, M. and A. Bock, *Maturation of [NiFe]-hydrogenases in Escherichia coli: the HypC cycle.* J Mol Biol, 2002. 324(2): p. 287-96.

83. Posewitz, M.C., et al., *Discovery of two novel radical S-adenosylmethionine proteins required for the assembly of an active [Fe] hydrogenase.* J Biol Chem, 2004. 279(24): p. 25711-20.

84. Pilkington, S.J., et al., *Relationship between mitochondrial NADH-ubiquinone reductase and a bacterial NAD-reducing hydrogenase.* Biochemistry, 1991. 30(8): p. 2166-75.

85. Fearnley, I.M. and J.E. Walker, *Conservation of sequences of subunits of mitochondrial complex I and their relationships with other proteins.* Biochim Biophys Acta, 1992. 1140(2): p. 105-34.

86. Albracht, S.P., *Intimate relationships of the large and the small subunits of all nickel hydrogenases with two nuclear-encoded subunits of mitochondrial NADH: ubiquinone oxidoreductase.* Biochim Biophys Acta, 1993. 1144(2): p. 221-4.

87. Albracht, S.P., *Nickel hydrogenases: in search of the active site.* Biochim Biophys Acta, 1994. 1188(3): p. 167-204.

88. Albracht, S.P., A. Mariette, and P. de Jong, *Bovine-heart NADH:ubiquinone oxidoreductase is a monomer with 8 Fe-S clusters and 2 FMN groups.* Biochim Biophys Acta, 1997. 1318(1-2): p. 92-106.

89. Kunkel, A., et al., *An Escherichia coli hydrogenase-3-type hydrogenase in methanogenic archaea.* Eur J Biochem, 1998. 252(3): p. 467-76.

90. Albracht, S.P. and R. Hedderich, *Learning from hydrogenases: location of a proton pump and of a second FMN in bovine NADH--ubiquinone oxidoreductase (Complex I).* FEBS Lett, 2000. 485(1): p. 1-6.

91. Adams, M.W., L.E. Mortenson, and J.S. Chen, *Hydrogenase.* Biochim Biophys Acta, 1980. 594(2-3): p. 105-76.

92. Bowien, B. and H.G. Schlegel, *Physiology and biochemistry of aerobic hydrogen-oxidizing bacteria.* Annu Rev Microbiol, 1981. 35: p. 405-52.

93. Thauer, R.K., A.R. Klein, and G.C. Hartmann, *Reactions with Molecular Hydrogen in Microorganisms: Evidence for a Purely Organic Hydrogenation Catalyst.* Chem Rev, 1996. 96(7): p. 3031-3042.

94. Thauer, R.K., *Biochemistry of methanogenesis: a tribute to Marjory Stephenson. 1998 Marjory Stephenson Prize Lecture.* Microbiology, 1998. 144 (Pt 9): p. 2377-406.

95. Reeve, J.N., et al., *Methanogenesis: genes, genomes, and who's on first?* J Bacteriol, 1997. 179(19): p. 5975-86.

96. Fauque, G., et al., *The three classes of hydrogenases from sulfate-reducing bacteria of the genus Desulfovibrio.* FEMS Microbiol Rev, 1988. 4(4): p. 299-344.

97. Meyer, J., B.C. Kelley, and P.M. Vignais, *Nitrogen fixation and hydrogen metabolism in photosynthetic bacteria.* Biochimie, 1978. 60(3): p. 245-60.

98. Vignais, P.M., et al., *Hydrogenase, nitrogenase, and hydrogen metabolism in the photosynthetic bacteria.* Adv Microb Physiol, 1985. 26: p. 155-234.

99. Weiner, J.H., et al., *A novel and ubiquitous system for membrane targeting and secretion of cofactor-containing proteins.* Cell, 1998. 93(1): p. 93-101.

100. Vignais, P.M., et al., *Characterization of the hydrogen-deuterium exchange activities of the energy-transducing HupSL hydrogenase and H(2)-signaling HupUV hydrogenase in Rhodobacter capsulatus.* J Bacteriol, 2000. 182(21): p. 5997-6004.

101. Meyer, J. and J. Gagnon, *Primary structure of hydrogenase I from Clostridium pasteurianum.* Biochemistry, 1991. 30(40): p. 9697-704.

102. Atta, M. and J. Meyer, *Characterization of the gene encoding the [Fe]-hydrogenase from Megasphaera elsdenii.* Biochim Biophys Acta, 2000. 1476(2): p. 368-71.

103. Malki, S., et al., *Characterization of an operon encoding an NADP-reducing hydrogenase in Desulfovibrio fructosovorans.* J Bacteriol, 1995. 177(10): p. 2628-36.

104. Horner, D.S., P.G. Foster, and T.M. Embley, *Iron hydrogenases and the evolution of anaerobic eukaryotes.* Mol Biol Evol, 2000. 17(11): p. 1695-709.

105. Bui, E.T. and P.J. Johnson, *Identification and characterization of [Fe]-hydrogenases in the hydrogenosome of Trichomonas vaginalis.* Mol Biochem Parasitol, 1996. 76(1-2): p. 305-10.

106. Plumper, E.P., Bradley P.J.,Johnson P.J., Protist, 1998. 149: p. 303-311.

107. Voordouw, G., *A universal system for the transport of redox proteins: early roots and latest developments.* Biophys Chem, 2000. 86(2-3): p. 131-40.

108. Voordouw, G. and S. Brenner, *Nucleotide sequence of the gene encoding the hydrogenase from Desulfovibrio vulgaris (Hildenborough).* Eur J Biochem, 1985. 148(3): p. 515-20.

109. Nicolet, Y., et al., *A novel FeS cluster in Fe-only hydrogenases.* Trends Biochem Sci, 2000. 25(3): p. 138-43.

110. Hatchikian, E.C., et al., *Carboxy-terminal processing of the large subunit of [Fe] hydrogenase from Desulfovibrio desulfuricans ATCC 7757.* J Bacteriol, 1999. 181(9): p. 2947-52.

111. Przybyla, A.E., et al., *Structure-function relationships among the nickel-containing hydrogenases.* FEMS Microbiol Rev, 1992. 8(2): p. 109-35.

112. Friedrich, B. and E. Schwartz, *Molecular biology of hydrogen utilization in aerobic chemolithotrophs.* Annu Rev Microbiol, 1993. 47: p. 351-83.

113. Vignais, P.M. and B. Toussaint, *Molecular biology of membrane-bound H2 uptake hydrogenases.* Arch Microbiol, 1994. 161(1): p. 1-10.

114. Volbeda, A., et al., *Crystal structure of the nickel-iron hydrogenase from Desulfovibrio gigas.* Nature, 1995. 373(6515): p. 580-7.

115. Higuchi, Y., T. Yagi, and N. Yasuoka, *Unusual ligand structure in Ni-Fe active center and an additional Mg site in hydrogenase revealed by high resolution X-ray structure analysis.* Structure, 1997. 5(12): p. 1671-80.

116. Fontecilla-Camps, J.C., et al., *Hydrogenase: a hydrogen-metabolizing enzyme. What do the crystal structures tell us about its mode of action?* Biochimie, 1997. 79(11): p. 661-6.

117. Montet, Y., et al., *Gas access to the active site of Ni-Fe hydrogenases probed by X-ray crystallography and molecular dynamics.* Nat Struct Biol, 1997. 4(7): p. 523-6.

118. Voordouw, G., *Evolution of Hydrogenase Genes.* Advances in Inorganic Chemistry, 1992. 38: p. 397-422.

119. Bairoch, A. and P. Bucher, *PROSITE: recent developments.* Nucleic Acids Res, 1994. 22(17): p. 3583-9.

120. Meek, L. and D.J. Arp, *The hydrogenase cytochrome b heme ligands of Azotobacter vinelandii are required for full H(2) oxidation capability.* J Bacteriol, 2000. 182(12): p. 3429-36.

121. Walker, C.C. and M.G. Yates, *The hydrogen cycle in nitrogen-fixing Azotobacter chroococcum.* Biochimie, 1978. 60(3): p. 225-31.

122. Weare, N.M. and J.R. Benemann, *Nitrogenase activity and photosynthesis in Plectonema boryanum.* J Bacteriol, 1974. 119(1): p. 258-65.

123. Bothe, H., E. Distler, and G. Eisbrenner, *Hydrogen metabolism in blue-green algae.* Biochimie, 1978. 60(3): p. 277-89.

124. Bianco, P., et al., *Reactivity of [Fe] and [Ni-Fe-Se] hydrogenases with their oxido-reduction partner: the tetraheme cytochrome c3.* Biochem Biophys Res Commun, 1992. 189(2): p. 633-9.

125. Morelli, X., et al., *Structural model of the Fe-hydrogenase/cytochrome c553 complex combining transverse relaxation-optimized spectroscopy experiments and soft docking calculations.* J Biol Chem, 2000. 275(30): p. 23204-10.

126. Aubert, C., et al., *A sequential electron transfer from hydrogenases to cytochromes in sulfate-reducing bacteria.* Biochim Biophys Acta, 2000. 1476(1): p. 85-92.

127. Lambert, G.R. and G.D. Smith, *Hydrogen uptake by the nitrogen-starved cyanobacterium Anabaena cylindrica.* Arch Biochem Biophys, 1981. 211(1): p. 360-7.

128. Houchins, J.P. and G. Hind, *Concentration and Function of Membrane-Bound Cytochromes in Cyanobacterial Heterocysts.* Plant Physiol, 1984. 76(2): p. 456-460.

129. Tamagnini, P., et al., *Hydrogenases and hydrogen metabolism of cyanobacteria.* Microbiol Mol Biol Rev, 2002. 66(1): p. 1-20, table of contents.

130. Elsen, S., et al., *The hupTUV operon is involved in negative control of hydrogenase synthesis in Rhodobacter capsulatus.* J Bacteriol, 1996. 178(17): p. 5174-81.

131. Black, L.K., C. Fu, and R.J. Maier, *Sequences and characterization of hupU and hupV genes of Bradyrhizobium japonicum encoding a possible nickel-sensing complex involved in hydrogenase expression.* J Bacteriol, 1994. 176(22): p. 7102-6.

132. Lenz, O., et al., *A hydrogen-sensing system in transcriptional regulation of hydrogenase gene expression in Alcaligenes species.* J Bacteriol, 1997. 179(5): p. 1655-63.

133. Schneider, K. and H.G. Schlegel, *Purification and properties of soluble hydrogenase from Alcaligenes eutrophus H 16.* Biochim Biophys Acta, 1976. 452(1): p. 66-80.

134. Kentemich T, B.M., Mayer F and Bothe H Naturforsch, 1989. 44C: p. 384-391.

135. Fox, J.D., et al., *Characterization of the CO-induced, CO-tolerant hydrogenase from Rhodospirillum rubrum and the gene encoding the large subunit of the enzyme.* J Bacteriol, 1996. 178(6): p. 1515-24.

136. Andrews, S.C., et al., *A 12-cistron Escherichia coli operon (hyf) encoding a putative proton-translocating formate hydrogenlyase system.* Microbiology, 1997. 143 (Pt 11): p. 3633-47.

137. Tersteegen, A. and R. Hedderich, *Methanobacterium thermoautotrophicum encodes two multisubunit membrane-bound [NiFe] hydrogenases. Transcription of the operons and sequence analysis of the deduced proteins.* Eur J Biochem, 1999. 264(3): p. 930-43.

138. Sapra, R., M.F. Verhagen, and M.W. Adams, *Purification and characterization of a membrane-bound hydrogenase from the hyperthermophilic archaeon Pyrococcus furiosus.* J Bacteriol, 2000. 182(12): p. 3423-8.

139. Silva, P.J., et al., *Enzymes of hydrogen metabolism in Pyrococcus furiosus.* Eur J Biochem, 2000. 267(22): p. 6541-51.

140. Verhagen, M.F., T. O'Rourke, and M.W. Adams, *The hyperthermophilic bacterium, Thermotoga maritima, contains an unusually complex iron-hydrogenase: amino acid sequence analyses versus biochemical characterization.* Biochim Biophys Acta, 1999. 1412(3): p. 212-29.

141. Nicolet, Y., et al., *Desulfovibrio desulfuricans iron hydrogenase: the structure shows unusual coordination to an active site Fe binuclear center.* Structure, 1999. 7(1): p. 13-23.

142. Adams, M.W., *The structure and mechanism of iron-hydrogenases.* Biochim Biophys Acta, 1990. 1020(2): p. 115-45.

143. Peters, J.W., et al., *X-ray crystal structure of the Fe-only hydrogenase (CpI) from Clostridium pasteurianum to 1.8 angstrom resolution.* Science, 1998. 282(5395): p. 1853-8.

144. Atta, M., et al., *Heterologous biosynthesis and characterization of the [2Fe-2S]-containing N-terminal domain of Clostridium pasteurianum hydrogenase.* Biochemistry, 1998. 37(45): p. 15974-80.

145. Kummerle, R., et al., *Structural similarities between the N-terminal domain of Clostridium pasteurianum hydrogenase and plant-type ferredoxins.* Biochemistry, 1999. 38(6): p. 1938-43.

146. Yeh, A.P., et al., *Structure of a thioredoxin-like [2Fe-2S] ferredoxin from Aquifex aeolicus.* J Mol Biol, 2000. 300(3): p. 587-95.

147. Chatelet, C., et al., *A [2Fe-2S] protein from the hyperthermophilic bacterium Aquifex aeolicus.* Biochem Biophys Res Commun, 1999. 261(3): p. 885-9.

148. Akhmanova, A., et al., *A hydrogenosome with a genome.* Nature, 1998. 396(6711): p. 527-8.

149. Frey, M., Fontecilla-Camps JC and Volbeda A, *Handbook of metalloproteins*, ed. H.R. Messerschmidt Albrecht, Poulos Thomas, Wieghardt Karl. 2001. 880-896.

150. Messerschimidt A, H.R., Poulos T and Wieghardt K, *Handbook of metalloproteins*. 2001: John Wiley and Sons.

151. Evans, D.J. and C.J. Pickett, *Chemistry and the hydrogenases.* Chem Soc Rev, 2003. 32(5): p. 268-75.

152. Tye, J.W., M.Y. Darensbourg, and M.B. Hall, *De novo design of synthetic di-iron(I) complexes as structural models of the reduced form of iron-iron hydrogenase.* Inorg Chem, 2006. 45(4): p. 1552-9.

153. Cammack, R., *The enzyme at the end of the food chain.* Nature, 1997. 390(6659): p. 443-4.

154. Happe, R.P., et al., *Biological activation of hydrogen.* Nature, 1997. 385(6612): p. 126.

155. Matias, P.M., et al., *[NiFe] hydrogenase from Desulfovibrio desulfuricans ATCC 27774: gene sequencing, three-dimensional structure determination and refinement at 1.8 A and modelling studies of its interaction with the tetrahaem cytochrome c3.* J Biol Inorg Chem, 2001. 6(1): p. 63-81.

156. Pierik, A.J., et al., *A low-spin iron with CN and CO as intrinsic ligands forms the core of the active site in [Fe]-hydrogenases.* Eur J Biochem, 1998. 258(2): p. 572-8.

157. De Lacey, A.L., et al., *Kinetic characterization of Desulfovibrio gigas hydrogenase upon selective chemical modification of amino acid groups as a tool for structure-function relationships.* Biochim Biophys Acta, 2000. 1481(2): p. 371-80.

158. Nicolet, Y., et al., *Crystallographic and FTIR spectroscopic evidence of changes in Fe coordination upon reduction of the active site of the Fe-only hydrogenase from Desulfovibrio desulfuricans.* J Am Chem Soc, 2001. 123(8): p. 1596-601.

159. Macor, K.A., et al., *An investigation of hydrogenase I and hydrogenase II from Clostridium pasteurianum by resonance Raman spectroscopy. Evidence for a [2Fe-2S] cluster in hydrogenase I.* J Biol Chem, 1987. 262(21): p. 9945-7.

160. Fu, W., et al., *Resonance Raman studies of iron-only hydrogenases.* Biochemistry, 1993. 32(18): p. 4813-9.

161. Moulis, J.M., et al., *Crystal structure of the 2[4Fe-4S] ferredoxin from Chromatium vinosum: evolutionary and mechanistic inferences for [3/4Fe-4S] ferredoxins.* Protein Sci, 1996. 5(9): p. 1765-75.

162. Stephens, P.J., D.R. Jollie, and A. Warshel, *Protein Control of Redox Potentials of Ironminus signSulfur Proteins.* Chem Rev, 1996. 96(7): p. 2491-2514.

163. Adams, M.W., *The mechanisms of H2 activation and CO binding by hydrogenase I and hydrogenase II of Clostridium pasteurianum.* J Biol Chem, 1987. 262(31): p. 15054-61.

164. Messick, T.E., et al., *Noncysteinyl coordination to the [4Fe-4S]2+ cluster of the DNA repair adenine glycosylase MutY introduced via site-directed mutagenesis. Structural characterization of an unusual histidinyl-coordinated cluster.* Biochemistry, 2002. 41(12): p. 3931-42.

165. Camba, R. and F.A. Armstrong, *Investigations of the oxidative disassembly of Fe-S clusters in Clostridium pasteurianum 8Fe ferredoxin using pulsed-protein-film voltammetry.* Biochemistry, 2000. 39(34): p. 10587-98.

166. Shirakawa, T., et al., *Identification of variant molecules of Bacillus thermoproteolyticus ferredoxin: crystal structure reveals bound coenzyme A and an unexpected [3Fe-4S] cluster associated with a canonical [4Fe-4S] ligand motif.* Biochemistry, 2005. 44(37): p. 12402-10.

167. Busch, J.L., et al., *[3Fe-4S] <--> [4Fe-4S] cluster interconversion in Desulfovibrio africanus ferredoxin III: properties of an Asp14 --> Cys mutant.* Biochem J, 1997. 323 (Pt 1): p. 95-102.

168. Gorwa, M.F., C. Croux, and P. Soucaille, *Molecular characterization and transcriptional analysis of the putative hydrogenase gene of Clostridium acetobutylicum ATCC 824.* J Bacteriol, 1996. 178(9): p. 2668-75.

169. Santangelo, J.D., P. Durre, and D.R. Woods, *Characterization and expression of the hydrogenase-encoding gene from Clostridium acetobutylicum P262.* Microbiology, 1995. 141 (Pt 1): p. 171-80.

170. Stokkermans, J., et al., *hyd gamma, a gene from Desulfovibrio vulgaris (Hildenborough) encodes a polypeptide homologous to the periplasmic hydrogenase.* FEMS Microbiol Lett, 1989. 49(2-3): p. 217-22.

171. Voordouw, G., J.D. Strang, and F.R. Wilson, *Organization of the genes encoding [Fe] hydrogenase in Desulfovibrio vulgaris subsp. oxamicus Monticello.* J Bacteriol, 1989. 171(7): p. 3881-9.

172. Crane, B.R., L.M. Siegel, and E.D. Getzoff, *Sulfite reductase structure at 1.6 A: evolution and catalysis for reduction of inorganic anions.* Science, 1995. 270(5233): p. 59-67.

173. Adams, M.W., E. Eccleston, and J.B. Howard, *Iron-sulfur clusters of hydrogenase I and hydrogenase II of Clostridium pasteurianum.* Proc Natl Acad Sci U S A, 1989. 86(13): p. 4932-6.

174. Thauer, R.K., et al., *The reaction of the iron-sulfur protein hydrogenase with carbon monoxide.* Eur J Biochem, 1974. 42(2): p. 447-52.

175. Erbes, D.L. and R.H. Burris, *The kinetics of methyl viologen oxidation and reduction by the hydrogenase from Clostridium pasteurianum.* Biochim Biophys Acta, 1978. 525(1): p. 45-54.

176. Lemon, B.J. and J.W. Peters, *Binding of exogenously added carbon monoxide at the active site of the iron-only hydrogenase (CpI) from Clostridium pasteurianum.* Biochemistry, 1999. 38(40): p. 12969-73.

177. Bennett, B., B.J. Lemon, and J.W. Peters, *Reversible carbon monoxide binding and inhibition at the active site of the Fe-only hydrogenase.* Biochemistry, 2000. 39(25): p. 7455-60.

178. Surerus, K.K., et al., *Further characterization of the spin coupling observed in oxidized hydrogenase from Chromatium vinosum. A Mossbauer and multifrequency EPR study.* Biochemistry, 1994. 33(16): p. 4980-93.

179. Razavet, M., et al., *Transient FTIR spectroelectrochemical and stopped-flow detection of a mixed valence (Fe(I)-Fe(II)) bridging carbonyl intermediate with structural elements and spectroscopic characteristics of the di-iron sub-site of all-iron hydrogenase.* Chem Commun (Camb), 2002(7): p. 700-1.

180. Cao, Z. and M.B. Hall, *Modeling the active sites in metalloenzymes. 3. Density functional calculations on models for [Fe]-hydrogenase: structures and vibrational frequencies of the observed redox forms and the reaction mechanism at the Diiron Active Center.* J Am Chem Soc, 2001. 123(16): p. 3734-42.

181. Zhao, X., et al., *H/D exchange reactions in dinuclear iron thiolates as activity assay models of Fe-H2ase.* J Am Chem Soc, 2001. 123(39): p. 9710-1.

182. Chen, Z., et al., *Infrared studies of the CO-inhibited form of the Fe-only hydrogenase from Clostridium pasteurianum I: examination of its light sensitivity at cryogenic temperatures.* Biochemistry, 2002. 41(6): p. 2036-43.

183. Gloaguen, F., J.D. Lawrence, and T.B. Rauchfuss, *Biomimetic hydrogen evolution catalyzed by an iron carbonyl thiolate.* J Am Chem Soc, 2001. 123(38): p. 9476-7.

184. Mejia-Rodriguez, R., et al., *The hydrophilic phosphatriazaadamantane ligand in the development of H2 production electrocatalysts: iron hydrogenase model complexes.* J Am Chem Soc, 2004. 126(38): p. 12004-14.

185. Borg, S.J., et al., *Electrocatalytic proton reduction by dithiolate-bridged diiron carbonyl complexes: a connection to the H-cluster?* Biochem Soc Trans, 2005. 33(Pt 1): p. 3-6.

186. Gloaguen, F., et al., *Bimetallic carbonyl thiolates as functional models for Fe-only hydrogenases.* Inorg Chem, 2002. 41(25): p. 6573-82.

187. Justice, A.K., et al., *Dihydrogen activation by a diruthenium analogue of the Fe-only hydrogenase active site.* J Am Chem Soc, 2004. 126(41): p. 13214-5.

188. van der Vlugt, J.I., et al., *Characterization of a diferrous terminal hydride mechanistically relevant to the Fe-only hydrogenases.* J Am Chem Soc, 2005. 127(46): p. 16012-3.

189. Greco, C., et al., *Insights into the mechanism of electrocatalytic hydrogen evolution mediated by Fe2(S2C3H6)(CO)6: the simplest functional model of the Fe-hydrogenase active site.* Inorg Chem, 2007. 46(1): p. 108-16.

190. Ensign, S.A., *Microbial metabolism of aliphatic alkenes.* Biochemistry, 2001. 40(20): p. 5845-53.

191. Dowd, P., et al., *Vitamin K and energy transduction: a base strength amplification mechanism.* Science, 1995. 269(5231): p. 1684-91.

192. Janc, J.W., M.H. O'Leary, and W.W. Cleland, *A kinetic investigation of phosphoenolpyruvate carboxylase from Zea mays.* Biochemistry, 1992. 31(28): p. 6421-6.

193. Knowles, J.R., *The mechanism of biotin-dependent enzymes.* Annu Rev Biochem, 1989. 58: p. 195-221.

194. Mattevi, A., A.J. Schierbeek, and W.G. Hol, *Refined crystal structure of lipoamide dehydrogenase from Azotobacter vinelandii at 2.2 A resolution. A comparison with the structure of glutathione reductase.* J Mol Biol, 1991. 220(4): p. 975-94.

195. Argyrou, A., J.S. Blanchard, and B.A. Palfey, *The lipoamide dehydrogenase from Mycobacterium tuberculosis permits the direct observation of flavin intermediates in catalysis.* Biochemistry, 2002. 41(49): p. 14580-90.

196. Jang, S.B., et al., *Crystallization and preliminary X-ray analysis of a NADPH 2-ketopropyl-coenzyme M oxidoreductase/carboxylase.* Acta Crystallogr D Biol Crystallogr, 2001. 57(Pt 3): p. 445-7.

197. Collaborative Computational Project, N., *The CCP4 suite: programs for protein crystallography.* Acta Crystallogr D Biol Crystallogr, 1994. 50(Pt 5): p. 760-3.

198. Brunger, A.T., et al., *Crystallography & NMR system: A new software suite for macromolecular structure determination.* Acta Crystallogr D Biol Crystallogr, 1998. 54(Pt 5): p. 905-21.

199. Jones, T.A., et al., *Improved methods for building protein models in electron density maps and the location of errors in these models.* Acta Crystallogr A, 1991. 47 (Pt 2): p. 110-9.

200. Laskowski, R.A., D.S. Moss, and J.M. Thornton, *Main-chain bond lengths and bond angles in protein structures.* J Mol Biol, 1993. 231(4): p. 1049-67.

201. Guex, N. and M.C. Peitsch, *SWISS-MODEL and the Swiss-PdbViewer: an environment for comparative protein modeling.* Electrophoresis, 1997. 18(15): p. 2714-23.

202. Christopher, J.A., R. Swanson, and T.O. Baldwin, *Algorithms for finding the axis of a helix: fast rotational and parametric least-squares methods.* Comput Chem, 1996. 20(3): p. 339-45.

203. ACDlabs, *Advanced Chemistry Development,Inc.* 2003: Toronto,Ontario,Canada.

204. Alexander, R.S., S.K. Nair, and D.W. Christianson, *Engineering the hydrophobic pocket of carbonic anhydrase II.* Biochemistry, 1991. 30(46): p. 11064-72.

205. Fierke, C.A., T.L. Calderone, and J.F. Krebs, *Functional consequences of engineering the hydrophobic pocket of carbonic anhydrase II.* Biochemistry, 1991. 30(46): p. 11054-63.

206. Nair, S.K. and D.W. Christianson, *Structural consequences of hydrophilic amino acid substitutions in the hydrophobic pocket of human carbonic anhydrase II.* Biochemistry, 1993. 32(17): p. 4506-14.

207. Mannervik, B., *A branching reaction mechanism of glutathione reductase.* Biochem Biophys Res Commun, 1973. 53(4): p. 1151-8.

208. Patel, M.P. and J.S. Blanchard, *Expression, purification, and characterization of Mycobacterium tuberculosis mycothione reductase.* Biochemistry, 1999. 38(36): p. 11827-33.

209. Pandey, A.S., et al., *Mechanistic implications of the structure of the mixed-disulfide intermediate of the disulfide oxidoreductase, 2-ketopropyl-coenzyme M oxidoreductase/carboxylase.* Biochemistry, 2006. 45(1): p. 113-20.

210. Fox, B. and C.T. Walsh, *Mercuric reductase. Purification and characterization of a transposon-encoded flavoprotein containing an oxidation-reduction-active disulfide.* J Biol Chem, 1982. 257(5): p. 2498-503.

211. Massey, V., Q.H. Gibson, and C. Veeger, *Intermediates in the catalytic action of lipoyl dehydrogenase (diaphorase).* Biochem J, 1960. 77: p. 341-51.

212. Massey, V. and C. Veeger, *Studies on the reaction mechanism of lipoyl dehydrogenase.* Biochim Biophys Acta, 1961. 48: p. 33-47.

213. Moore, E.C., P. Reichard, and L. Thelander, *Enzymatic Synthesis of Deoxyribonucleotides.V. Purification and Properties of Thioredoxin Reductase from Escherichia Coli B.* J Biol Chem, 1964. 239: p. 3445-52.

214. Searls, R.L., J.M. Peters, and D.R. Sanadi, *alpha-Ketoglutaric dehydrogenase. X. On the mechanism of dihydrolipoyl dehydrogenase reaction.* J Biol Chem, 1961. 236: p. 2317-22.

215. Thorpe, C. and C.H. Williams, Jr., *Differential reactivity of the two active site cysteine residues generated on reduction of pig heart lipoamide dehydrogenase.* J Biol Chem, 1976. 251(12): p. 3553-7.

216. Thorpe, C. and C.H. Williams, Jr., *Spectral evidence for a flavin adduct in a monoalkylated derivative of pig heart lipoamide dehydrogenase.* J Biol Chem, 1976. 251(23): p. 7726-8.

217. Miller, S.M., et al., *Use of a site-directed triple mutant to trap intermediates: demonstration that the flavin C(4a)-thiol adduct and reduced flavin are kinetically competent intermediates in mercuric ion reductase.* Biochemistry, 1990. 29(11): p. 2831-41.

218. O'Donnell, M.E. and C.H. Williams, Jr., *Reconstitution of Escherichia coli thioredoxin reductase with 1-deazaFAD. Evidence for 1-deazaFAD C-4a adduct formation linked to the ionization of an active site base.* J Biol Chem, 1984. 259(4): p. 2243-51.

219. Sahlman, L., A.M. Lambeir, and S. Lindskog, *Rapid-scan stopped-flow studies of the pH dependence of the reaction between mercuric reductase and NADPH.* Eur J Biochem, 1986. 156(3): p. 479-88.

220. Hopkins, N. and C.H. Williams, Jr., *Characterization of lipoamide dehydrogenase from Escherichia coli lacking the redox active disulfide: C44S and C49S.* Biochemistry, 1995. 34(37): p. 11757-65.

221. Deonarain, M.P., et al., *Directed mutagenesis of the redox-active disulphide bridge in glutathione reductase from Escherichia coli.* Proc Biol Sci, 1990. 241(1302): p. 179-86.

222. Borges, A., et al., *Site-directed mutagenesis of the redox-active cysteines of Trypanosoma cruzi trypanothione reductase.* Eur J Biochem, 1995. 228(3): p. 745-52.

223. Sheldrick, G.M.S., T. R., *SHELXL (refinement): SHELXL: high resolution refinement* Methods in Enzymology, ed. J.R.M.S. CW Carter. Vol. 277. 1997. pp. 319-343.

224. Murshudov, G.N., A.A. Vagin, and E.J. Dodson, *Refinement of macromolecular structures by the maximum-likelihood method.* Acta Crystallogr D Biol Crystallogr, 1997. 53(Pt 3): p. 240-55.

225. Pannu, N.S., et al., *Incorporation of prior phase information strengthens maximum-likelihood structure refinement.* Acta Crystallogr D Biol Crystallogr, 1998. 54(Pt 6 Pt 2): p. 1285-94.

226. Winn, M.D., M.N. Isupov, and G.N. Murshudov, *Use of TLS parameters to model anisotropic displacements in macromolecular refinement.* Acta Crystallogr D Biol Crystallogr, 2001. 57(Pt 1): p. 122-33.

227. Gouet, P., X. Robert, and E. Courcelle, *ESPript/ENDscript: Extracting and rendering sequence and 3D information from atomic structures of proteins.* Nucleic Acids Res, 2003. 31(13): p. 3320-3.

228. Mizuguchi, K., et al., *JOY: protein sequence-structure representation and analysis.* Bioinformatics, 1998. 14(7): p. 617-23.

229. Sali, A. and T.L. Blundell, *Definition of general topological equivalence in protein structures. A procedure involving comparison of properties and relationships through simulated annealing and dynamic programming.* J Mol Biol, 1990. 212(2): p. 403-28.

230. Bond, C.S., *TopDraw: a sketchpad for protein structure topology cartoons.* Bioinformatics, 2003. 19(2): p. 311-2.

231. Schierbeek, A.J., et al., *X-ray structure of lipoamide dehydrogenase from Azotobacter vinelandii determined by a combination of molecular and isomorphous replacement techniques.* J Mol Biol, 1989. 206(2): p. 365-79.

232. Kuriyan, J., et al., *X-ray structure of trypanothione reductase from Crithidia fasciculata at 2.4-A resolution.* Proc Natl Acad Sci U S A, 1991. 88(19): p. 8764-8.

233. Krauth-Siegel, R.L., et al., *Glutathione reductase from human erythrocytes. The sequences of the NADPH domain and of the interface domain.* Eur J Biochem, 1982. 121(2): p. 259-67.

234. Herzberg, O. and J. Moult, *Analysis of the steric strain in the polypeptide backbone of protein molecules.* Proteins, 1991. 11(3): p. 223-9.

235. Stoddard, B.L. and S. Pietrokovski, *Breaking up is hard to do.* Nat Struct Biol, 1998. 5(1): p. 3-5.

236. Weiss, M.S., A. Jabs, and R. Hilgenfeld, *Peptide bonds revisited.* Nat Struct Biol, 1998. 5(8): p. 676.

237. Wang, P.F., et al., *A stable mixed disulfide between thioredoxin reductase and its substrate, thioredoxin: preparation and characterization.* Biochemistry, 1996. 35(15): p. 4812-9.

238. Arscott, L.D., D.M. Veine, and C.H. Williams, Jr., *Mixed disulfide with glutathione as an intermediate in the reaction catalyzed by glutathione reductase from yeast and as a major form of the enzyme in the cell.* Biochemistry, 2000. 39(16): p. 4711-21.

239. Benen, J., et al., *Lipoamide dehydrogenase from Azotobacter vinelandii: site-directed mutagenesis of the His450-Glu455 diad. Spectral properties of wild type and mutated enzymes.* Eur J Biochem, 1991. 202(3): p. 863-72.

240. Nordhoff, A., et al., *Folding of the four domains and dimerization are impaired by the Gly446-->Glu exchange in human glutathione reductase. Implications for the design of antiparasitic drugs.* Biochemistry, 1993. 32(15): p. 4060-6.

241. Rao, S.T. and M.G. Rossmann, *Comparison of super-secondary structures in proteins.* J Mol Biol, 1973. 76(2): p. 241-56.

242. Wierenga, R.K., J. Drenth, and G.E. Schulz, *Comparison of the three-dimensional protein and nucleotide structure of the FAD-binding domain of p-hydroxybenzoate hydroxylase with the FAD- as well as NADPH-binding domains of glutathione reductase.* J Mol Biol, 1983. 167(3): p. 725-39.

243. Schiltz, E., R. Blatterspiel, and R. Untucht-Grau, *Glutathione reductase from human erythrocytes. Amino-acid sequence of a major fragment that links the FAD, NADP and interface domains.* Eur J Biochem, 1979. 102(1): p. 269-78.

244. Schulz, G.E., *Binding of nucleotides to proteins.* Current opinion in structural biology, 1992. 2: p. 61-67.

245. Schulz, G.E. and R.H. Schirmer, *Topological comparison of adenyl kinase with other proteins.* Nature, 1974. 250(462): p. 142-4.

246. Schulz, G.E., R.H. Schirmer, and E.F. Pai, *FAD-binding site of glutathione reductase.* J Mol Biol, 1982. 160(2): p. 287-308.

247. Eggink, G., et al., *Rubredoxin reductase of Pseudomonas oleovorans. Structural relationship to other flavoprotein oxidoreductases based on one NAD and two FAD fingerprints.* J Mol Biol, 1990. 212(1): p. 135-42.

248. Vallon, O., *New sequence motifs in flavoproteins: evidence for common ancestry and tools to predict structure.* Proteins, 2000. 38(1): p. 95-114.

249. Veeger, C. and V. Massey, *A new NAD-dependent spectral species of lipoamide dehydrogenase.* Biochim Biophys Acta, 1963. 67: p. 679-81.

250. van den Berg, W.A.M., Vervoort J., Moonen C.T.W. and Muller, *13C-NMR study on the active sites of lipoamide dehydrogenase and glutathione reductase*, in *Flavins and Flavoproteins*, R. Bray, Engel, PC and Mayhew, SG, Editor. 1984, Walter de Gruyter: Berlin.

251. Matthews, R.G. and C.H. Williams, Jr., *Measurement of the oxidation-reduction potentials for two-electron and four-electron reduction of lipoamide dehydrogenase from pig heart.* J Biol Chem, 1976. 251(13): p. 3956-64.

252. Arscott, L.D., C. Thorpe, and C.H. Williams, Jr., *Glutathione reductase from yeast. Differential reactivity of the nascent thiols in two-electron reduced enzyme and properties of a monoalkylated derivative.* Biochemistry, 1981. 20(6): p. 1513-20.

253. Maeda-Yorita, K., et al., *Properties of lipoamide dehydrogenase altered by site-directed mutagenesis at a key residue (I184Y) in the pyridine nucleotide binding domain.* Biochemistry, 1991. 30(51): p. 11788-95.

254. Picaud, T. and A. Desbois, *Electrostatic control of the isoalloxazine environment in the two-electron reduced states of yeast glutathione reductase.* J Biol Chem, 2002. 277(35): p. 31715-21.

255. Carugo, O. and P. Argos, *NADP-dependent enzymes. I: Conserved stereochemistry of cofactor binding.* Proteins, 1997. 28(1): p. 10-28.

256. Mao, L., et al., *Molecular determinants for ATP-binding in proteins: a data mining and quantum chemical analysis.* J Mol Biol, 2004. 336(3): p. 787-807.

257. Karplus, P.A., E.F. Pai, and G.E. Schulz, *A crystallographic study of the glutathione binding site of glutathione reductase at 0.3-nm resolution.* Eur J Biochem, 1989. 178(3): p. 693-703.

258. Krauth-Siegel, R.L., et al., *Role of active site tyrosine residues in catalysis by human glutathione reductase.* Biochemistry, 1998. 37(40): p. 13968-77.

259. Berry, A., N.S. Scrutton, and R.N. Perham, *Switching kinetic mechanism and putative proton donor by directed mutagenesis of glutathione reductase.* Biochemistry, 1989. 28(3): p. 1264-9.

260. Ziegler, G.A. and G.E. Schulz, *Crystal structures of adrenodoxin reductase in complex with NADP+ and NADPH suggesting a mechanism for the electron transfer of an enzyme family.* Biochemistry, 2000. 39(36): p. 10986-95.

261. Scrutton, N.S., A. Berry, and R.N. Perham, *Redesign of the coenzyme specificity of a dehydrogenase by protein engineering.* Nature, 1990. 343(6253): p. 38-43.

262. Mittl, P.R., et al., *Structural differences between wild-type NADP-dependent glutathione reductase from Escherichia coli and a redesigned NAD-dependent mutant.* J Mol Biol, 1993. 231(2): p. 191-5.

263. Rescigno, M. and R.N. Perham, *Structure of the NADPH-binding motif of glutathione reductase: efficiency determined by evolution.* Biochemistry, 1994. 33(19): p. 5721-7.

264. Rossman, M.G. and A. Liljas, *Letter: Recognition of structural domains in globular proteins.* J Mol Biol, 1974. 85(1): p. 177-81.

265. Kluger, R. and K. Nakaoka, *Inhibition of acetoacetate decarboxylase by ketophosphonates. Structural and dynamic probes of the active site.* Biochemistry, 1974. 13(5): p. 910-4.

266. Otwinowski, Z.a.M., W., *Processing of X-ray diffaction data collected in oscillation mode*. Methods in Enzymology: Macromolecular crystallographyt, Part A, ed. C.W.C.J.a.R.M. Sweet. Vol. 276. 1997: Academic Press.

267. DeLano, W., *The PyMOL molecular graphics system*. 2002, DeLano Scientific: San Carlos, CA, USA.

268. Cleland, W., *The Chemistry of Carbanions and Carbanion Like Transition States*. Comprehensive Biological Catalysis, ed. S. M. Vol. 2. 1998: Academic Press.

269. White, D., *The Physiology and Biochemistry of Prokaryotes*. 2nd Edition ed. 2000: Oxford University Press. 338-362.

270. Wood HG, L.L., *Autotrophic character of the acetogenic bacteria*. Variations in Autotrophic Life, ed. J.a.B. Shively. 1991, New York: Academic Press. 201-250.

271. Wolfe, R., *Novel coenzymes of archaebacteria*. The molecular basis of bacterial metabolism, ed. G.a.T.R. Hauska. 1990, Springer-Verlag, Berlin.

272. Begley, T.P. and S.E. Ealick, *Enzymatic reactions involving novel mechanisms of carbanion stabilization.* Curr Opin Chem Biol, 2004. 8(5): p. 508-15.

273. Leslie, A., *Joint CCP4 and ESF-EACBM Newsletter on Protein Crystallography.* 1992. N26.

274. Magid, E. and B.O. Turbeck, *The rates of the spontaneous hydration of CO2 and the reciprocal reaction in neutral aqueous solutions between 0 degrees and 38 degrees.* Biochim Biophys Acta, 1968. 165(3): p. 515-24.

275. Cronk, J.D., et al., *Identification of a novel noncatalytic bicarbonate binding site in eubacterial beta-carbonic anhydrase.* Biochemistry, 2006. 45(14): p. 4351-61.

276. Kimber, M.S. and E.F. Pai, *The active site architecture of Pisum sativum beta-carbonic anhydrase is a mirror image of that of alpha-carbonic anhydrases.* Embo J, 2000. 19(7): p. 1407-18.

277. Mitsuhashi, S., et al., *X-ray structure of beta-carbonic anhydrase from the red alga, Porphyridium purpureum, reveals a novel catalytic site for CO(2) hydration.* J Biol Chem, 2000. 275(8): p. 5521-6.

278. Harris, P., et al., *Structural basis for the catalytic mechanism of a proficient enzyme: orotidine 5'-monophosphate decarboxylase.* Biochemistry, 2000. 39(15): p. 4217-24.

279. Wu, N., et al., *Electrostatic stress in catalysis: structure and mechanism of the enzyme orotidine monophosphate decarboxylase.* Proc Natl Acad Sci U S A, 2000. 97(5): p. 2017-22.

280. Akhtar, M., *The modification of acetate and propionate side chains during the biosynthesis of haem and chlorophylls: mechanistic and stereochemical studies.* Ciba Found Symp, 1994. 180: p. 131-51; discussion 152-5.

281. Lyon, E.J., et al., *UV-A/blue-light inactivation of the 'metal-free' hydrogenase (Hmd) from methanogenic archaea.* Eur J Biochem, 2004. 271(1): p. 195-204.

282. Bagley, K.A., et al., *Infrared-detectable groups sense changes in charge density on the nickel center in hydrogenase from Chromatium vinosum.* Biochemistry, 1995. 34(16): p. 5527-35.

283. Zilberman, S., et al., *Resolving the CO/CN ligand arrangement in CO-inactivated [FeFe] hydrogenase by first principles density functional theory calculations.* Inorg Chem, 2006. 45(15): p. 5715-7.

284. Tard, C., et al., *Synthesis of the H-cluster framework of iron-only hydrogenase.* Nature, 2005. 433(7026): p. 610-3.

285. Adman, E., K.D. Watenpaugh, and L.H. Jensen, *NH---S hydrogen bonds in Peptococcus aerogenes ferredoxin, Clostridium pasteurianum rubredoxin, and Chromatium high potential iron protein.* Proc Natl Acad Sci U S A, 1975. 72(12): p. 4854-8.

286. Swartz, P.D., B.W. Beck, and T. Ichiye, *Structural origins of redox potentials in Fe-S proteins: electrostatic potentials of crystal structures.* Biophys J, 1996. 71(6): p. 2958-69.

287. Dolan, E.A., et al., *Protein control of electron transfer rates via polarization: molecular dynamics studies of rubredoxin.* Biophys J, 2004. 86(4): p. 2030-6.

288. Chen, J.S. and L.E. Mortenson, *Purification and properties of hydrogenase from Clostridium pasteurianum W5.* Biochim Biophys Acta, 1974. 371(2): p. 283-98.

289. Georgiadis, M.M., et al., *Crystallographic structure of the nitrogenase iron protein from Azotobacter vinelandii.* Science, 1992. 257(5077): p. 1653-9.

290. Sheldrick, G.a.S., TR, *Methods in Enzymology.* 1997. 277: p. 319-343.

291. McRee, D.E., *XtalView/Xfit--A versatile program for manipulating atomic coordinates and electron density.* J Struct Biol, 1999. 125(2-3): p. 156-65.

292. Boyke, C.A., et al., *Diferrous cyanides as models for the Fe-only hydrogenases.* J Am Chem Soc, 2005. 127(31): p. 11010-8.

293. Darensbourg, M.Y., et al., *The organometallic active site of [Fe]hydrogenase: models and entatic states.* Proc Natl Acad Sci U S A, 2003. 100(7): p. 3683-8.

294. Gloaguen, F., et al., *Synthetic and structural studies on [Fe2(SR)2(CN)x(CO)6-x](x-) as active site models for Fe-only hydrogenases.* J Am Chem Soc, 2001. 123(50): p. 12518-27.

295. Georgakaki, I.P., M.L. Miller, and M.Y. Darensbourg, *Requirements for functional models of the iron hydrogenase active site: D2/H2O exchange activity in ((mu-SMe)(mu-pdt)[Fe(CO)2(PMe3)]2+)[BF4-].* Inorg Chem, 2003. 42(8): p. 2489-94.

296. Peters, J.W., *Structure and mechanism of iron-only hydrogenases.* Curr Opin Struct Biol, 1999. 9(6): p. 670-6.

297. Lyon, E.J., et al., *Coordination sphere flexibility of active-site models for Fe-only hydrogenase: studies in intra- and intermolecular diatomic ligand exchange.* J Am Chem Soc, 2001. 123(14): p. 3268-78.